



**COSMETICS FROM RAMBUTAN PEELS EXTRACTS**

**SIRILUK PONGPUNYAYUEN**

**MASTER OF SCIENCE**

**IN**

**COSMETIC SCIENCE**

**SCHOOL OF COSMETIC SCIENCE**


**MAE FAH LUANG UNIVERSITY**

**2011**

**©COPYRIGHT BY MAE FAH LUANG UNIVERSITY**

# **COSMETICS FROM RAMBUTAN PEELS EXTRACTS**

**SIRILUK PONGPUNYAYUEN**



**THIS THESIS IS A PARTIAL FULFILLMENT OF  
THE REQUIREMENTS FOR THE DEGREE OF  
MASTER OF SCIENCE  
IN  
COSMETIC SCIENCE**

**SCHOOL OF COSMETIC SCIENCE**

**MAE FAH LUANG UNIVERSITY**

**2011**

**©COPYRIGHT BY MAE FAH LUANG UNIVERSITY**

# **COSMETICS FROM RAMBUTAN PEELS EXTRACTS**

SIRILUK PONGPUNYAYUEN

THIS THESIS HAS BEEN APPROVED  
TO BE A PARTIAL FULFILLMENT OF THE REQUIREMENTS  
FOR THE DEGREE OF MASTER OF SCIENCE

IN  
COSMETIC SCIENCE  
2011

THESIS COMMITTEE

.....CHAIRPERSON  
(Asst. Prof. Dr. Mayuree Kanlayavattanakul)

.....ADVISOR  
(Asst. Prof. Dr. Nattaya Lourith)

.....EXTERNAL EXAMINER  
(Asst. Prof. Dr. Sirivan Athikomkulchai)

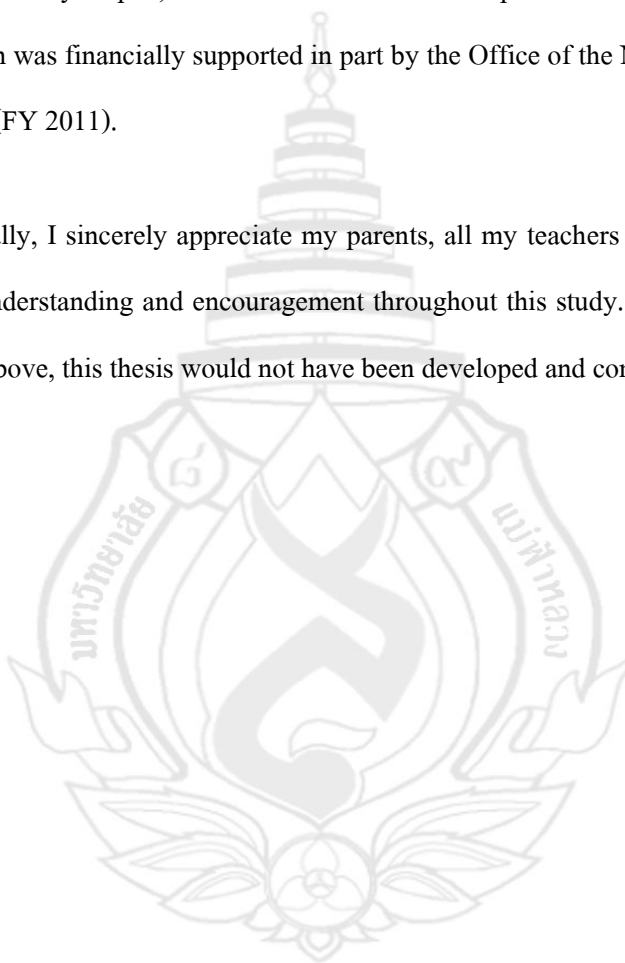
©COPYRIGHT BY MAE FAH LUANG UNIVERSITY

## ACKNOWLEDGEMENTS

I was very grateful to Asst. Prof. Dr. Nattaya Lourith who has encouraged this study. She has intensively helped, led and advised me to solve problems and to complete this thesis. This research was financially supported in part by the Office of the National Research Council of Thailand (FY 2011).

Finally, I sincerely appreciate my parents, all my teachers and friends for their love, tolerance, understanding and encouragement throughout this study. Without all these persons mentioned above, this thesis would not have been developed and completed.

Siriluk Pongpunyayuen



<b>Thesis Title</b>	Cosmetics from Rambutan peels extracts
<b>Author</b>	Siriluk Pongpunyayuen
<b>Degree</b>	Master of Science (Cosmetic Science)
<b>Advisor</b>	Asst. Prof. Dr. Nattaya Lourith

## ABSTRACT

*Nephelium lappaceum* Linn. peels were macerated in 70% EtOH (5.556 %w/w) and partitioned with *n*-hexane and EtOAc, respectively. Extractive yield was found highest in Aq. (5.556 %w/w) extract, followed by EtOAc (0.705 %w/w) and *n*-hexane extracts (0.071 %w/w), respectively. The extracts were evaluated on ABTS<sup>++</sup> scavenging and antityrosinase activities. Total phenolic content was determined by Folin Ciocalteu method. HPLC was used for quantification of phenolics in extracts. The EtOAc extract was the most potent antioxidant extract with an IC<sub>50</sub> of 2.915 ± 0.022 ppm, which was significantly better than ascorbic acid (IC<sub>50</sub> = 6.288 ± 0.098). In addition, the EtOAc extract posed the strongest tyrosinase inhibitory effect (89.010 ± 0.420 %). Therefore, it was evaluated on IC<sub>50</sub> (430.838 ± 0.568 ppm). However, it was less active than kojic acid (IC<sub>50</sub> = 38.984 ± 0.514 ppm). Total phenolic content was found highest in the EtOAc extract (45.500 ± 0.866 g GAE/ 100 g crude extract). Total phenolic content was related with antioxidant ( $r = 0.955$ ) and antityrosinase activities ( $r = 0.844$ ). The EtOAc extract was non-cytotoxic in Vero cells at 50 ppm. HPLC analysis found ferulic acid (3.235 ± 0.023 g/ kg), gallic acid (2.434 ± 0.044 g/ kg), rosmarinic acid (1.743 ± 0.151g/ kg), caffeic acid (1.267 ± 0.218 g/ kg), kojic acid (0.932 ± 0.023 g/ kg), chlorogenic acid (0.388 ± 0.032 g/ kg) and quercetin (0.885 ± 0.156 g/ kg) highest in the EtOAc extract. Therefore, the EtOAc extract was further

incorporated into a stable base emulsion (0.005% w/w). The formulation was physically and chemically stabled following accelerated tests and long term storage at different temperatures for 6 months.

**Keywords:** Rambutan/Antioxidant/Antityrosinase/Phenolic/Anti–wrinkle cosmetic



## TABLE OF CONTENTS

	<b>Page</b>
<b>ACKNOWLEDGEMENTS</b>	<b>(3)</b>
<b>ABSTRACT</b>	<b>(4)</b>
<b>LIST OF TABLES</b>	<b>(8)</b>
<b>LIST OF FIGURES</b>	<b>(9)</b>
<b>ABBREVIATIONS AND SYMBOLS</b>	<b>(11)</b>
 <b>CHAPTER</b>	
<b>1 INTRODUCTION</b>	<b>1</b>
1.1 Background of the study	1
1.2 Objective of the study	2
1.3 Scope of the study	3
1.4 Significances of the study	3
 <b>2 LITERATURE REVIEW</b>	 <b>4</b>
2.1 Skin structure	4
2.2 Skin ageing and skin wrinkle	6
2.3 Skin color	9
2.4 Free radical	12
2.5 Antioxidant	14
2.6 Phenolic compounds	16
2.7 Emulsion	19
2.8 Stability test	23
2.9 Rambutan	24

## TABLE OF CONTENTS (continued)

	Page
<b>CHAPTER</b>	
<b>3 MATERIAL AND METHODS</b>	<b>27</b>
3.1 Chemicals and reagents	27
3.2 Equipments	28
3.3 Methodology	29
<b>4 RESULTS AND DISCUSSION</b>	<b>35</b>
4.1 Sample preparation and extraction	35
4.2 Antioxidant and antityrosinase activities	36
4.3 Total phenolic content	38
4.4 Quantification of phenolic compounds by HPLC	40
4.5 Cytotoxicity	42
4.6 Correlation between biological activities, total phenolic content and actives	43
4.7 Fundamental properties of Rambutan peels extracts	44
4.8 Preparation of emulsion	44
4.9 Incorporation of Rambutan peels extract in the emulsion	46
<b>5 CONCLUSION</b>	<b>49</b>
<b>REFERENCE</b>	<b>50</b>
<b>CURRICULUM VITAE</b>	<b>57</b>



## LIST OF TABLES

Table	Page
2.1 Classes of Phenolic Compounds in Plants	17
3.1 Mobile Phase System	32
3.2 Formulation of Cosmetic Base	34
4.1 Proportion and Extractive Yield of Rambutan Peels Extracts	36
4.2 ABTS Scavenging Activity ( $IC_{50}$ ) of Rambutan Peels Extracts	37
4.3 Phenolic Compounds in Rambutan Peels Extracts	42
4.4 Physical Evaluation of Cosmetic Emulsion	46
4.5 Physical Stability of Rambutan Peels Emulsion under Long Time Storages	47

## LIST OF FIGURES

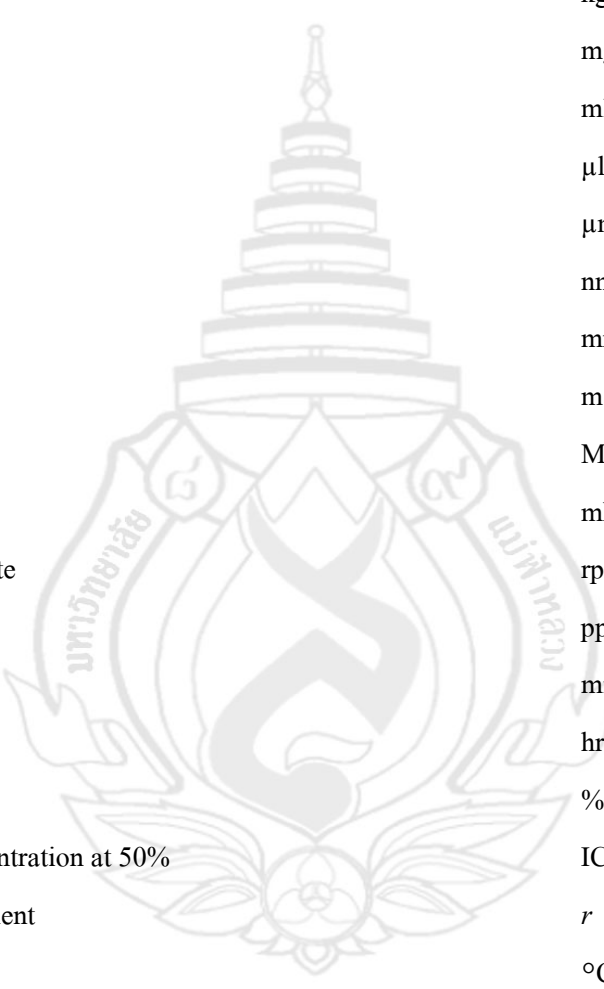
Figure	Page
2.1 Structure of Skin	5
2.2 Photo Ageing	7
2.3 Types of Wrinkles	8
2.4 Melanogenesis Pathway	11
2.5 Example of Hydrobenzoic Acid	18
2.6 Examples Hydroxycinnamic Acid	18
2.7 Generic Structure of a Flavonoid Molecule	19
2.8 Generic Structure of Major Classes of Flavonoids	21
2.9 Type of Emulsions	22
2.10 Structure of Geraniin (a), Ellagic acid (b), Coliragin (c)	26
3.1 Rambutan Peels Extraction	30
4.1 ABTS <sup>+</sup> Scavenging Activity of Ascorbic Acid and Rambutan Peels Extracts	37
4.2 Antityrosinase Activity of Rambutan Peels Extracts	38
4.3 Phenolic Content of Each Rambutan Peels Extracts	39
4.4 Correlation between Antioxidant Activity and Total Phenolic Content of Rambutan Peels Extracts	39
4.5 Correlation between Total Phenolic Content and Antityrosinase Activity and between Antioxidant and Antityrosinase Activities	40
4.6 HPLC Chromatogram of Phenolics and Rambutan Peels, EtOAc Extract, 70% EtOH Extract and Aq. Extract	41
4.7 Correlation between Actives and Antioxidant (a), Antityrosinase Activities (b), and Total Phenolic Content	45

## LIST OF FIGURES ( continued)

Figure	Page
4.8 Physical Stability of Rambutan Peels Extract in Emulsion Evaluated in Acceralated Test	47
4.9 Physical Stability of Rambutan Peels Emulsion	
4.10 Chemical Stability of Rambutan Peels Emulsion in Terms of Antioxidant Activity and Total Phenolic Content	48



## ABBREVIATIONS AND SYMBOLS



Gram	g
Kilogram	kg
Milligram	mg
Milliliter	ml
Microliter	$\mu$ l
Micrometer	$\mu$ m
Nanometer	nm
Milimeter	mm
Meter	m
Molar	M
Milimolar	mM
Round per minute	rpm
Part per million	ppm
Minute	min
Hour	hr
Percentage	%
Inhibition concentration at 50%	IC <sub>50</sub>
Relation coefficient	<i>r</i>
Degree Celsius	°C
Centipoints	cPs
Gallic acid equivalent	GAE
Butyl hydroxyl toluene	BHT
2,2'-Azino-bis-3-ethylbenzthiazoline-6-sulphonic acid	ABTS
1,1-Diphenyl-2-picrylhydrazyl	DPPH

## ABBREVIATIONS AND SYMBOLS (continued)

Sodium dihydrogen phosphate	$\text{NaH}_2\text{PO}_4 \cdot \text{H}_2\text{O}$
Disodium hydrogen phosphate	$\text{Na}_2\text{HPO}_4$
Sodium carbonate	$\text{Na}_2\text{CO}_3$
Ferrous ion	$\text{Fe}^{2+}$
Ferric ion	$\text{Fe}^{3+}$
Trolox equivalent antioxidant capacity	TEAC
Disodium dihydrogenethylenediamine tetra acetic dehydrate	EDTA 2 Na
2,4,6-Tri-2-pyridyl-1,3,5-triazine	TPTZ
Ferric reducing antioxidant power	FRAP
Ethanol	EtOH
Ethyl acetate	EtOAc
Deionized water	DI water
Acetic acid	AcOH
Acetonitrile	AcCN
High-performance liquid chromatography	HPLC
Weight by weight	w/w
Weight by volume	w/v
Aqueous	Aq.
Methanol	MeOH
6-Hydroxy-2,5,7,8-tetramethylchroman-2-carboxylic acid	Trolox

## **CHAPTER 1**

### **INTRODUCTION**

#### **1.1 Background of the study**

Skin is an organ of the body usually and directly exposed to prooxidative environment including ultraviolet radiation (UV) and pollutions. UV radiation stimulate reactive oxygen species (ROS) productions and other free radicals in cellular metabolism; however, free radicals are neutralized by cellular antioxidant defense system to deprive the resulting harmful effect (Darr & Fridovich, 1994). ROS resulting stimulates the synthesis of collagen degrading enzyme. Loss of collagen will lead to wrinkles and ageing of skin (Ajiboye, 2011). Therefore, administration of antioxidant prevents oxidation and scavenges free radicals in the body, and applications of antioxidants were widely applicable (Berger, 2005). At present, popular of botanical cosmetics are increasingly and largely accepted because all most consumers are concerning on safety of natural cosmetics largely free from adverse effect (Lupo, 2001). Botanical antioxidants comprehensively used in cosmetics are contributed by phenolic compounds as active ingredient. Rich source of antioxidant and phenolics have been exhaustively investigated in agriculture waste. Research apply for value added up agriculture waste into cosmetic products were reported in Tamarind and Mangosteen (Nattaya Lourith, Mayuree Kanlayavattanakul & Setinee Chanpirom, 2009; Hunt, Shaokang & Ernst, 2010).

Rambutan is an economic fruit of Thailand. Large quantity of waste for instance seeds and peels from processing and consumptions are increasing in turn every year. Therefore, this fruit residue is encored to be transform into value added up material. Rambutan

peels methanolic extract showed antioxidant activity ( $IC_{50}$  0.46  $\mu$ g/ml) by lipid peroxidation assay (Nont Thitilerdecha, Apiwat Teerawutgulrag & Nuansri Rakariyatham, 2008). This fraction was chromatographed presenting ellagic acid, corilagin and geraniin (Nont Titilerdacha & Nuansri

Rakariyatham, 2011). Rambutan 95% ethanol peels extract scavenged  $ABTS^{++}$  and non-cytotoxic as evaluated in Caco-2 cells. (Siriporn Okonogi, Chadarat Duangrat, Songyot Anuchpreeda, Suganya Tachakittirungrod, & Sombat Chowwanapoonpohn, 2007) Therefore, Rambutan peels are potentially to be applied in healthcare products including cosmetics. However, some of biological activity relevant to cosmetics and phenolic constituents are rarely reported.

Thus, this study subjectively evaluates the biological activity of Rambutan peels extracts prepared by a modified extraction method to archive greater activities and explored more actives. The great potential extract was confirmed on its safety in Vero cells. Total phenolic content and characterization of phenolics in Rambutan peels s were determined and correlated with biological activities. This, will be feasible for quality control and the economy standardization of Rambutan peels extracts. Furthermore, the formulated cosmetics containing Rambutan peels extract was evaluated in terms of physical and chemical stabilities.

## 1.2 Objectives of the study

- 1.2.1 To prepare active principle of the Rambutan peels extracts
- 1.2.2 To study on antioxidant and antityrosinase activities of Rambutan peels extracts
- 1.2.3 To evaluate the extracts' safety in Vero cells
- 1.2.4 To determine total phenolic contents in Rambutan peels extracts
- 1.2.5 To characterize and quantify phenolics in Rambutan peels extracts
- 1.2.6 To correlate biological activities, total phenolic content and actives in Rambutan peels extracts
- 1.2.7 To study on the fundamental properties of Rambutan peels extracts
- 1.2.8 To formulate emulsion containing Rambutan peels extract
- 1.2.9 To evaluate physical and chemical stabilities of the developed formulation

### **1.3 Scope of the study**

1.3.1 Literature reviews

1.3.2 Preparation of biological activity extract from Rambutan peels by maceration and liquid – liquid extractions

1.3.3 Assessment of antioxidant and antityrosinase activities

1.3.4 Safety evaluation in Vero cells

1.3.5 Total phenolic content determination

1.3.6 Characterization of phenolics by HPLC

1.3.7 Study on fundamental properties of Rambutan peels extracts

1.3.8 Cosmetic formulation (emulsion) and physical properties evaluation

1.3.9 Physical and chemical stabilities evaluation of the formulation

### **1.4 Significances of the study**

1.4.1 Biological activities relevant to cosmetics of a safe Rambutan peels extracts

1.4.2 The concise and practical extraction method meeting economic feasibility of Rambutan peels extract in industrial aspects

1.4.3 Accurate and concise standardization of Rambutan peels extracts is offered

1.4.4 Fundamental properties of Rambutan peels extract for healthcare product applications including cosmetics

1.4.5 Stable cosmetic formulation containing Rambutan peels extract

1.4.6 Value added up of Rambutan and the fruit residues

1.4.7 Novel safe and efficient ecological friendly cosmetic raw material



## **CHAPTER 2**

### **LITERATURE REVIEWS**

#### **2.1 Skin structure**

The skin is the body's largest organ. It has many functions, including regulating body temperature, maintaining water, electrolytes balance and sensing painful. Skin is composed of three layers; epidermis, dermis and subcutaneous tissue (Jouni, 1979) as shown in Figure 2.1. Each layer presents specific characteristics and functions as followings;

##### **2.1.1 Epidermis**

It is the most superficial layer of the skin. The epidermis composes of three main types of cells; the keratinocytes which made the protein keratin, the melanocytes which produces the pigment melanin and the Langerhans cells which are part of the immune system and intercept foreign substances those try to pass though the skin. Epidermis is divided to 5 layers. Stratum basale is the deepest layer of epidermis and has a single layer of keratinocytes, it also known as stratum germinativum. Stratum spinosum is superficial to the stratum basale. It provides both strength and flexibility to the skin. This layer consists of 8-10 layers of keratinocytes. Stratum granulosum consists of protein keratin. It consists of 3-5 layers of flattened keratinocytes. Keratinocytes are membrane enclosed lamellar granules which release lipid rich secretion. The secretion fills the space between cells of stratum granulosum, stratum lucidum and stratum corneum. They act as a water repellent sealant that helps retard loss of body fluids and entry of foreign materials. Stratum lucidum is present only areas in thick skin. It consists of large amount of keratin and thickened plasma membrane. And stratum corneum consists of dead keratinocyte cells. These are continuously shed and replaced by cells from the deeper strata. This layer consists

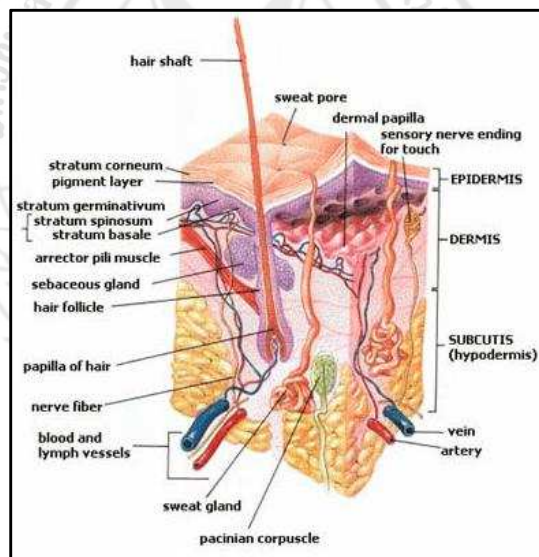
of mostly keratin and lipid secretions from lamellar granules which make this layer an effective water repellent barrier.

### 2.1.2 Dermis

It is composed mainly of connective tissues containing collagen and elastin. Collagen is a primary structural component of the dermis and the most abundant protein found in humans. It is responsible for conferring the strength and support to human skin. Elastin is a protein in the connective tissue that is elastin and allows many tissues in the body to resume their shape after stretching or contraction. It helps the skin to return to its original position when it is pinched or poked.

### 2.1.3 Subcutaneous

It is the deepest layer of the skin. It locates beneath the dermis. The subcutaneous is composed mostly of fat that is an important energy source for the body.



**From** Jouni, U. (1979). Biochemistry of the Elastic fibers in Normal Connective Tissues and its Alterations in Diseases. **Journal of Investigative Dermatology**, 72(1), 1-10.

**Figure 2.1** Structure of Skin

## 2.2 Skin ageing and skin wrinkle

The ageing process is noticeable within all organs of the body and manifests itself visibly in the skin. Ageing is the result of free radical damage that irradiation of living thing know to induced the formation of free radicals shortened their life span and produced changes the resembled ageing. Since, free radicals were also known to be a natural by-product of aerobic metabolism (2-3% of oxygen consumed by a cell is converted into free radicals). Ageing and age-related disease might be due to the long term effects of oxidative damage which, in turn, is modifiable by genetic and environmental factors. Since then, support for the involvement of free radicals in ageing has increased progressively and become plausible one of the more the ageing process. Free radical activity has also been shown to oxidize and cross-link protein including enzymes and connective tissue. In particular, the amino acid residues of protein are highly susceptible to oxidative attack and it has been shown that there is a progressive increase in form of damage in cells and tissues of the body as a function of age. Indeed, oxidized protein in an old animal may represent 30-50% of the total cellular protein and is slowly the catalytic activity of many enzymes decreases with ages. The reaction of an oxygen radical with DNA can knock out a cause breakage, with the potential to produce a harmful (Wickens, 2001).

Chronologically, aged skin is thin, relatively flattened, dry and unblemished, with some loss of elasticity and age-related loss of architectural regularity. The extracellular matrix is reflected by a decrease in the number of fibroblasts. Reduced levels of collagen and elastin, with impaired organization are primarily because of decreased protein synthesis affecting types I and III collagen in the dermis, with an increased breakdown of extracellular matrix proteins. Oxidative stress is considered of primary importance in driving the ageing process. The original free radical theory of ageing purported that the molecular basis of ageing was derived from a lifetime accumulation of oxidative damage to cells resulting from ROS produced as a consequence of aerobic metabolism. ROS is generated the oxidative cellular metabolism including superoxide and hydroxyl radicals and other activated forms of oxygen such as hydrogen peroxide and singlet oxygen. The primary of productions of ROS is the mitochondria and other major sources of ROS include phagocytosis, non-enzymatic reactions of oxygen and ionizing

radiation etc. Skin ageing is influenced by several factors including genetic and environmental exposure (Callaghan & Wilhelm, 2008).



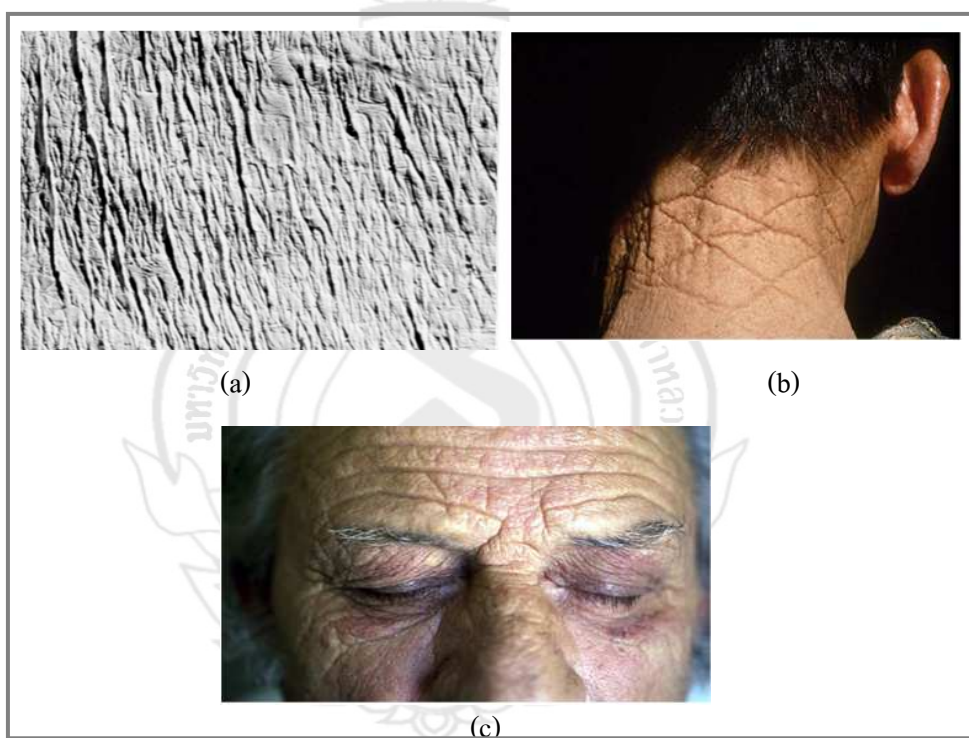
**From** Gonderdi, X. (2008). Photoageing. Retrieved January 10, 2012, from <http://www.xprodosit.com/yazi/photo-ageing-nedir>

**Figure 2.2** Photo Aging

Photoageing and chronological skin ageing have been considered distinct entities. Although the typical appearance of photo-aged and chronologically aged human skin can be readily distinguished, recent evidence indicates that chronologically aged and UV radiated skin share important molecular features including altered signal transduction pathways that promote matrix-metalloproteinase (MMP) expression, decreased pro-collagen synthesis and connective tissue damage. Oxidative stress is central role in initiating the signalling events that lead to cellular response following UV radiation. UV radiation of skin increases hydrogen peroxides and other ROS production and decreases anti-oxidant enzymes. These features are also observed in

chronologically aged human skin. In both cases, increased ROS production alters gene and protein structure and function leading to skin damage as shown in Figure 2.2 (Callaghan and Wilhelm, 2008).

Wrinkles are an obvious and important indicator of ageing. The wrinkles of ageing are classified into three morphological types. Crinkles are a very fine micro-wrinkle of the skin surface in aged skin, fine elastic fibers that keep the epidermis tight with the dermis (Figure 2.3a). Glyphic wrinkles appear on skin area with elastin degeneration caused by UV radiation (Figure 2.3b). Linear facial wrinkles are the first to appear at the site of expression lines and deepest wrinkles of ageing skin (Figure 2.3c) (Hatzis, 2004).



**From** Hatzis, J. (2004). The wrinkle and its measurement-A skin surface profilometric method. **Micron**, 35(1), 201-209.

**Figure 2.3** Types of Wrinkles: Crinkle (a), Glyphic Wrinkle (b) and Linear Facial Wrinkle (c)

## 2.3 Skin color

Human skin color stems from in the outermost layer of the skin, the epidermis where the pigment-producing cells melanocytes are localized to produce melanin. Upon exposure of the skin to UV radiation, melanogenesis is enhanced by the activation of the key enzyme of melanogenesis, tyrosinase is a glycoprotein located in the membrane of the melanosome, a vesicle inside the melanocyte. Melanogenesis occurs in the melanosome. Two types of melanin are synthesized eumelanin and pheomelanin. Eumelanin is a dark brown-black insoluble, whereas pheomelanin is light red yellow sulphur-containing soluble polymer (Kongshoj, Thorleifsson & Wulf, 2006).

Melanogenesis pathway as shown in Figure 2.4, the concentration of *L*-tyrosine depends on the conversion of the *L*-phenylalanine by intracellular phenylalanine hydroxylase (PAH) and in contrast to *L*-tyrosine. Tyrosinase catalyses the first two steps of melanin production, the hydroxylation of *L*-tyrosine to *L*-dihydroxyphenylalanine (*L*-DOPA) and the subsequent oxidation of this *o*-diphenol to the corresponding quinone, *L*-dopaquinone. Following the formation of *L*-dopaquinone was converted to dopachrome. In the eumelanin pathway, dopachrome is either spontaneously converted to 5, 6-dihydroxyindole or converted to 5, 6-dihydroxyindole-2-carboxylic acid by dopachrome tautomerase (DCT), also referred to as tyrosine-related protein-2 (TRP-2). There are two tyrosinase-related proteins, TRP-1 and TRP-2, which are structurally related to tyrosinase and share approximately 40% amino acid. The polymerization of indoles and quinones leads to eumelanin formation. The pheomelanin pathway, at the *L*-dopaquinone depends on the presence of cysteine which is actively transported through the melanosome. Cysteine reacts with *L*-dopaquinone to form cysteinyl-dopa, then converted to quinoleimine, alanine-hydroxyl dihydrobenzothiazine and polymerized to pheomelanin production (Gillbro & Olsson, 2011).

Tyrosinase inhibitors from both natural and synthetic source have been identified. Many putative inhibitors are examined in the presence of tyrosine or dopa as the enzyme substrate, and activity is assessed in terms of dopachrome formation. Thus, the inhibition of tyrosinase activity can be accomplished by following;

Reducing agents causing chemical reduction of *L*-dopaquinone, was used a melanogenesis inhibitor because of its capacity to reduce back *o*-dopaquinone to dopa thus, avoiding dopachrome and melanin formations.

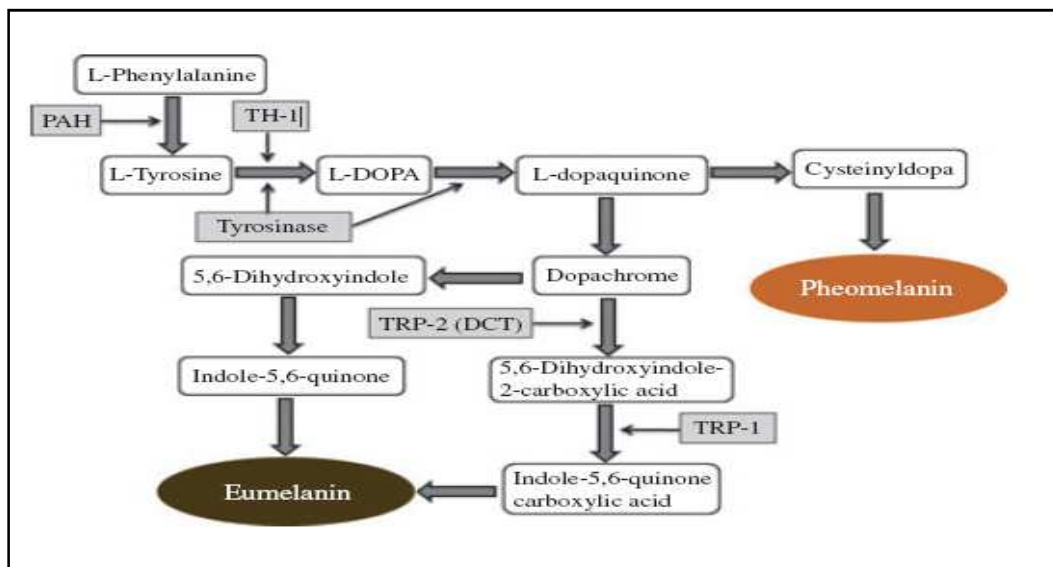
*o*-Dopaquinone scavenger such as most thio-containing compounds, which are well-known melanogenesis inhibitors and react with *L*-dopaquinone to form colorless products. The melanogenetic process is therefore slowed until all the scavenger is consumed, and then it goes at its original rate.

Alternative enzyme substrates such as some phenolic compounds, whose quinoid was reaction products absorb in a spectral range different from that of *L*-dopachrome. When these phenolics show a good affinity for the enzyme, dopachrome formation is prevented, and they could be mistakenly classified as inhibitors.

Nonspecific enzyme was inactivators such as acids or bases, which non-specifically denature the enzyme, thus inhibiting its activity.

Specific tyrosinase inactivators such as mechanism-based inhibitors. These inhibitors can be catalyzed by tyrosinase and form covalent bond with the enzyme, thus irreversibly inactivating the enzyme during catalytic reaction. They inhibited tyrosinase activity by inducing the enzyme catalyzing (Chang, 2009).

However, the skin color is determines by number of factors, the most important of that is amount and distribution of melanin pigmentation. In fact, melanin is protected the skin from UV radiation damage by absorbing UV radiation whereas, overexpose to UV radiation can lead to increase in melanogenesis (Gillbro & Olsson, 2011). Abnormal melanin pigmentation is derived from the accumulation of an excessive amount of melanin in epidermis including dark spots and freckles that are serious esthetic problem in human beings suppressing self's confidence. Therefore, a number of whitening agents have been developed for cases of undesirable skin.



**From** Gillbro, J. & Olsson, M. (2011). The melanogenesis and mechanism of skin-lightening agents – existing and new approaches. **International Journal of Cosmetic Science**, 33(3), 1-16.

**Figure 2.4** Melanogenesis Pathway

Now a day, there are many known substances that can reduce the level of melanin pigmentation in the skin. There are also substance known to have an effect on the transfer of melanin from melanocytes to keratinocytes in epidermis, leading to an overall lighter skin color such as nicotinamide and soybean. Many of the actives have a tyrosinase-inhibiting effect leading to reduce total melanin production, for examples kojic acid, arbutin, quercetin and epigallocatechin. These actives inhibited tyrosinase activity by their ability to chelate the copper in the active site on the melanogenesis (Kim & Uyama, 2005).



## 2.4 Free radical

Free radicals are a byproduct of normal cell function. When cells create energy, they also produce unstable oxygen molecules. These molecules, called free radicals, have a free electron. This electron makes the molecule highly unstable. The free radical bonds to other molecules in the body causing proteins and other essential molecules to not function as they should. However, antioxidants can minimize free radical damage. There are many types of radicals but the most important free radicals in the body are the radical derivatives of oxygen better known ROS (Halliwell, 2009; Wickens, 2001; Scgeibmeria et al., 2005).

Individual species of ROS are as followings;

### 2.4.1 Superoxide anion ( $\text{O}_2^-$ )

The superoxide free radical anion is formed when oxygen is reduced by the transfer of a single electron to its outer shells. The major source of superoxide in vivo is the electron leakage that results from the electron transfer chain of the mitochondria. However, the superoxide radical anion appears to play a central role as other reactive intermediates are formed from it. Its main significance lies in its being a main source for the generation of hydrogen peroxide and as a reductant of transition metals, which are precursors to the formation of the lethal hydroxyl radical.

### 2.4.2 Hydroxyl radical ( $\text{OH}^\bullet$ )

The hydroxyl radical is an extremely reactive oxidising radical that will react to most biomolecules at diffusion controlled rates, which means that reactions will occur immediately with biomolecules. The hydroxyl free radical is important in radiobiological damage and is several orders of magnitude more reactive towards cellular constituents than superoxide radicals (and many orders more reactive than hydrogen peroxide).

### 2.4.3 Hydrogen peroxide ( $\text{H}_2\text{O}_2$ )

Hydrogen peroxide is not a free radical but falls in the category of reactive oxygen species. It is an oxidizing agent that is not particularly reactive but its main significance lies in that it is the main source of hydroxyl radicals in the presence of transition metal ions. It is also

involved in the production of HOCl by neutrophils. Hydrogen peroxide can be generated from the two electron reduction of oxygen. In biological systems hydrogen peroxide is generated by the production of superoxide: two superoxide molecules can react together to form hydrogen peroxide and oxygen.

#### **2.4.4 Nitric oxide (·NO)**

It is a common gaseous free radical. It is now recognized to play a role in vascular physiology and is also known as endothelium derived relaxing factor. Vascular endothelium produces nitric oxide, as do neutrophils and macrophages from arginine using the enzyme nitric oxide synthetase. This event can be stimulated by cytokines, tumour necrosis factor, or interleukins. Inhibition of production is known to reduce microbicidal and tumouricidal activities of macrophages.

#### **2.4.5 Hypochlorous acid (HOCl)**

Hypochlorous acid can cross cell membranes and, in the presence of transitional metal ions, generate hydroxyl radicals. Highly reactive hydroxyl radicals can be formed from HOCl/OCl<sup>-</sup> on reaction with reductants that are one-electron donors. HOCl has been shown to be capable of initiating lipid peroxidation, combining with H<sub>2</sub>O<sub>2</sub> to damage DNA and DNA repair processes and altering intracellular free Ca<sup>2+</sup> and pH. It may contribute to tissue damage during the inflammatory process.

#### **2.4.6 Ozone (O<sub>3</sub>)**

This natural compound present in the higher atmosphere and in the lower atmosphere of our polluted cities is a major pollutant formed by photochemical reactions between hydrocarbons and nitrogen oxides. Ozone is not a free radical but, as singlet oxygen, may produce them, stimulates lipid peroxidation and thus induces damages at the lipid and protein levels *in vivo* mainly in airways. The exact chemistry of ozone-mediated stimulation of peroxidation is not entirely known. Ozone may add on across a double bond and decomposes to form a free radical.

### 2.4.7 Thiyl radicals (RS<sup>•</sup>)

The thiolate specie is one of the most reactive functional groups found in proteins. It can react as a nucleophile and attack a disulfide bond. In the absence of oxygen, a thiyl radical was shown to induced cis/trans-isomerization of linoleic acid and led to several isomers.

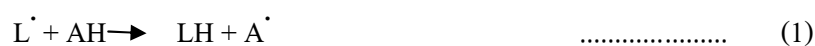
### 2.4.8 Carbon centered radicals (O<sub>2</sub>CCl<sub>3</sub>)

The formation of these reactive free radical is observed in cells treated with CCl<sub>4</sub>. The action of the cytochrome P450 system generates the trichloromethyl radical (•CCl<sub>3</sub>) which is able to react with oxygen to give several peroxy radicals such as O<sub>2</sub>CCl<sub>3</sub>.

However free radicals damage living cells causing lipid protein, DNA as well as noncellular element such as lost of amount of collagen and elastin in ageing of skin.

## 2.5 Antioxidant

An antioxidant may be defined as any substance that when present at low concentrations, compared with those of the oxidizable substrate, significantly delays or inhibits oxidation of that substrate'. For convenience, antioxidants have been traditionally divided into two classes, primary or chain breaking antioxidants and secondary or preventative antioxidants. Secondary or preventative antioxidants are compounds that retard the rate of oxidation (Antolovich, Prenzler, Patsalides, McDonald & Robard, 2002; Miller, Rigehof, Prakash & Kanter, 2000; Muller, Frohlich & Bolm, 2011). This may be achieved in a number of ways including removal of substrate or singlet oxygen quenching. Primary antioxidants, AH, when present in trace amounts, may either delay or inhibit the initiation step by reacting with a lipid radical or inhibit the propagation step by reacting with peroxy or alkoxyl radicals:



The antioxidant free radical may further interfere with chain propagation reactions by forming peroxy antioxidant compounds:



The activation energy of the above reactions increases with increasing A–H and L–H bond dissociation energy. Therefore, the efficiency of the antioxidant increases with decreasing A–H bond strength. Chain-breaking antioxidants may occur naturally maybe produced synthetically as ascorbic acid and BHT, natural antioxidant has been promoted.

Strategies have been develop for measuring the antioxidant activity as the ability to scavenge free radicals generated in Aq. and lipophilic phase.

### 2.5.1 ABTS scavenging assay

ABTS assay, the procedure based on inhibition of the production of the  $ABTS^{++}$ . The accumulation of  $ABTS^{++}$  can be inhibited by presence of an antioxidant in the reaction, to an extent dependent on the antioxidant in the reaction. The relative ability of hydrogen donating antioxidant to scavenge  $ABTS^{++}$  generated which can be measured spectrophotometrically, by 750 nm. Antioxidant direct reduction of the  $ABTS^{++}$  very similar establishing that the action of antioxidant activity was scavenging of the  $ABTS^{++}$  and not by inhibition of its formation through reduction of reaction with hydrogen peroxide (Miller & Rice-Evans, 1997). Results were express by comparison with standard amounts of Trolox to give rinsed to the TEAC. The TEAC is equal to the milimolar concentration of a trolox solution whose antioxidant capacity is equivalent to one milligram of the extract. TEAC reflects relative ability of hydrogen or electron-donating antioxidant to scavenge the  $ABTS^{++}$  compared with the Trolox.

### 2.5.2 DPPH scavenging assay

A method has been developed to determine the antioxidant activity of material utilizes the stable  $DPPH^{\bullet}$ . Higher free radical scavenging ability indicate a greater capacity for neutralizing free radicals which is expected to reduce or destroy ROS and help prevent or slow the visible signs of ageing. The odd electron in the DPPH free radical gives a strong absorption

maximum at 517 nm and is purple in color. The color turns from purple to yellow as the molar absorptivity of the DPPH radical at 517 nm reduces when the odd electron of DPPH radical becomes paired with a DPPH-H. Result was reported as the  $IC_{50}$  that is the concentration sample that cause 50% inhibition of DPPH radical.

### 2.5.3 FRAP assay

The method is based on the reduction of a ferroin analog, the  $Fe^{3+}$  complex of tripyridyltriazine Fe (TPTZ)<sup>3+</sup>, to the intensely blue coloured  $Fe^{2+}$  complex  $Fe - (TPTZ)^{2+}$  by antioxidants in acidic medium. Results are obtained as absorbance increases at 595 nm and can be expressed as micromolar  $Fe^{2+}$  equivalents or relative to an antioxidant standard.

## 2.6 Phenolic compounds

Phenolic compounds are secondary metabolites. These compounds, one of the most widely occurring groups of photochemical, are of considerable physiological and morphological importance in plants. Phenolic compounds play an important role in growth and reproduction, providing protection against pathogens and predators, besides contributing towards the color and sensory characteristics of fruits and vegetables. The beneficial effects derived from phenolic compounds have been attributed to their antioxidant activity. Phenolic compounds could be a natural source of antioxidants (Rice-Evans, Miller & Paganga, 1996; Soobtattee, Neeragheen, Luximon-Rama, Aruoma & Bahorum, 2005; Kroon & Willamson, 1999).

### 2.6.1 Chemistry of phenolic compound

Structurally, phenolic compounds comprise an aromatic ring, bearing one or more hydroxyl substituents, and range from simple phenolic molecules to highly polymerized compounds. Despite this structural diversity, the groups of compounds are often referred to as 'polyphenols'. Most naturally occurring phenolic compounds are present as conjugates with mono- and polysaccharides, linked to one or more of the phenolic groups, and may also occur as functional derivatives such as esters and methyl esters. Though such structural diversity results in

the wide range of phenolic compounds that occur in nature, phenolic compounds can basically be categorized into several classes as shown in Table 2.1.

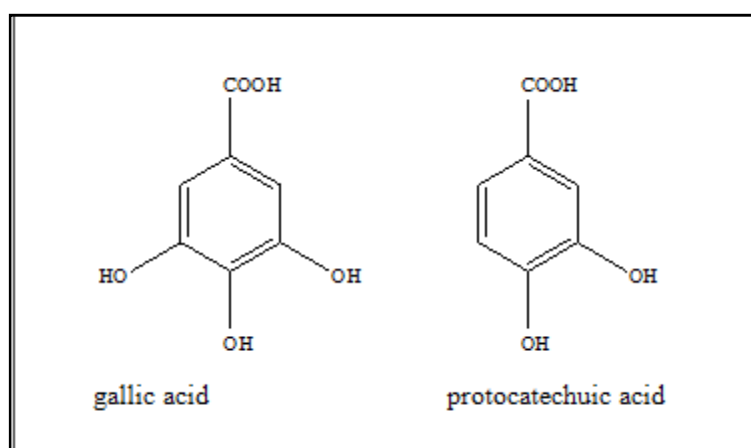
**Table 2.1** Classes of Phenolic Compounds in Plants

Class	Structure
Simple phenolics, benzoquinones	$C_6$
Hydroxybenzoic acids	$C_6-C_1$
Acetophenones, phenylacetic acids	$C_6-C_2$
Hydroxycinnamic acids, phenylpropanoids (coumarins, isocoumarins, chromones, chromenes)	$C_6-C_3$
Naphthoquinones	$C_6-C_4$
Xanthenes	$C_6-C_1-C_6$
Stilbenes, anthraquinones	$C_6-C_2-C_6$
Flavonoids, isoflavonoids	$C_6-C_3-C_6$
Lignans, neolignans	$(C_6-C_3)_2$
Bioflavonoids	$(C_6-C_3-C_6)_2$
Lignins	$(C_6-C_3)_n$
Condensed tannins (proanthocyanidins or flavanols)	$(C_6-C_3-C_6)_n$

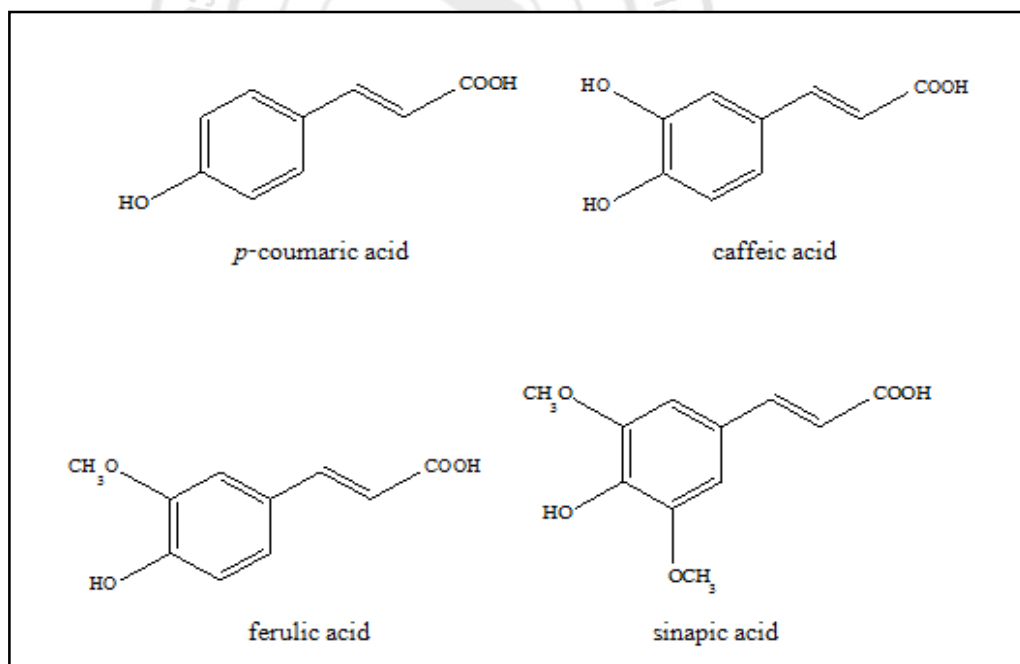
Phenolic acids consist of two subgroups, i.e., the hydroxybenzoic (Figure 2.5) and hydroxycinnamic acids (Figure 2.6). Hydroxybenzoic acids include gallic, *p*-hydroxybenzoic, protocatechuic, vanillic and syringic acids, which in common have the  $C_6-C_1$  structure. Hydroxycinnamic acids, on the other hand, are aromatic compounds with a three-carbon side chain ( $C_6-C_3$ ), with caffeic, ferulic, *p*-coumaric and sinapic acids being the most common.

Determination of total phenolic is used the Folin Ciocalteu reagent, which is the mixture of phosphomolybdate and phosphotungstate used for colorimetric assay of phenolic and polyphenolic antioxidants. It is reduced to a blue-color complex in alkaline solution by phenol. The intensity of the blue color produced is measured with a spectrophotometer at 765 nm. Gallic

acid is an organic acid used as a standard for analysis of the phenol content by the Folin Ciocalteu assay. The total phenolic contents are expressed in grams gallic acid equivalents (GAE) per 100 gram crude extract (Shui & Leong, 2006).

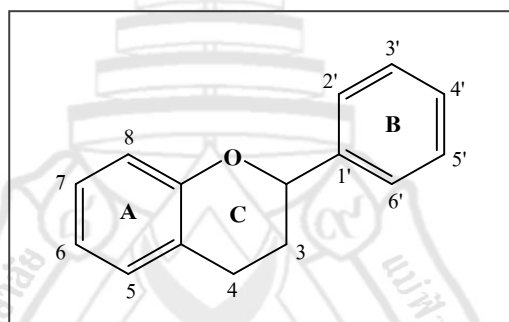


**Figure 2.5** Examples of Hydroxybenzoic Acid



**Figure 2.6** Examples of Hydroxycinnamic Acids

Flavonoids constitute the largest group of plant phenolics, accounting for over half of the eight thousand naturally occurring phenolic compounds. Flavonoids are low molecular weight compounds, consisting of fifteen carbon atoms, arranged in a  $C_6-C_3-C_6$  configuration. Essentially the structure consists of two aromatic rings A and B, joined by a 3-carbon bridge, usually in the form of a heterocyclic ring, C (Figure 2.7). Variations in substitution patterns to ring C result in the major flavonoid classes, i.e., flavonols, flavones, flavanones, flavanols (or catechins), isoflavones, flavanonols, and anthocyanidins (Figure 2.8), of which flavones and flavonols are the most widely occurring and structurally diverse. Substitutions to rings A and B give rise to the different compounds within each class of flavonoids.



**Figure 2.7** Generic Structure of a Flavonoid Molecule

## 2.7 Emulsion

Out of the range of cosmetic product, the emulsion is the form that is probable the most used for reasons; skin feeling, consumer appeal and easy for application. The best known cosmetic products based on cream and lotion (Tadros, 2009).

Emulsion is composed as liquid droplets dispersed in a liquid. The dispersed phase is also called the internal phase, in contrast to the external or continuous phase. If the internal phase, lipophilic (oil) such as vegetable oil and mineral oil dispersed in the external hydrophilic (water) phase, an emulsion of type oil in water (O/W) emulsion. In the other hand, there is water in oil (W/O) emulsion with the hydrophilic phase dispersed in the continuous lipophilic phase (Figure 2.9). Stabilization of emulsion, emulsifiers are required.



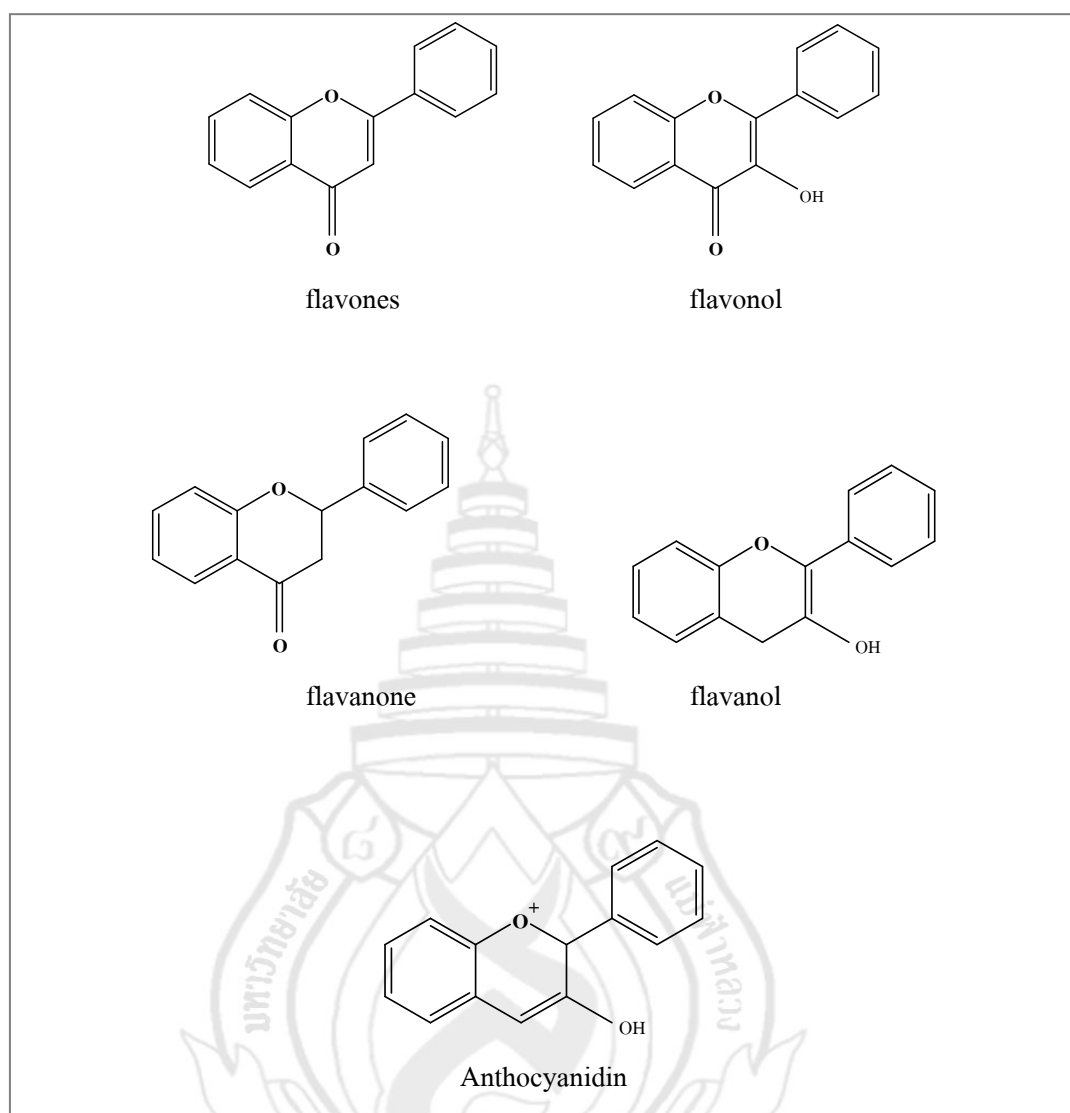
Out of the range of cosmetic product, the emulsion is the form that is probable the most used for reasons; skin feeling, consumer appeal and easy for application. The best known cosmetic products based on cream and lotion.

Emulsion is composed as liquid droplets dispersed in a liquid. The dispersed phase is also called the internal phase, in contrast to the external or continuous phase. If the internal phase, lipophilic (oil) such as vegetable oil and mineral oil dispersed in the external hydrophilic (water) phase, an emulsion of type oil in water (O/W) emulsion. In the other hand, there is water in oil (W/O) emulsion with the hydrophilic phase dispersed in the continuous lipophilic phase (Figure 2.9). Stabilization of emulsion, emulsifiers are required.

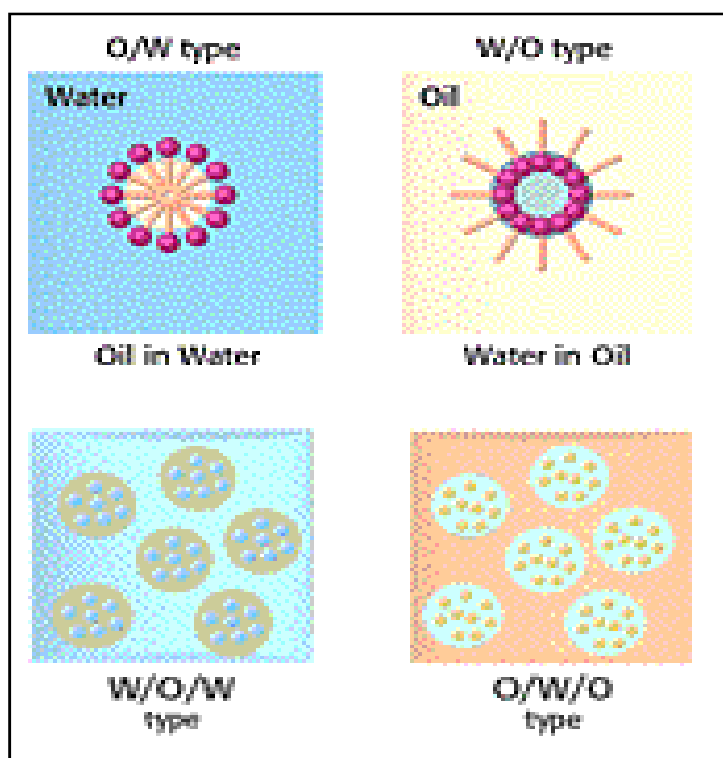
W/O emulsion permits direct contact of skin by the oil phase, giving an immediate occlusive effect and skin little cooling sensation. This type of emulsion is more difficult to produce because the oil phase is continuous and cannot provide the stabilizing properties of an electrical double layer. The end feeling typically produced by this emulsion type is rich and lubricious treatment effect.

O/W emulsion permits cooling of the skin by allowing water evaporating. In this kind of lotion, the initially non-occlusive oil phase slowly coalesces to form a continuous film on the skin. Advantages of emulsion are more stable liquid system, non-oil application, dry end feel for sheer, light-bodied cosmetics effects.

Multiple emulsions are emulsions in which the dispersion phase contains another dispersion phase. Thus, water in oil in water (W/O/W) emulsion is a system in which the globules of water is dispersed in globules of oil and the oil globules are themselves dispersed in water system. A parallel arrangement exists in oil in water in oil (O/W/O) emulsion that internal oil phase is dispersed in water globules, which are themselves dispersed within an external oil phase in Figure 2.9. Advantages of multiple emulsions are the claim sustain release the entrapped active ingredients in the innermost layer and separation of various incompatible ingredients in the formulation.



**Figure 2.8** Generic Structure of Major Classes of Flavonoids



**From** Morante, N. (2011). **Basic Emulsion.** Retrieved June 15, 2011, from [http://www.specialchem4cosmetics.com/services/articles.aspx?id=3875&or=s151357\\_101\\_3875&q=emulsion+](http://www.specialchem4cosmetics.com/services/articles.aspx?id=3875&or=s151357_101_3875&q=emulsion+)

**Figure 2.9** Types of Emulsions

Emulsion represented a mixture of two or more raw materials that are not miscible in each other, it is inherently unstable. The degree and speed of instability are quite variable. Emulsion destabilizing has revealed three processes leading to instability, flocculation, creaming and coalescence.

Flocculation is characterized by a weak, reversible association between droplets of the emulsions' internal phase. Each individual droplet maintained its own identity, thus, there is no change in the basic droplet size. Flocculation represented a less serious sign of instability that can be reversed by shaking very well.

Creaming is particles of emulsion aggregation; there was a tendency for sedimentation. This caused a partial separation of the emulsion into two emulsions, one of which is richer in the internal phase and the other richer in the external phase. It can be reversed by agitation.

Coalescence is an aggregation between two particles can, if the two particles combined, lead to the formation of one larger particle. This process represented a more serious stability. Both of these processes are irreversible and can eventually lead to complete separation of internal and external phase of the emulsion.

## 2.8 Stability test

The purpose of stability testing cosmetic products is to ensure that a new or modified product meets the intended physical, chemical and microbiological quality standards as well as functionality and aesthetics when stored under appropriate conditions. Either conducted in real time or under accelerated conditions, tests should be done in order to assure stability and physical integrity of cosmetic products under appropriate conditions of storage, transport and use, chemical stability, microbiological stability and the compatibility between the bulks and the container (Barel, Paye & Maibach, 2001; Achisi, maccione, Sinico & Valenti, 2001)

Because of the many of cosmetic products and their included complexity, standard stability tests cannot be prescribed, each manufacturer must be adjusted to their activity. However, there are the guidelines in order to assure the stability of products in the market place as follows;

### 2.8.1 General stability tests

Temperature stability tests; the products are tested at different temperature to observe and measure the changes in the properties of the samples with the lapse of time. The temperature, such as  $-10^{\circ}\text{C}$ ,  $-5^{\circ}\text{C}$ ,  $4^{\circ}\text{C}$ ,  $25^{\circ}\text{C}$ ,  $30^{\circ}\text{C}$ ,  $37^{\circ}\text{C}$ ,  $45^{\circ}\text{C}$ , etc., is selected according to store the samples with 1, 2 and 6 months or 1-3 years.

Photo stability tests; the products are tested at different light source such as sunlight, artificial light and fluorescent light to observe and measure the changes in the properties of the samples with the lapse of time.

### 2.8.2 Special accelerated stability tests

Temperature and humidity combination tests: special accelerated testing is performed by combining various temperatures ( $37^{\circ}\text{C}$  -  $50^{\circ}\text{C}$ ) and humidities (75-98%). Cyclical temperature tests; these tests are not conducted at a fixed temperature and humidity. To stimulate the yearly and daily changes in temperature, the test temperature is changed cyclically a number of times each day. Temperature cycling and/or freeze-thaw tests can reveal some types of defects more quickly than can storage at a constant temperature. Freeze-thaw testing should be considered for certain types of products such as suspension problems, instability of emulsions, package design, corrosion of internal of the container (Baby et al., 2007).

Stress test: this test considers the overall stress and time period of actual usage. It predicts the stable lifetime of the product from the physical changes induced by stress over a fixed level. Stress test includes centrifugal separation assay (Rolim et al., 2006) which the product was subjected to centrifuge at 3000 round per minute for 30 min and the separation was measured

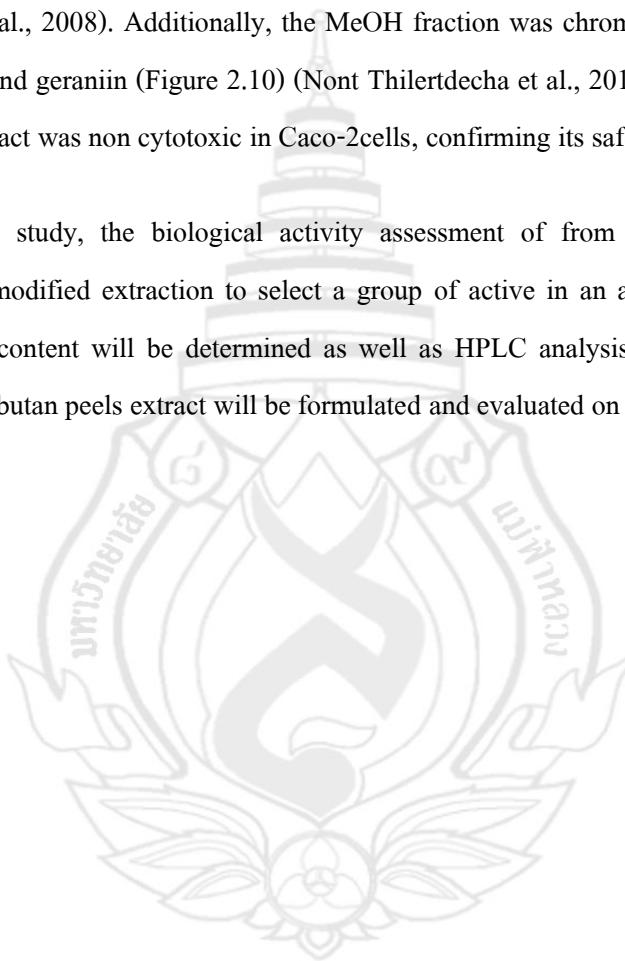
## 2.9 Rambutan

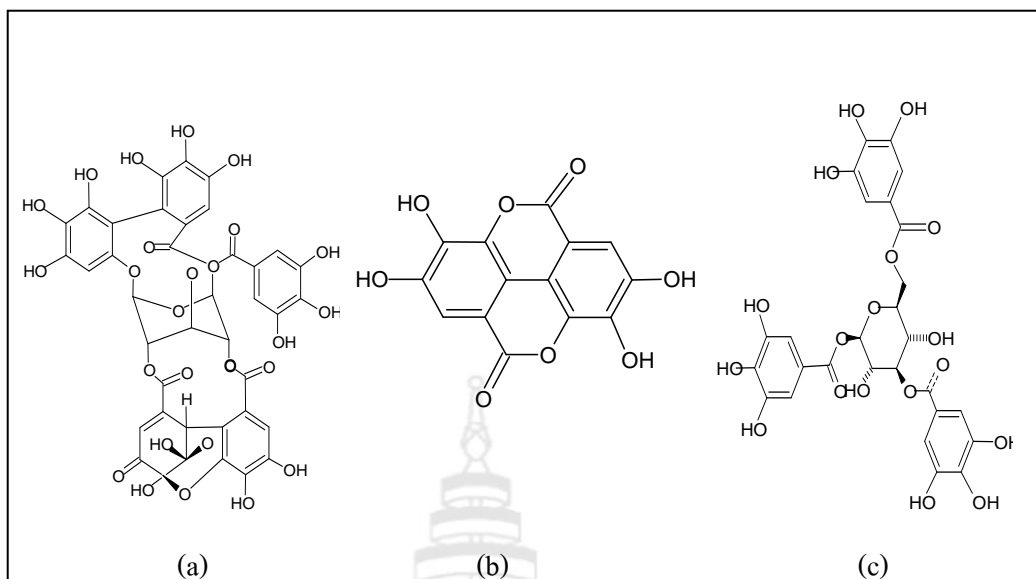
*Naphelium lappaceum* L., known as Rambutan, it is a popular tropical fruit and belonging to Sapindaceae family. Rambutan is widely distributed in South East Asia especially Malaysia, Indonesia and Thailand (Mortan, 1987). In Thailand, two types of Rambutan are Rong-Rien and Si-Chompu. Rong-Rien is popular cultivar because the flavor of the juicy aril is a blend of sweet and sour. Rambutan is an economic fruit which is consumed fresh, canned or processed. The fruit residue discard from the agri-industrial is increasing every to serve a highly demand accordingly (UNESCSP, 2007).

Recently, Rambutan peels were macerated in EtOH and water, respectively and tested on their antioxidant activity. The EtOH extract was shown the greatest activity ( $\text{IC}_{50}$   $1.70 \pm 0.10$  ppm) and it was better activity than ascorbic acid ( $\text{IC}_{50}$   $7.70 \pm 0.10$  ppm) on ABTS scavenging activity. EtOH extract was posed the strongest superoxide scavenging activity ( $41.40 \pm 0.50$  %) (Palanisamy et al., 2008). In addition, Rambutan peels macerated in ether, MeOH and water, respectively and evaluated on their lipid peroxidation inhibitory effect base on ferric

thiocyanated method. The strongest inhibitory was found in MeOH (0.46 ppm), followed by water (0.55 ppm) and ether fractions (0.81 ppm), respectively, which was no significantly potent antioxidant activity with BHT. Furthermore, MeOH fraction was shown the highest inhibited DPPH radical scavenging activity ( $IC_{50}$   $4.49 \pm 0.26$  ppm). All peels fractions were antibacterial activity against five pathogenic bacteria and MeOH fraction was highest inhibition effect on *Staphylococcus epidermidis* (MIC = 2.00 mg/ml) which most found in epidermis (Nont Thilertdecha et al., 2008). Additionally, the MeOH fraction was chromatographed giving ellagic acid, corilagin and geraniin (Figure 2.10) (Nont Thilertdecha et al., 2011). In addition, Rambutan peels EtOH extract was non cytotoxic in Caco-2 cells, confirming its safety (Okonogi et al., 2007).

In this study, the biological activity assessment of from Rambutan peels extracts prepared by a modified extraction to select a group of active in an attempt to archive greater. Total phenolic content will be determined as well as HPLC analysis. Furthermore, Cosmetics containing Rambutan peels extract will be formulated and evaluated on its stability as well.






**From** Nont Thitilertdecha, Apiwat Teerawutgulrag & Nuansri Rakariyatham. (2011). Identification of major phenolic compound from *Nephelium lappaceum* L. extracts and their antioxidant activity. **Molecules**, 15(1), 1453-1465.

**Figure 2.10** Structures of Geraniin (a), Ellagic acid (b) and Corilagin (c)

## CHAPTER 3

### METERIALS AND METHODS

#### 3.1 Chemicals and reagents

- 
- |   |                            |
|---|----------------------------|
| 1. ABTS   | (Fluka, USA)               |
| 2. Ascorbic acid                                      | (Sigma, USA)               |
| 3. Mushroom tyrosinase                                | (Sigma, USA)               |
| 4. <i>L</i> -dopa                                     | (Sigma, USA)               |
| 5. Kojic acid   | (Fluka, USA)               |
| 6. $\text{NaH}_2\text{PO}_4 \cdot \text{H}_2\text{O}$ | (Ajax Finechem, Australia) |
| 7. $\text{Na}_2\text{HPO}_4$                          | (Ajax Finechem, Australia) |
| 8. Potassium persulfate                               | (Fluka, USA)               |
| 9. Folin Ciocalteau reagent                           | (Carlo erba, Italy)        |
| 10. $\text{Na}_2\text{CO}_3$                          | (Ajax Finechem, Australia) |
| 11. Gallic acid                                       | (Fluka, USA)               |
| 12. Caffeic acid                                      | (Fluka, USA)               |
| 13. Ferulic acid                                      | (Fluka, USA)               |
| 14. Chlorogenic acid                                  | (MP Biomedical, France)    |
| 15. Rosmarinic acid                                   | (Sigma, USA)               |
| 16. Quercetin   | (Acros, USA)               |
| 17. EDTA 2 Na   | (Namsiang, Thailand)       |
| 18. Carbopol ultrez <sup>®</sup> 21                   | (Namsiang, Thailand)       |
| 19. Propylene glycol                                  | (Namsiang, Thailand)       |
| 20. Jojoba oil  | (Namsiang, Thailand)       |
| 21. Cyclomethicone                                    | (Namsiang, Thailand)       |



22. Glyceryl monosterate	(Namsiang, Thailand)
23. Cetyl alcohol	(Namsiang, Thailand)
24. Stearic acid	(Namsiang, Thailand)
25. Triethanolamine 99%	(Namsiang, Thailand)
26. Liquid germall <sup>®</sup> plus	(Namsiang, Thailand)
27. <i>n</i> -Hexane	(Zen point, Thailand)
28. EtOAc	(Zen point, Thailand)
29. 95% EtOH	(Zen point, Thailand)
30. DI water	(Milli-Q, Thailand)
31. AcOH	(Carlo erba, Italy)
32. AcCN	(Labscan, Ireland)
33. Absolute EtOH	(Merck, Germany)
34. Glycerine	(Namsiang, Thailand)

### 3.2 Equipments

1. Rotary evaporator	(Eyela/ CCA-1110, Japan)
2. 2-Digit digital balance	(Adventurer/ ARC 120, USA)
3. 4-Digit digital balance	(Sartorius/ BT 2245, Germany)
4. Incubator shaker	(Q.nic/ IS-40, Thailand)
5. Microplate reader	(Asys/ UVM 340, UK)
6. Sonicator	(Crest/ 690DAE, Malaysia)
7. HPLC	(Alliance/ WATER 2695, USA)
8. Water bath	(Mettler/ WB 22, Germany)
9. Homogenizer	(Ika/ T25D, Germany)
10. pH meter	(Mettler Toledo/S 20, USA)
11. Viscometer	(Brookfied/ RVDV-II+PRO, USA)
12. Colorimeter	(Hunterlab/ ULTRASCAN <sup>®</sup> , USA)
13. Centrifugation	(Spectrafuge/ 16M, UK)
14. Hot air oven	(Mettler/ UM 500, Germany)

15. Micropipette

(Mettler Toledo/ Rainin, USA)

### 3.3 Methodology

#### 3.3.1 Rambutan peels extraction

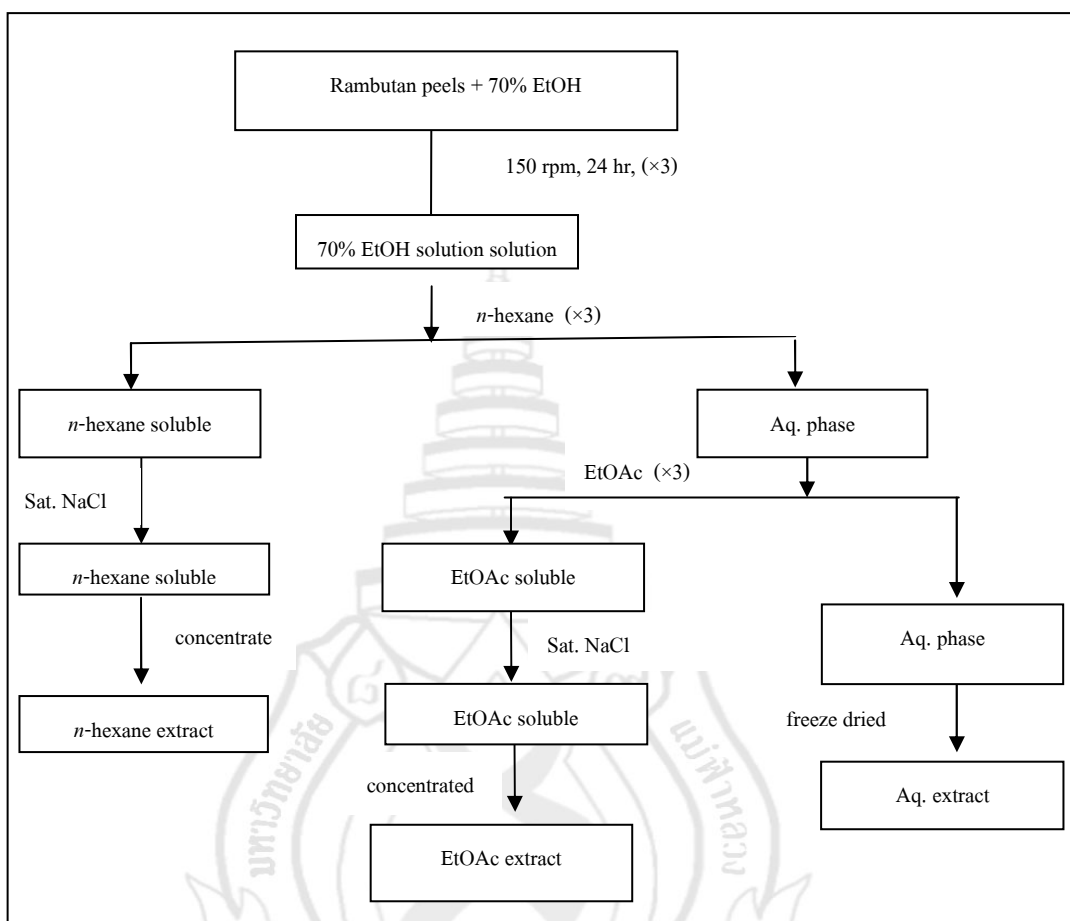
Rambutan fruits were collected from a local market in Chiang Rai during May, 2009. These peels were washed, subsequently cut into small pieces and dried in hot air oven at 50 °C. The dried peels of Rambutan (63.390 g) were extracted with 70% EtOH (500 ml) by a vigorously shaking at 150 rpm under room temperature for 24 hr. The extract was repeated for three times. The whole was filtrated and combined. The filtrate was concentrated under *vacuo* yielded crude 70% EtOH extract. The 70% EtOH extract was reconstituted (30 ml) and partitioned with *n*-hexane (1:3, v/v) for three times. The organic layers were collected and washed by sat. NaCl and concentrated to give *n*-hexane extract. The aqueous (Aq.) layer was further partitioned with EtOAc for three times by the same procedure to give crude EtOAc extract. The remaining Aq. phase was freeze dried to afford crude Aq. extract, eventually (Figure 3.1).

#### 3.3.2 ABTS radical scavenging activity

The antioxidant activity was determined ABTS assay (Kanlayavattakul & Lourith, 2011). This method is widely used for assessment of antioxidant activity, it is applicable for lipophilic and hydrophilic compounds (Rice – Evan *et al.*, 1996).

##### 3.3.2.1 Preparation of the ABTS<sup>•+</sup>

ABTS<sup>•+</sup> was produced by reacting 7 mM ABTS solution with 2.45 mM potassium persulfate solution. The mixture was kept in the dark at room temperature for 16-18 hr. Before used, the ABTS<sup>•+</sup> solution was diluted in absolute EtOH (1:20, v/v) to obtain an absorbance of  $0.700 \pm 0.200$  at 750 nm by a microplate reader.



**Figure 3.1** Rambutan Peels Extraction

### 3.3.2.3 Determination of $IC_{50}$

The  $IC_{50}$  value was the concentration of the test sample that cause 50% inhibition of free radicals. An  $IC_{50}$  value was obtained by plotting % inhibitions with concentrations of the free radical inhibitor. The percent inhibition of antioxidant activity was calculated as follows;

$$\% \text{ inhibition} = (A-B) / (A) \times 100$$

Where;  $A$  an absorbance at 750 nm after incubation without test sample

$B$  an absorbance at 750 nm after incubation with test sample

### 3.3.3 Antityrosinase activity

The tyrosinase inhibitory activity was determined by a modified dopachrome method using *L*-dopa as the substrate (Mayuree Kanlayavattakul & Nattaya Lourith, 2011). Dopachrom is one of the intermediates in the melanogenesis. The pink color of dopachrome can be detected by visible. The potential tyrosinase inhibitor could show minimal dopachrome absorption.

#### 3.3.3.1 Preparation of 20 mM phosphate buffer (pH 6.8)

$\text{NaH}_2\text{PO}_4 \cdot \text{H}_2\text{O}$  (31.20 mg) in 10 ml of DI water and  $\text{Na}_2\text{HPO}_4$  (28.40 mg) in 10 ml of DI water were mixed giving phosphate buffer pH 6.8.

#### 3.3.3.2 Preparation of substrate and tyrosinase solution

*L*-Dopa solution (0.85 mM) was prepared in phosphate buffer 20 mM (pH 6.8). Mushroom tyrosinase enzyme (240 unit/ ml) was dispersed in the phosphate buffer.

#### 3.3.3.3 Preparation of the samples

All sample extracts were preliminary antityrosinase activity screened at 1,000 ppm. The greatest inhibitory extract was further evaluated on its  $\text{IC}_{50}$  compared with kojic acid as a positive control.

#### 3.3.3.4 Preparation of reaction

The samples (40  $\mu\text{l}$ ) was added to 80  $\mu\text{l}$  of 20 mM phosphate buffer (pH 6.8) and 40  $\mu\text{l}$  of mushroom tyrosinase solution in one well of a 96-well plate. Each well was mixed and pre-incubated at  $25^\circ\text{C}$  for 10 min. Then, 40  $\mu\text{l}$  of 0.85 mM *L*-dopa was added and incubated at  $25^\circ\text{C}$  for 20 min. There was a corresponding blank of each sample, and this blank contained all components except for tyrosinase solution. The absorbance was measured at 490 nm with the microplate reader. Each assay was performed in triplicate.

#### 3.3.3.5 Evaluation of tyrosinase activity

Activity was measured and calculated as percent inhibition that using the following equation;

$$\% \text{ inhibition} = (A-B) / (A) \times 100$$

Where; *A* an absorbance at 490 nm after incubation without test sample

*B* an absorbance at 490 nm after incubation with test sample

### 3.3.4 Total phenolic content

Total phenolic content of all extracts were determined with the using of Folin Ciocalteu method (Mayuree Kanlayavattakul & Nattaya Lourith, 2011).

#### 3.3.4.1 Preparation of the samples

Sample extracts were prepared in MeOH to a final concentration of 100 ppm. Gallic acid was prepared in final concentrations of 5, 10, 20, 30 and 40 ppm.

#### 3.3.4.2 Preparation of reaction

Each sample (4  $\mu$ l) was mixed with DI water (112  $\mu$ l) and Folin Ciocalteu reagent (4  $\mu$ l) in a 96-well plate and shook for 5 min. Thereafter, 7.5%  $\text{Na}_2\text{CO}_3$  (80  $\mu$ l) was added. The mixture was incubated for 1 hr. The absorbance was measured at 765 nm with the microplate reader. All of tests were done in triplicate and expressed as g of gallic acid equivalents per 100 g of crude extract (g GAE/100 g crude extract).

### 3.3.5 Quantification of phenolic compounds by HPLC

HPLC was used for quantification of phenolics in the extracts. It was done by means of a Water 2695 Alliance equipped with a Water 2996 photodiode array detector. The reversed phase column (Alltech, Prevail  $\text{C}_{18}$  5  $\mu$ m, 250  $\times$  4.6 mm, stainless steel with Alltech, Prevail all guard cartridge  $\text{C}_{18}$  5  $\mu$ m, 7.5  $\times$  4.6 mm) was eluted by a gradient solvent system composing of AcCN and 3% AcOH in DI water (Table 3.1). A flow rate was controlled at 1 ml/min with an injection volume of 10  $\mu$ l.

**Table 3.1** Mobile Phase System

Time (min)	AcCN (%)	3% aq. AcOH (%)
0-3	0	100
3-5	15	85
5-10	20	80
10-15	25	75
15-20	30	70
20-30	50	50

#### 3.3.5.1 Preparation of the extracts and the standards for HPLC analysis

All extracts (1 mg) were accurately weighed into 1 ml of AcCN. Kojic acid, gallic acid, chlorogenic acid, caffeic acid, ferulic acid, rosmarinic acid and quercetin were accounted as the standards. A calibration curve was prepared from standard concentrated 5 – 500 ppm. All samples were analyzed in triplicate, content of the phenolics in each sample was calculated and expressed as g/kg crude extract.

#### 3.3.6 Cytotoxicity

Cytotoxic against Vero cell lines (Africal green monkey kidney cell lines) were conducted by the National Center for Genetic Engineering and Biotechnology (Biotec) using of Green fluorescent protein (GFP) detection method compared with Elliptine as a positive control (Shrivastava, Ravikumar, Shanmugasundaram, Babu & Nair, 2005).

#### 3.3.7 Fundamental properties of Rambutan peels extracts

Solubility was determined by dissolving of each Rambutan peels extract (0.5 mg) in propylene glycol (100 mg) and glycerine (100 mg), separately. The solubility of each solvent and pH was evaluated.

#### 3.3.8 Cosmetic emulsion and physical properties evaluation

Emulsions containing the ingredients as shown in Table 3.2, were formulated by mixing water and oil phases at 75°C and homogenized (6,000 rpm) for 10 min. The whole was cooled down and added preservative. The formula was accelerated stability test by heating – cooling 6 cycles (45 and 4 °C, 24 hr, each) (Barel et al., 2001). The appearance, pH, viscosity and centrifugation under this condition (3,000 rpm, 30 min) were evaluated (Rolim et al., 2006).

#### 3.3.9 Incorporation of Rambutan peels extract in the base emulsion

From the antioxidant activity and total phenolic content, the extract which shown the highest free radical scavenging activity and highest total phenolic content, was chosen to incorporate into the cosmetic emulsion at 50 ppm (0.005% w/w) with EtOAc extract. Stability

test was conducted physical and chemical stability tests were monitored including heating – cooling 6 cycled and long time storage at 4, 25 and 45 °C for 6 months.

Chemical stability was determined by dissolved 0.30 g emulsion in 5 ml of absolute EtOH and centrifuged at 3,500 rpm for 5 min at room temperature. Total phenolic content and antioxidant activity of the supernatant were analyzed (Nataya Lourith et al., 2009).

**Table 3.2** Formulation of Cosmetic Base

Part	INCI Name	Function	% (w/w)			
			1	2	3	4
A:	EDTA 2 Na	Chelating agent	0.10	0.10	0.10	0.10
	Carbopol ulterz <sup>®</sup> 21	Thickening agent	-	-	-	0.15
	Propylene glycol	Humectant	3.00	3.00	3.00	3.00
	DI water	Diluent	81.40	79.40	79.90	81.25
B:	Jobba oil	Emollient	2.00	2.00	2.00	2.00
	Cyclomethicone	Emollient	3.00	3.00	3.00	3.00
	Glyceryl monostearate	Co- Emulsifier	1.50	1.50	1.50	1.50
	Cetyl alcohol	Emollient	3.00	5.00	3.00	3.00
	Stearic acid	Emulsifier	2.00	2.00	3.50	2.00
	Triethanolamine					
C:	99%	Emulsifier	0.50	0.50	0.50	0.50
	DI water	Diluent	3.00	3.00	3.00	3.00
D:	Liquid germall <sup>®</sup> plus	Preservative	0.50	0.50	0.50	0.50
<b>Total</b>			<b>100.00</b>	<b>100.00</b>	<b>100.00</b>	<b>100.00</b>

### 3.3.10 Statistic analysis

Statistical assessment was carried out by the software system named SPSS (16.0) for Windows using one-way. The results were presented as means ± standard deviations.

## CHAPTER 4

### RESULTS AND DISCUSSION

#### 4.1 Sample preparation and extraction

It is already known that most of the natural derived plant ingredients that are phenolic compounds such as gallic acid, quercetin and catechin have antioxidant and antityrosinase activity, with broad solubility propensities due to their molecular properties (Sultana, Anwar & Asharf, 2009). In natural extract preparation typically, solvent extract is the most frequently used technique for isolation of plant antioxidant compounds. However, the extractive yields and phenolic compounds of plants are strongly depend on the nature of extracted solvent polarity. Polar solvents are frequently employed for antioxidant phenolics isolation from plants. The most suitable of solvents are Aq. containing EtOH, MeOH and EtOAc (Javanmardi, Stushnaff, Locke & Vivaco, 2003; Kin et al., 2007). For instance, EtOAc extract of antioxidant phenolics from onion and citrus peels and methanolic water extraction in rice bran (Zhou & Yu, 2004). In addition, 70% EtOH have been extensively used to extract antioxidant and antityrosinase compounds from the seeds (Nattaya Lourith et al., 2009).

In this study, Rambutan peels were extracted with 70% EtOH by a modified method. (Nattaya Lourith et al., 2009) The 70% EtOH extract indicated that extracting produced the overall effectiveness of bioactive compounds including phenolics (Zhou & Yu, 2004). Consequently, 70% EtOH extract (3.526 g, 5.556 % w/w) was liquid – liquid extracted with *n*-hexane and EtOAc, respectively. *n*-Hexane was used to clean up the extract by isolating low polar substances such as wax and fat. Meanwhile, EtOAc extracted higher polarity compound including phenolic compounds. The highest weight and extractive yield were found in the crude Aq., followed by EtOAc and *n*-hexane extracts, respectively (Table 4.1).



**Table 4.1** Proportion and Extractive Yield of Rambutan Peels Extracts

Extracts	Weight (g)	% Yield (w/w)
<i>n</i> -hexane	0.045	0.071
EtOAc	0.443	0.705
Aq.	3.214	5.350

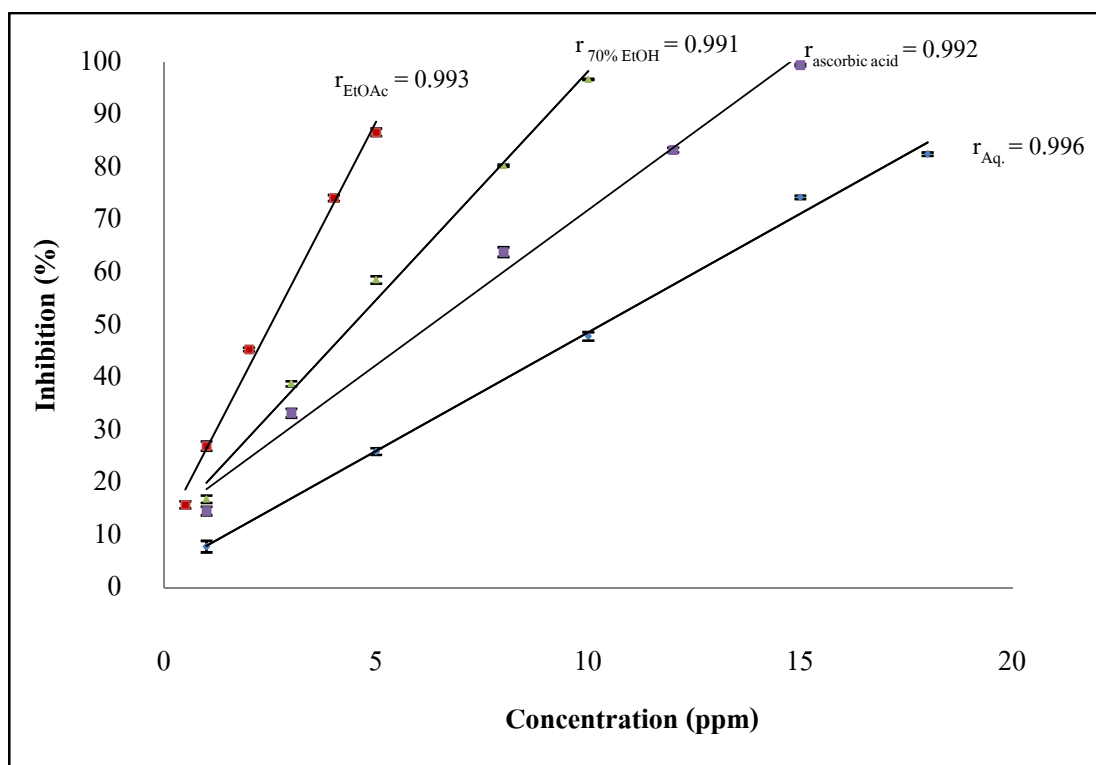
#### 4.2 Antioxidant and antityrosinase activities

Antioxidant activity of each extract to scavenge ABTS<sup>++</sup> was evaluated except *n*-Hexane extract because it was used to clean up the extract. Anti-radical activity of each sample at various concentrations including the standard ascorbic acid was compared as shown in Figure 4.1.

The greatest antioxidant activity was exhibited by EtOAc extract, followed by 70% EtOH and Aq. extracts, respectively. The Rambutan peels EtOAc and 70% EtOH extracts were more potent than ascorbic acid, which was used as a positive control (Table 4.2). Furthermore, radical scavenging activity of EtOAc and 70% EtOH extract was significantly better than ascorbic acid ( $p < 0.001$ ). In particular, the EtOAc extract was significantly more potent than 70% EtOH extract ( $p < 0.001$ ).

Antityrosinase activity was preliminarily screened at 1,000 ppm of the extract. The activity was found highest in EtOAc extract, followed by the 70% EtOH and Aq. extracts, respectively, as shown in Figure 4.2. Although, at a lower concentration of EtOAc extract (600 ppm), it was significantly ( $p < 0.001$ ) more potent than 70% EtOH and Aq. extracts (Figure 4.2).

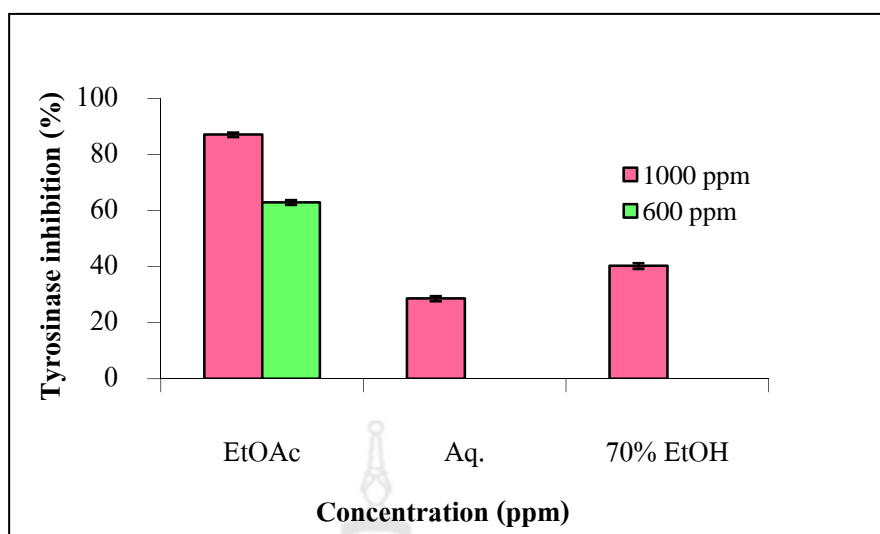
EtOAc extract was further examined on its IC<sub>50</sub> compared with kojic acid. However, EtOAc extract shown less skin lightening activity than kojic acid (IC<sub>50</sub> = 430.838 ± 0.588 and 38.984 ± 0.513 ppm).



**Figure 4.1** ABTS<sup>++</sup> Scavenging Activity of Ascorbic Acid (■) and Rambutan Peels EtOAc (●), 70% EtOH (▲) and Aq. (◆) Extracts

**Table 4.2** ABTS Scavenging Activity (IC<sub>50</sub>) of Rambutan Peels Extracts

Samples	IC <sub>50</sub> (ppm)	IC <sub>50</sub> sample/IC <sub>50</sub> ascorbic acid	<i>p</i>
EtOAc extract	2.915 ± 0.022	0.464	< 0.001
70% EtOH extract	4.447 ± 0.047	0.707	< 0.001
Aq. extract	9.012 ± 0.003	1.433	< 0.001
Ascorbic acid	6.288 ± 0.098	1	-

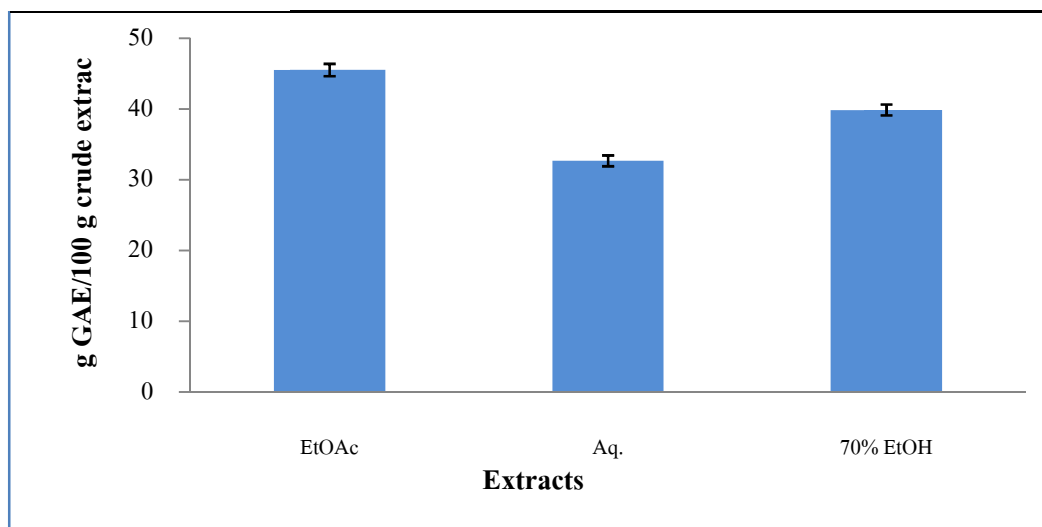


**Figure 4.2** Antityrosinase Activity of Rambutan Peels Extracts

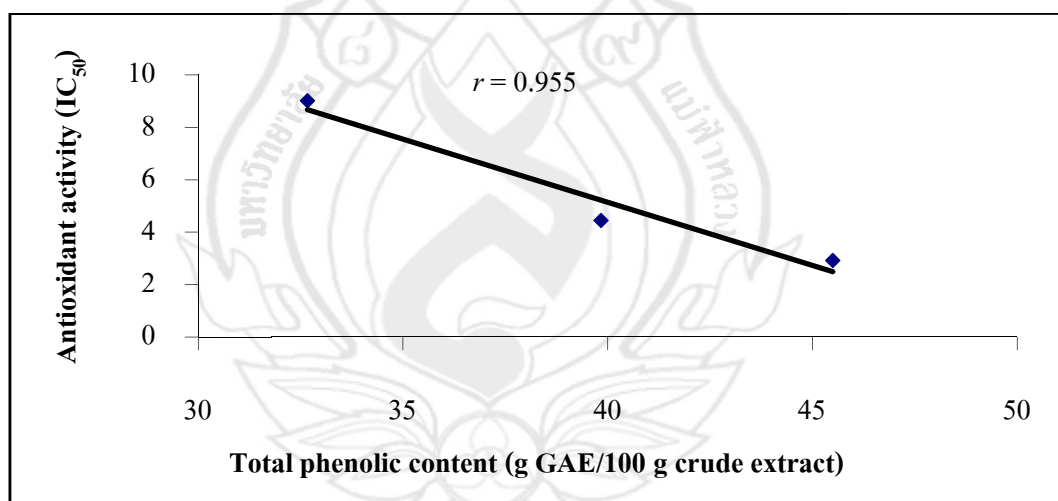
### 4.3 Total phenolic content

It is well known that protective effect have been attributed, in large part, to the antioxidant present including the antioxidant natural source including vegetables, fruits and agriculture wastes. The actions of phenolics are mostly ascribed to their antioxidant capacities, chelation of redox active metal ion as well (Soobratte et al., 2005). Respecting to antioxidant and antityrosinase activities, Rambutan peels extracts were evaluated on total phenolic content by Folin Ciocalteu method (Figure 4.3).

Maximum phenolic content was found in EtOAc extract ( $45.500 \pm 0.866$  g GAE/ 100 g crude extract) followed by 70% EtOH ( $39.833 \pm 0.764$  g GAE/ 100 g crude extract) and Aq. extracts ( $32.667 \pm 0.764$  g GAE/ 100 g crude extract). Total phenolic content was evaluated in an attempt to relate antioxidant activity with the active principles. The phenolic content in EtOAc extract was significantly ( $p < 0.001$ ) higher than the others. Furthermore, total phenolic compound of this modified extract method was correlated with antioxidant activity ( $r = 0.955$ ) as shown in Figure 4.4.



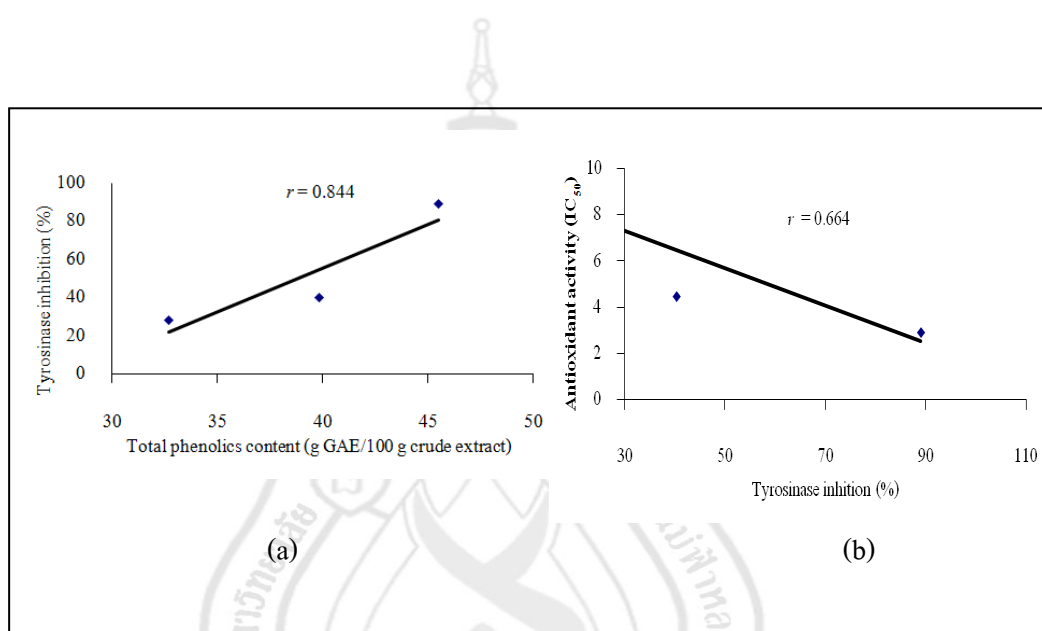
**Figure 4.3** Phenolic Content of Each Rambutan Peels Extract



**Figure 4.4** Correlation between Antioxidant Activity and Total Phenolic Content of Rambutan Peels Extracts

Thus, higher phenolic content extract possesses a stronger antioxidant activity. The presenting relationship was greater than the previous reported, in lipid peroxidation inhibitory effect by  $\beta$  - carotene bleaching assay ( $r = 0.610$ ) and antioxidant activity by thiocyanate method

( $r = 0.680$ ) (Nont Thilertdecha et al., 2008). However, free radical scavenging activity by DPPH assay was comparative ( $r = 0.960$ ) (Nont Thilertdecha et al., 2011), respecting to the similar antioxidant's mechanism on hydrogen donating ABTS assay (Rice - Evan et al., 1995). Furthermore, correlation between total phenolic content and tyrosinase inhibitory activity was exhibited ( $r = 0.844$ , Figure 4.5a). Tyrosinase inhibitory effect was related with antioxidant activity ( $r = 0.644$ ) as well (Figure 4.5b).

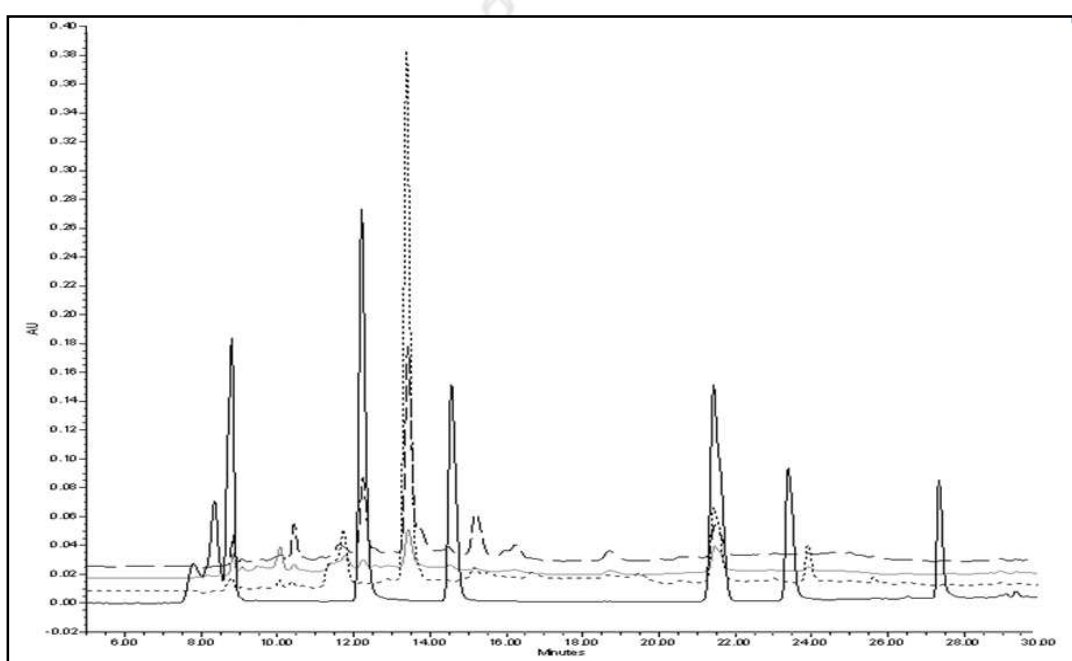


**Figure 4.5** Correlation between Total Phenolic Content and Antityrosinase (a) and between Antioxidant and Antityrosinase Activities (b)

#### 4.4 Quantification of phenolic compounds by HPLC

Phenolic compounds in each Rambutan peels extracts were analyzed by HPLC. Analysis of gallic acid, kojic acid, chlorogenic acid, caffeic acid, ferulic acid, rosmarinic acid and quercetin by gradient mobile phase system containing 3% aq. AcOH and AcCN was successively afforded the fingerprint of the extracts. The analytical phenolics are widely distributed in plants and known as antioxidant and antityrosinase activities used in healthcares (Kim & Uyama, 2005). These

compounds receiving a high interest for pharmacological application including cosmetic products. However, these phenolics are rarely presented in Rambutan as only ellagic acid, coliragin and gerananin were reported (Nont Thilertdecha et al., 2011). In this study, HPLC fingerprint of Rambutan peel extracts was shown in Figure 4.6. The fingerprint is suitable for control of chemical compound in Rambutan for quality control of extract. Quantification of active compounds were revealed as shown in Table 4.3.



**Figure 4.6** HPLC Chromatogram of Phenolics (—), Rambutan Peels EtOAc Extract (.....), 70%EtOH Extract (---) and Aq. Extract (-.-)

Ferulic, gallic, rosmarinic and kojic acids and quercetin were found highest in EtOAc extract except chlorogenic acid and caffeic acid. Caffeic acids and ester (chlorogenic acid) were found in Aq. and 70% EtOH, which are the higher polarity solvents. Additionally, phenolic compounds content in EtOAc extract that possessing highest biological activities and total phenolic content was significantly higher than the other extracts ( $p < 0.001$ ).

**Table 4.3** Phenolic Compounds in Rambutan Peels Extracts

Rambutan peels extracts	Phenolic compounds (g/kg crude extract)						
	Kojic acid	Gallic acid	Chlorogenic acid	Caffeic acid	Ferulic acid	Rosmarinic acid	Quercetin
EtOAc	0.932 ± 0.627	2.434 ± 0.044	0.388 ± 0.032	1.267 ± 0.218	3.235 ± 0.023	1.743 ± 0.151	0.885 ± 0.156
Aq.	0.234 ± 0.105	2.369 ± 0.075	3.771 ± 0.787	0.303 ± 0.008	1.034 ± 0.066	0.186 ± 0.067	0.671 ± 0.162
70% EtOH	0.054 ± 0.028	1.945 ± 0.258	1.283 ± 0.086	1.531 ± 0.551	0.777 ± 0.041	0.150 ± 0.016	0.203 ± 0.032

#### 4.5 Cytotoxicity

The use of *in vitro* cytotoxicity studied provides important tools to enhance of hazardous effects by chemical and for predicting these effects on human. *In vitro* system is used principally for screening propose and for generating more comprehensive toxicological effectives (Eisenbrand et al., 2002). Cytotoxicity is considered primarily as the potential of compounds to induce cell death. In the previous report, Rambutan seed extract was non-cytotoxic in Caco-2 cells (Okonogi et al., 2007), which is mammalian cells from human colon adenocarcinoma cells (Artursson & Kalsson, 1991). That generally used to test on safety of pharmaceutical applications (Eisenbrand et al., 2002).

In this present study, the most potent extract with the highest total phenolic content and highest biological activities, EtOAc extract, was evaluated on its safety toward Vero cells. Vero cell was established from monkey and was tested because the cells are sensitive to chemical compounds and show good metabolic activities for the toxin, which is usually in healthcare products (Eisenbrand et al., 2002). The EtOAc extract was found non toxicity to the cells at the maximum concentration (50 ppm), which was much greater than its antioxidant active

concentration. The safety of this agriculture waste is consistence with Caco-2 cells (Okonogi et al., 2007), confirming its potential for cosmetic applications.

#### 4.6 Correlation between biological activities, total phenolic content and actives

Rambutan peels EtOAc extract was the most potent antioxidant and antityrosinase inhibitor having the highest total phenolic content. The characterized phenolics in the extract were related with the radical scavenging (Figure 4.7a) and antityrosinase activities (Figure 4.7b) and total phenolic (Figure 4.7c). Quercetin was shown as the principal phenolic responsible in antioxidant activity ( $r = 0.995$ ), and was indicated active in total phenolic content ( $r = 0.980$ ). In addition, rosmarinic acid was related with antityrosinase activity ( $r = 0.959$ ). Quercetin acts as hydrogen donating free radical scavenging agent and cofactor or substance of tyrosinase (Kim & Uyama, 2005). It inhibits tyrosinase activity by the ability to chelate the copper in the active site, leading to irreversible inactivation of tyrosinase and neautizes free radical in oxidantion. Rosmarinic acid neutralizes free radical generated oxidation, melanogenesis and down regulates tyrosinase activity. In similar to antioxidant activities of ferulic, caffeic and chlorogenic acids as well as metalloproteinase chelating effect that limit enzyme activity (Kim & Uyama, 2005; Chang, 2009). Additionally, phenolic compounds are receiving a high interesting for pharmacological applications particularly in cosmetics respecting to their biological activities. Especially, ferulic acid, which is approved as an antioxidant agent in Japan (Graf, 1992) including kojic acid, which is depigmentation agent. Kojic acid strongly inhibits tyrosinase by chelating efficiency in a non – competitive mechanism in similar to gallic acid that melanin production is reduced and neutralizes free radical generation (Kim & Uyama, 2005).

Thus, Rambutan peels EtOAc extract was exhibited as a potential source of ferulic acid. In addition, water is the most optimized solvent for isolation of chlorogenic acid from the peel. Furthermore, correlation between total phenolic content and activities is a convenience and practical method in quality control of Rambutan peels application. Total phenolic content determination could be used alternatively for antioxidant activity observation respecting to its low-cost comparing to ABTS assay. In similar, it could be more feasible than HPLC analyses in an industrial practice.



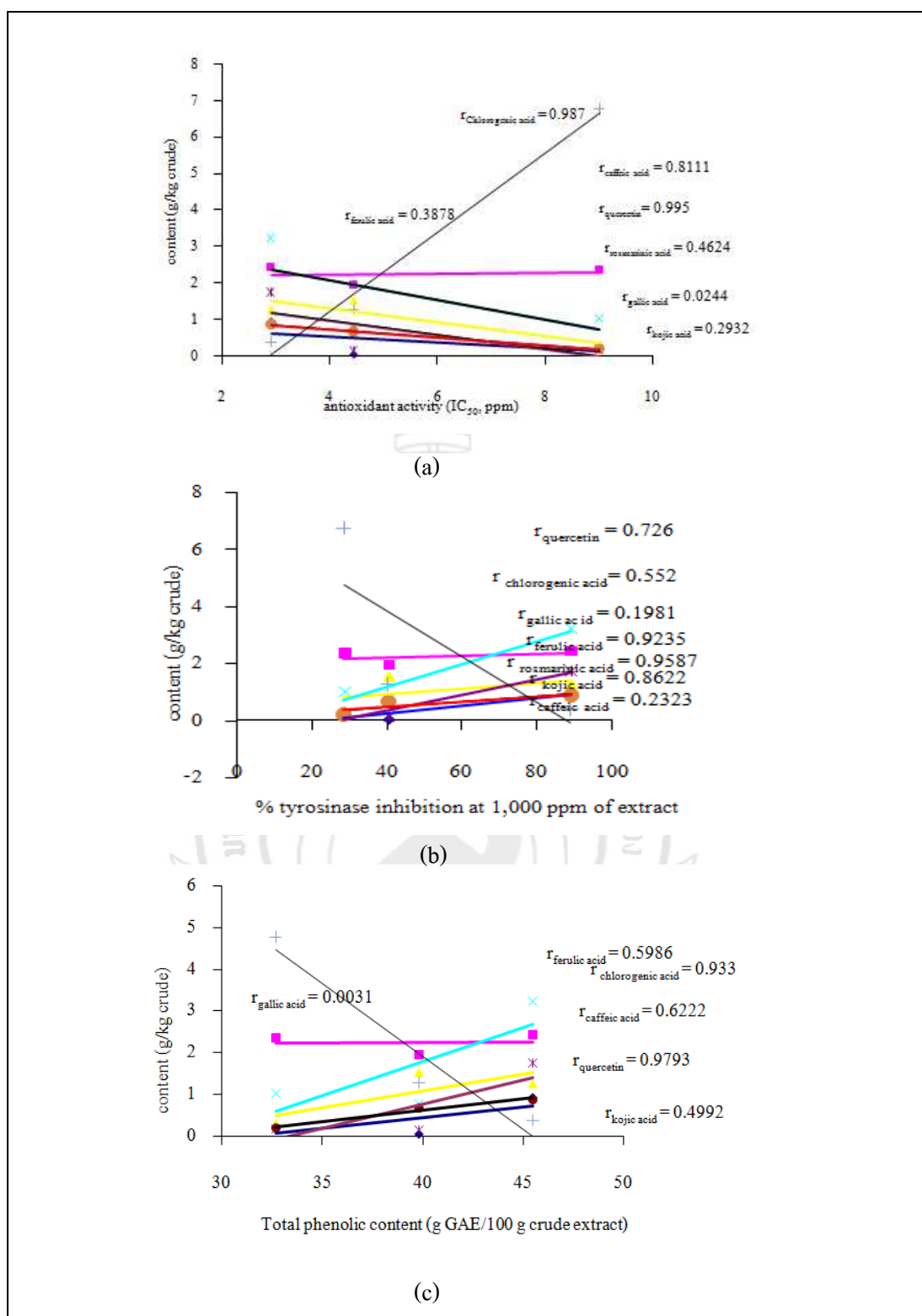
#### 4.7 Fundamental properties of Rambutan peels extracts

EtOAc extract, the most potent biological activity, was chosen to do solubility and pH of extract. EtOAc extract in propylene glycol was better and easy soluble than glycerine. The solubility was effected viscosity of solvent. Viscosity of propylene glycol is lower than glycerin (Dow, 2011) therefore, it was easy to soluble. pH of  $7.020 \pm 0.000$  and  $6.520 \pm 0.006$  was reported in propylene glycol and glycerine, respectively.

#### 4.8 Preparation of emulsion

Emulsion was formulated by dispersing of carbopol ultrez<sup>®</sup> 21 in water with heating to 75°C, propylene glycol and EDTA 2 Na were added. Then, oil phase (jojoba oil, cyclomethicone, glyceryl monostearate, cetyl alcohol and stearic acid) was heated to 75°C and added to water phase. Triethanolamine was added with homogenize (6,000 rpm, 10 min). The emulsion was cooled down (40°C) and preservative was added finally. Formulations were white, opaque and smooth texture but they were difficult to spread on skin except the formula 4. This formulation had 0.15% carbopol ultrez<sup>®</sup> 21, which was thickening agent and improved spread ability. Therefore, formula 4 was further evaluated on physical stability as shown in Table 4.4.

Emulsion was evaluated in terms of pH, color and viscosity. They were insignificantly ( $p > 0.05$ ) changed at 95% confident interval as observed in heating - cooling 6 cycles. pH was ranged 6.32-6.34 and viscosity was 36,000- 39,000 cPs that in similar to 1 month. Viscosity of this developed emulsion was in the range of typical flowability of cream and lotion. (Schlossman, 2000) Therefore, the formulated emulsion not only physically stable but afforded the acceptable texture for topical application.



**Figure 4.7** Correlation between Actives and Antioxidant (a), Antityrosinase Activities (b) and Total Phenolic Content (c)

**Table 4.4** Physical Evaluation of Cosmetic Emulsion

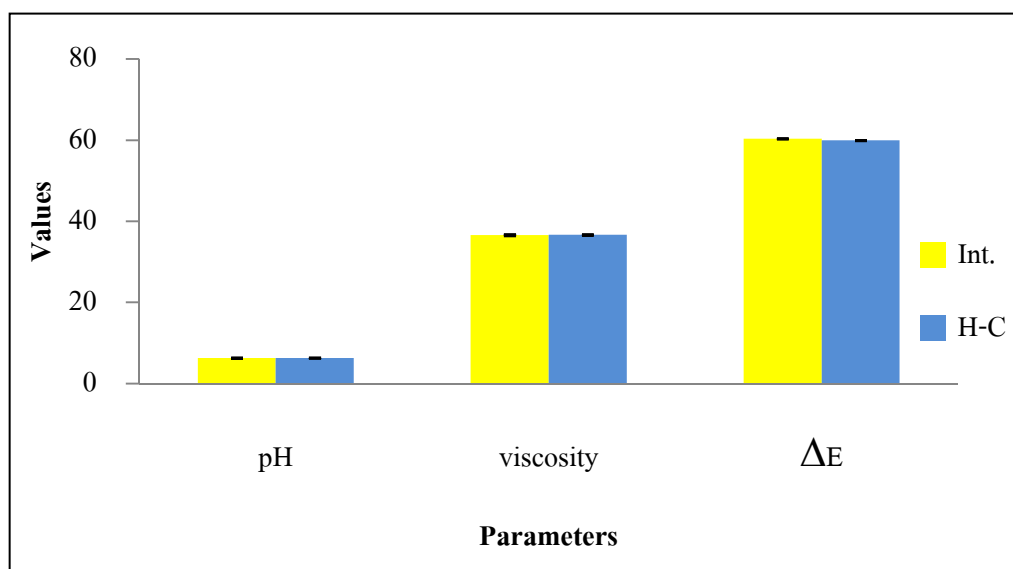
Conditions	Appearance	pH	viscosity (cPs)	$\Delta E$
Initial	white, smooth, opaque	$6.323 \pm 0.006$	$36,612 \pm 152.050$	$64.250 \pm 0.010$
Heating-cooling				
6 cycles	white, smooth, opaque	$6.323 \pm 0.015$	$36,656 \pm 124.070$	$64.297 \pm 0.010$
	at 4°C	$6.323 \pm 0.006$	$38,256 \pm 176.850$	$65.327 \pm 0.012$
1 month	at 25°C	$6.323 \pm 0.006$	$38,760 \pm 40.327$	$64.670 \pm 0.000$
	at 45°C	$6.337 \pm 0.006$	$38,500 \pm 204.150$	$64.697 \pm 0.006$

#### 4.9 Incorporation of Rambutan peels extract in the emulsion

The EtOAc extract, the most potent free radical scavenging activity and highest total phenolic content, was chosen to incorporate into the emulsion. It was incorporated at 50 ppm, the maximum concentration that non-cytotoxic and higher than the antiradical dose ( $IC_{50} = 2.915 \pm 0.022$  ppm). Physical stability was evaluated following heating - cooling 6 cycles (Figure 4.8). Physiochemical characterizes were consitstanced with the initial state. Thus, the emulsion was physically stabled.

Rambutan peels emulsion was further stored at 4, 25 and 45 °C for 1, 3 and 6 months. The emulsion was stabled following centrifugation assay and long term stability emulsion evaluation at various conditions (Table 4.5). pH and color of emulsion were insignificantly ( $p > 0.05$ ) differenced. Viscosity was not increased ( $p > 0.05$ ) at 90% confident. However, at the low temperature (4 °C), the formulation trended to decrease in viscosity (Figure 4.9). This might be regulated by jojoba oil containing in the base as the freezing point of the oil is 3.7 – 7.0 °C (Wikipedia, 2011).

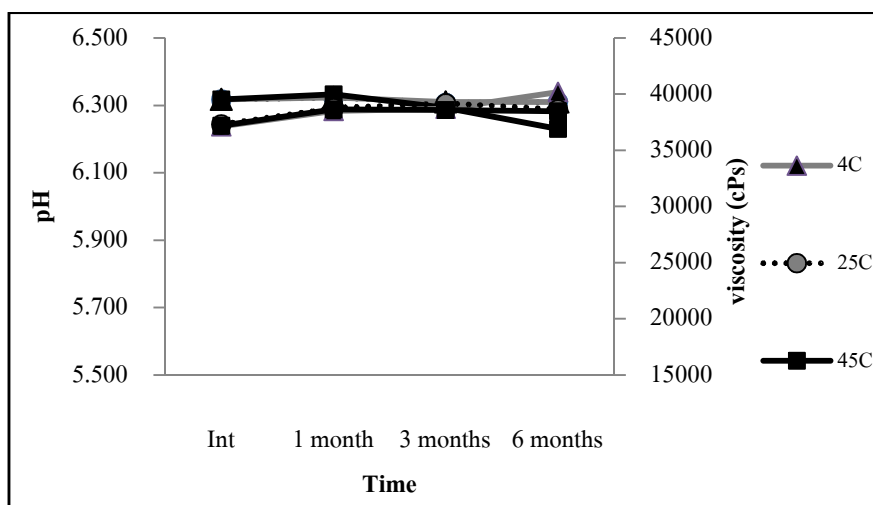
Additionally, chemical stability of Rambutan peels emulsion as evaluated. Total phenolic content and antioxidant activity ( $3,298 \pm 9.00$  µg GAE/ml and  $80.842 \pm 0.41\%$ ) were not change following heating – cooling 6 cycles ( $3,296 \pm 16.00$  µg GAE/ml and  $80.120 \pm 0.34$ ) in Figure 4.10.



**Figure 4.8** Physical Stability of Rambutan Peels Extract in Emulsion Evaluated in Accelerated Test

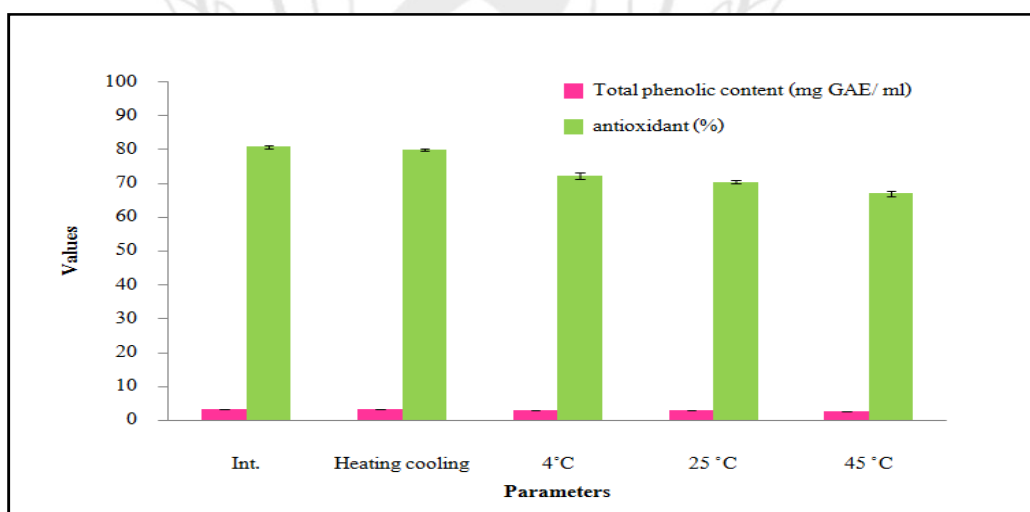
**Table 4.5** Physical Stability of Rambutan Peels Emulsion under Long Time Storages

Conditions		Appearance	pH	Viscosity (cPs)	ΔE
Initial		light yellow, smooth, opaque	6.308 ± 0.013	38,399 ± 79.720	59.868 ± 0.518
1 month	4°C	light yellow, smooth, opaque	6.323 ± 0.006	38,490 ± 64.667	60.637 ± 0.015
	25°C	light yellow, smooth, opaque	6.323 ± 0.015	38,760 ± 65.333	60.637 ± 0.012
	45°C	light yellow, smooth, opaque	6.333 ± 0.006	38,637 ± 64.689	60.187 ± 0.006
3 months	4°C	light yellow, smooth, opaque	6.307 ± 0.006	38,710 ± 115.333	59.640 ± 0.015
	25°C	light yellow, smooth, opaque	6.310 ± 0.000	39,177 ± 33.556	60.350 ± 0.000
	45°C	light yellow, smooth, opaque	6.293 ± 0.012	38,637 ± 177.850	59.163 ± 0.038
6 months	4°C	light yellow, smooth, opaque	6.310 ± 0.000	40,173 ± 268.578	60.637 ± 0.015
	25°C	light yellow, smooth, opaque	6.310 ± 0.010	38,570 ± 60.833	62.803 ± 0.006
	45°C	light yellow, smooth, opaque	6.230 ± 0.010	38,477 ± 49.666	59.317 ± 0.009



**Figure 4.9** Physical Stability of the Rambutan Peels Emulsion

In addition, chemical stability at the long term for 6 months under various temperatures was conducted (Figure 4.10). The formulated Rambutan peels emulsion was stable in terms of total phenolic content and antioxidant activity. Thus, this presenting natural cosmetic is physical and chemical stables.



**Figure 4.10** Chemical Stability of Rambutan Peels Emulsion in Terms of Antioxidant Activity and Total Phenolic Content

## CHAPTER 5

### CONCLUSION

Rambutan peels were macerated with 70% EtOH and further liquid – liquid extracted to select the group of active principles in extract. This method was exhibited as feasible and practical method to recover the biological activities from the fruit residues. The highest extractive yield was found Aq. (5.350%), followed by EtOAc (0.705%) and *n*-hexane (0.071%) extracts. Total phenolic content was found highest in EtOAc extract ( $45.50 \pm 0.866$  g GAE/ 100 g crude extract), followed by 70% EtOH and Aq. extracts ( $39.833 \pm 0.764$  and  $32.667 \pm 0.764$  g GAE/ 100 g crude extract, respectively). Total phenolic content was related with antioxidant activity ( $r = 0.955$ ). The EtOAc was shown to have the highest capacity to scavenge free radical with an  $IC_{50}$  of  $2.915 \pm 0.022$  ppm, followed by 70% EtOH and Aq. extracts ( $IC_{50}$   $4.447 \pm 0.047$  and  $9.012 \pm 0.003$  ppm, respectively) as assessed by ABTS assay. Consequently, extracts were preliminary screened at 1,000 ppm for antityrosinase activity. EtOAc extract posed the strongest inhibitory effect ( $89.010 \pm 0.420\%$ ), followed by the 70% EtOH and Aq. extracts ( $40.404 \pm 0.945$  and  $28.638 \pm 0.940\%$ , respectively). The EtOAc extract of Rambutan peels was non-cytotoxic in Vero cells confirming its safety in healthcare applications including cosmetics. Ferulic acid, gallic acid, caffeic acid, chlorogenic acid, rosmarinic acid, kojic acid and quercetin were characterized in the Rambutan peels extracts by HPLC. Over all contents of their actives were found highest in EtOAc extract, followed by Aq. and 70% EtOH extracts, respectively.

The Rambutan peels EtOAc extract was further incorporated into the stable base emulsion (0.005% w/w). The Rambutan peels emulsion had light yellow color with a luxury feeling, pH of  $6.323 \pm 0.006$  and appropriated viscosity at  $36,612 \pm 152.050$  cPs. The formulation was physically and chemically stabled following acceralated tests by centrifugation assay and heating – cooling 6 cycles, in addition to long term storage under 4, 25, 45 °C for 6 months.



## REFERENCES

## REFERENCES

- Ajiboye, T. (2011). In vivo antioxidant potentials of *Piliostigma thonningii* (Schum) leaves: Studies on hepatic marker enzyme, antioxidant system, drug detoxifying enzyme and lipid peroxidation. **Human & Experimental Toxicology**, **30**(1), 55-62.
- Anchisi, C., Maccioni, A., Sinico, C. & Valenti, D. (2001). Stability studies of new cosmetic formulations with vegetable extracts as functional agents. **IL Farmaco**, **56**(5), 427-431.
- Antolovich, M., Prenzler, P. D., Patsalides, E., McDonald, S. & Robard, K. (2002). Method for testing antioxidant activity. **Analyst**, **127**(1), 183-198.
- Artursson, P. & Kalsson, J. (1991). Correlation between oral drug absorption in humans and apparent drug permeability coefficients in human intestinal epithelial (Caco-2) cells. **Biochemical and Biophysical Research Communication**, **175**(3), 830-885.
- Baby, A., Migliato, K., Maciel, C., Zague, V., Pinto, C., Salgado, H., Kanekp, T. & Velasco, M. (2007). Accelerated chemical stability data of o/w fluid emulsions contain the extract of *Trichilia catigua* Adr. Juss and *Ptychopetalum olacoides* Benth. **Journal of Pharmaceutical Sciences**, **43**(3), 405-412.
- Barel, A. O., Paye, M. & Maibach, H. I. (2001). **Handbook of cosmetic science and technology**. New York: Dekker.
- Berger, M. (2005). Can oxidative damage be treated nutritionally. **Journal of Clinical Nutrition**, **24**(2), 172-183.



- Callagham, T. M. & Wilhelm, K. (2008). A review of ageing and an examination of clinical methods in the assessment of ageing skin. Part I: cellular and molecular perspective of skin ageing. **International Journal of Cosmetic Science**, 30(5), 313-322.
- Chang, S. T. (2009). An update review of tyrosinase inhibitors. **International Journal of Molecule Science**, 10(6), 1440-2475.
- Darr, D & Fridovich, I. (1994). Free Radicals in Cutaneous Biology. **Journal of Investigative Dermatology**, 102(5), 671-675.
- Dow. (2011). **Viscosity of polypl**. Retrived January 12, 2012, from: [https://www.dow-answer.custhelp.com/app/answers/detail/a\\_id/7457/~~/propylene-glycols---viscosity-information](https://www.dow-answer.custhelp.com/app/answers/detail/a_id/7457/~~/propylene-glycols---viscosity-information)
- Eisenbrand, G., Pool-Zabel, B., Baker, V., Balls, M., Blaauboer, B. J., Boobis, A., Carere, A., Kerekordes, S., Lhugenot, C. J., Pieter, R. & Kleiner, J. (2002). Method of *in vitro* toxicology. **Food and Chemical Toxicology**, 40(2), 193-236.
- Gillbro, J. & Olsson, M. (2011). The melanogenesis and mechanism of skin-lightening agents – existing and new approaches. **International Journal of Cosmetic Science**, 33(3), 1-16.
- Gonderdi, X. (2008). **Photoageing**. Retrieved January 10, 2012, from <http://www.xprodosit.com/yazi/photo-ageing-nedir>
- Graf, E. (1992). Antioxidant potential of ferulic acid. **Free Radical Biology & Medicine**, 12(4), 435-438.
- Halliwell, B. (2009). The wandering of a free radical. **Free Radical Biology & Medicine**, 46(1), 531-542.

Hatzis, J. (2004). The wrinkle and its measurement-A skin surface profilometric method.

**Micron**, **35**(1), 201-209.

Hunt, K., Shao Kang, H. & Ernst, E. (2010). Botanical Extract as Anti-Aging Preparations for

the skin: A Systematic Review. **Drugs & Aging**, **27**(12), 973-985.

Javanmardi, J. J., Stushnoff, C. C., Locke, E. E. & Vivanco, J. M. (2003). Antioxidant activity and total phenolic content of Iranian *Ocimum* accessions. **Food Chemistry**, **83**(4), 547.

Jouni, U. (1979). Biochemistry of the Elastic fibers in Normal Connective Tissues and its

Alterations in Diseases. **Journal of Investigative Dermatology**, **72**(1), 1-10.

Mayuree Kanlayavattakul. & Nattaya Lourith. (2011). Sapodella seed coat as a multifunction

ingredient for cosmetic application. **Process Biochemistry**, **46**(11), 2215-2218.

Kim, Y. J. & Uyama, H. (2005). Tyrosinase inhibitors from natural and synthetic sources:

structure, inhibition mechanism and perspective for the future. **Cellular and Molecular Life Sciences**, **62**(15), 1707-1723.

Kin, J., Chan, S., Kim, L., Kim, Y., Hwang, J., Kim, K. & Kim, W. (2007). Design of optimal

solvent for extract of bio-active ingredients for mulberry leaves. **Biochemical Engineering Journal**, **37**(3), 271-278.

Kongshoj, B., Thorleifsson, A. & Wulf, H. (2006). Pheomelanin and eumelanin in human skin

determined by high-performance liquid chromatography and its relation to in vivo reflectance measurements. **Photodermatology, Photoimmunology & Photomedicine**, **22**(3), 141-147.

Kroon, P. A. & Williamson, G. (1999). Hydroxycinamates in plants and food: Current as future

perspectives. **Journal of the Science of Food and Agriculture**, **79**(3), 355-361.

- Nattay Lourith, Mayuree Kanlayavattanakul & Seetinee Chanpirom. (2009). Free radical scavenging efficacy of tamarind seed coat and its cosmetics application. **Journal of Health Research**, **23**(4), 159-162.
- Nont Thitilertdecha & Nuansri Rakariyatham. (2011). Phenolic content and free radical scavenging activities in rambutan during fruit maturation. **Molecules**, **129**(2), 247-252.
- Nont Thitilertdecha, Apiwat Teerawutgulrag & Nuansri Rakariyatham. (2011). Identification of major phenolic compound from *Nephelium lappaceum* L. extracts and their antioxidant activity. **Molecules**, **15**(1), 1453-1465.
- Nont Thitilertdecha, Apiwat Teerawutgulrag & Nuansri Rakariyatham. (2008). Antioxidant and antibacterial activities of *Nephelium lappaceum* L. extracts. **LWT- Food Science and Technology**, **41**(10), 2029-2035.
- Lupo, M. (2001). Antioxidant and vitamin in cosmetics. **Journal of Clinics in Dermatology**, **19**(4), 467-473.
- Miller, H. E., Rigelhof, F., Marquart, L., Prakash, A. & Kanter, M. (2000). Antioxidant content of whole grain breakfast cereals, fruits and vegetables. **Journal of the American College of Nutrition**, **19**(3), 312-319.
- Morton, J. F. (1987). Fruit of warm climates. Rambutan. **NC: Creative Resource Systems**.  
Florida: Julia
- Morante, N. (2011). **Basic Emulsion**. Retrieved June 15, 2011, from [http://www.specialchem4cosmetics.com/services/articles.aspx?id=3875&or=s151357\\_101\\_3875&q=emulsion+](http://www.specialchem4cosmetics.com/services/articles.aspx?id=3875&or=s151357_101_3875&q=emulsion+)
- Muller, L., Frohlich, K. & Bolm, V. (2011). Comparative antioxidant activity of carotenoids measured by ferric reducing antioxidant power (FRAP), ABTS bleaching assay (TEAC), DPPH assay and peroxy radical scavenging assay. **Food Chemistry**, **129**(10), 139-148.

- Okonogi, S., Duangrat, C., Anuchpreeda, S., Tachakittirungrod, S. & Chowwanapoonpohn, S. (2007). Comparison of antioxidant capacities and cytotoxicities of certain fruit peels. **Food Chemistry**, **103**(3), 839-846.
- Palanisamy, U., Cheng, H., Masilamani, T., Subramaniam, T., Ling, L. & Radhakrishnan, A. K. (2008). Rind of the rambutan, *Nephelium lappaceum*, a potential source of natural antioxidants. **Food Chemistry**, **109**(1), 54-63.
- Rice-Evan, C., Miller, J. & Paganga, G. (1996). Structure-antioxidant activity relationships of flavonoid and phenolic acids. **Free Radical Biology & Medicine**, **20**(7), 933-956.
- Rolim, A., Oishi, T., Macial, C., Zague, V., Pinto, C., Kaneko, T., Consiglieri, V. & Velasco, M. (2006). Total flavonoids quantification from O/W emulsion with extract of Brazilian plants. **International Journal of Pharmaceutics**, **308**(1), 107-114.
- Scgeibmeria, H. D., Christensen, K., Whitakers, S. H., Jegaethesan, J., Clancy, R. & Pierce, J. D. (2005). A review of free radical and antioxidants for critical care nurses. **Intensive and Critical Care Nursing**, **21**(1), 24-28.
- Schlossman, M. (2000). **The chemistry and manufacture of cosmetics volume I**. New york: Allured.
- Shrivastava, Y., Ravikumar, Y., Shanmugasundaram, N., Babu, M. & Nair, N. (2005). Cytotoxicity studies of chromium (III) complexes on human dermal fibroblasts. **Free Radical Biology & Medicine**, **38**(1), 58-69.
- Shui, G. & Leong, P. L. (2006). Residue from star fruit as valuable source for functional food ingredients and antioxidant nutraceuticals. **Food Chemistry**, **97**(1), 277-284.

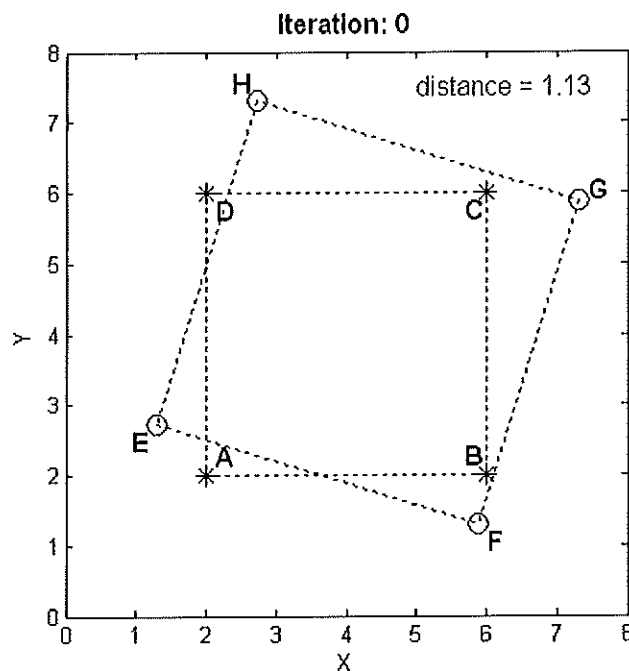
- Soobrattee, M. A., Neeragheen, V. S., Luximon-Ramma, A., Aruoma, O. I. & Bahorun, T. (2005). Phenolics as potential antioxidant therapeutic agents: Mechanism and actions. **Mutation Research**, **579**(1), 200-213.
- Sultana, B., Anwar, F. & Asharf, M. (2009). Effect of extract solvent/technique on the antioxidant activity of selected medicinal plant extracts. **Molecules**, **14**(1), 2167-2180.
- Tadros, F. T. (2009). **Emulsion science and technology**. German: Wiley.
- United Nations Economic and Social Commission for Asia and the Pacific (UNESCAP). (2007). **Rambutan**. Retrieved January 10, 2012, from <http://www.unapcaem.org/publication/F-fruits.PDF>
- Wickens, A. P. (2001). Ageing and the free radical theory. **Respiration Physiology**, **128**, 379-391.
- Wikipedia. (2011). **Jobba oil**. Retrieved November 12, 2011, from [http://en.wikipedia.org/wiki/jobba\\_oil](http://en.wikipedia.org/wiki/jobba_oil).
- Wikipedia. (2011). **Rambutan**. Retrieved June 20, 2011, from <http://en.wikipedia.org/wiki/Rambutan>.
- Zhou, K. & Yu, L. (2004). Effects of extraction solvent on wheat bran antioxidant activity estimation. **LWT- Food Science and Technology**, **37**(7), 717-721.

## **APPENDICES**

## APPENDIX A

### DEMONSTRATION OF ITERATIVE CLOSEST POINT PERFORMANCE

In Chapter 3 we mentioned about using Iterative Closest Point (ICP) algorithm to align the skulls to be the same position, orientation, and proportion. The purpose of this section is to presents the progression of the algorithm to clarify the idea of the ICP algorithm. The demonstration was presented in 2D version of the ICP algorithm to simplify the understanding.



**Figure A1** The Static Object with Asterisk-Marked at the Corner and the Moving Object with Circle-Marked at the Corner

To demonstrate the performance of the ICP algorithm, please see Figure A1, let the rectangle with asterisk-marked at the corners be the static object or target object and the rectangle with circle-marked at the corners be the moving object to be transformed to be the same position, orientation, and proportion as the target object using the ICP algorithm. In this section, the ICP algorithm from Chapter 3 was simplified from 3D approach to 2D approach to clarify the understanding. The ICP algorithm to align the moving object to the target object is as follows:

The ICP Algorithm

1. Initial transformation
2. Iterative procedure to minimize the average distance of closest point pairs between the target object and the moving object
  - 1) Calculate the distance between the target object and the moving object for the current iteration
  - 2) Calculate the distance between the target object and the moving object for the simulation of transforming the moving object as follows:
    - A. Move the object a small step in the following directions: up, down, left, and right
    - B. Rotate the object clockwise and counterclockwise for a small angle step
    - C. Scale the object up and down for a small step size
  - 3) Transform the object after the simulation that gives the minimum distance which is less than the distance of current iteration
  - 4) Terminate if there are no transformation that reduce the distance between the target object and the moving object

From the ICP algorithm, the initial transformation is presented in Figure A.1. From step 1, the distance between the target object and the moving object of this iteration or iteration 0 is 1.13. Definition of the distance between objects is the average value of the distance between closest point pairs from the objects. In this case, the closest point pairs between the objects are as follows: A and E, B and F, C and G, and H and I. The equation to calculate the distance between the objects is in equation (A.1).

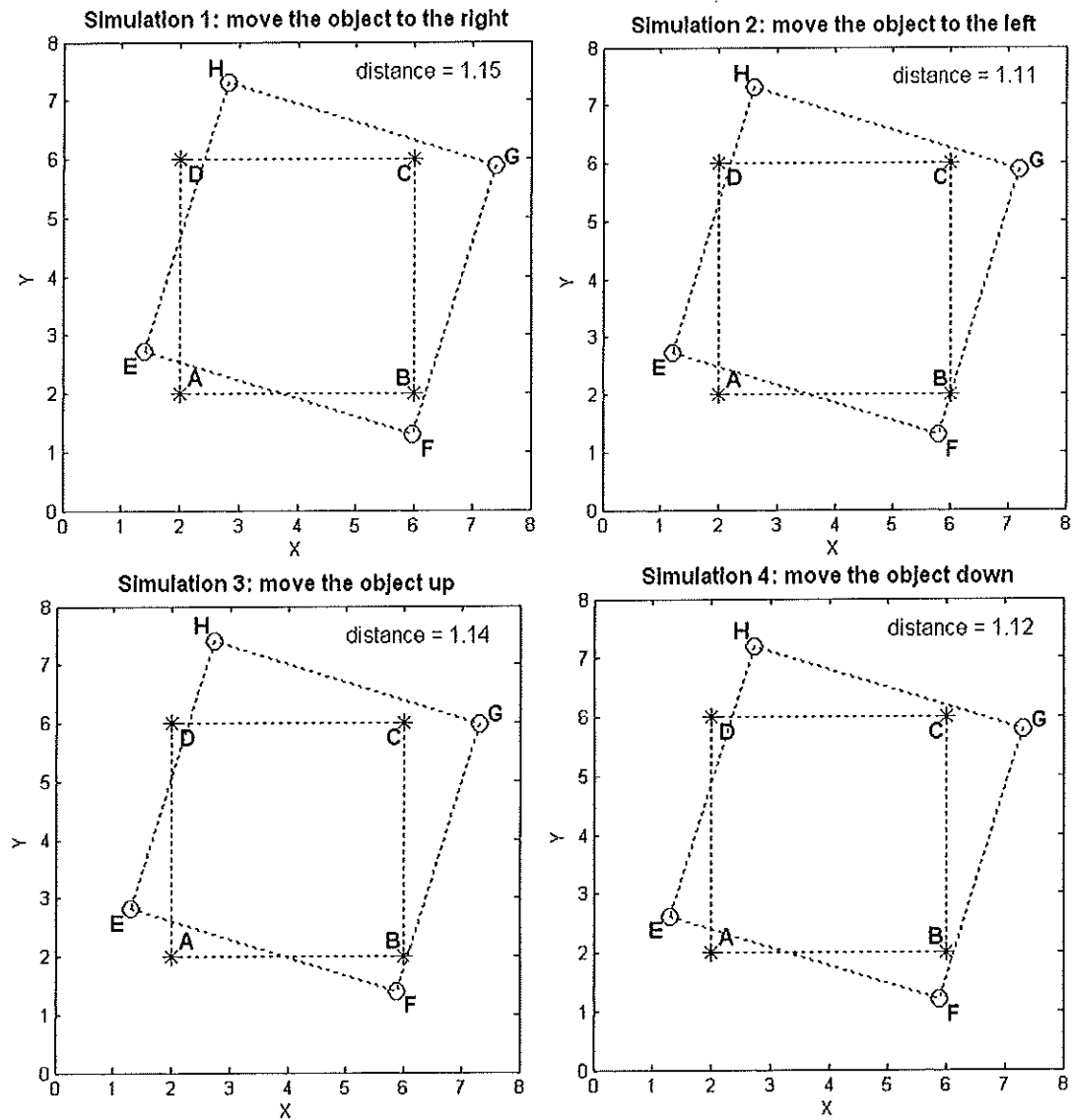
$$\text{distance} = (\overline{AE} + \overline{BF} + \overline{CG} + \overline{DH})/4 \quad (\text{A.1})$$



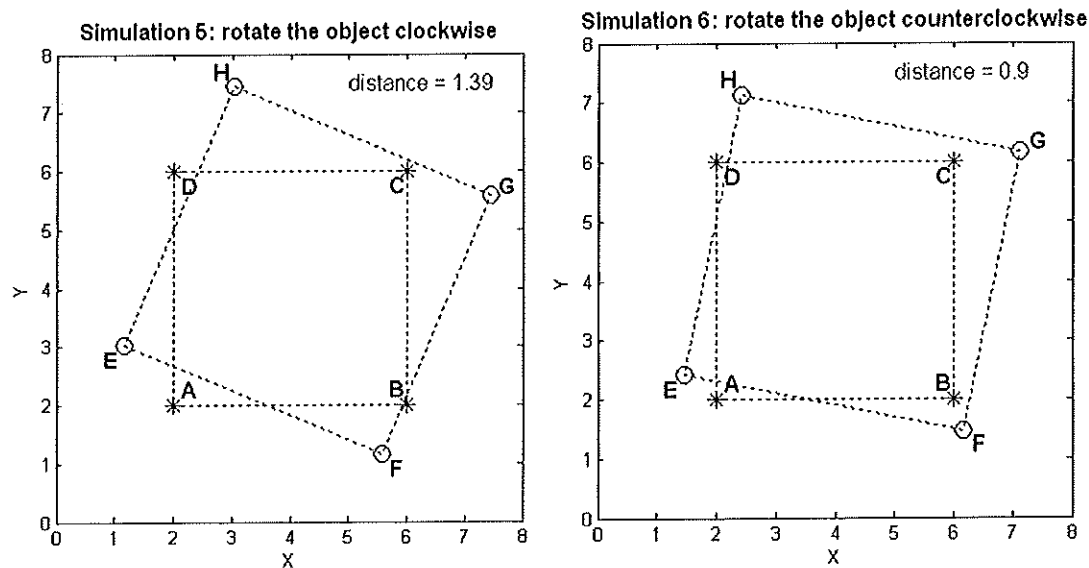
From step 2, all candidate transformations of the moving object were simulated. The simulations of moving object to the right, to the left, up, and down are presented in Figure A2. The simulations of rotation object clockwise and counterclockwise are presented in Figure A3. The simulations of scaling object down and up are presented in Figure A4.

From step 3, transformed the moving object after the simulation that gives the minimum distance which is less than the distance of current iteration. From Figure A2 to A.4, we found that the simulation of rotation the object counterclockwise in Figure A3 gives the minimum distance of 0.9 which is less than current iteration distance of 1.13. Hence, the object was then counterclockwise rotated and the next iteration was processed. The progression of the ICP algorithm implementation from iteration 0 to 27 is presented in Figure A5. At the iteration 27, since, there are no transformation that reduces the distance between the target object and the moving object, then the processing was terminated in step 4.

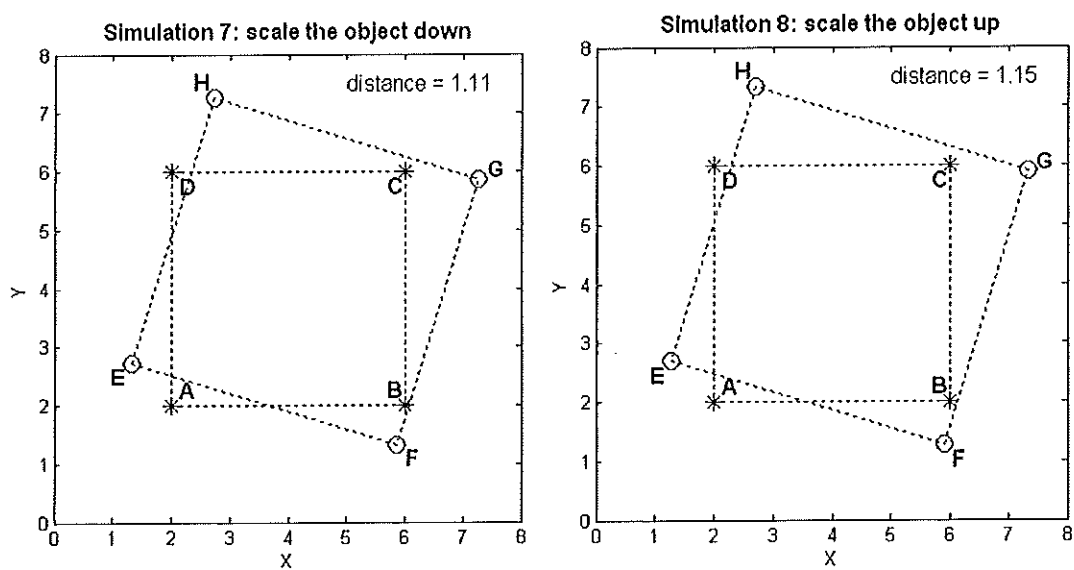
From Figure A5, we can see the progression of the ICP algorithm implementation from iteration 0 to 27. The moving object was iteratively moved, rotated, and scaled with the intention of providing the best transformation that minimized the distance between the moving object and the target object. From Figure A6 and Table A1, we can see the progression of the distance from the distance of 1.13 at iteration 0 to the distance of 0.00 at the iteration 27. In this case, we can see the convergence of the progression but please note that in general case the pre-alignment processing is needed prior processing the ICP algorithm to prevent the local minima phenomenon.



**Figure A2** The Simulations of Moving Object to the Right, to the Left, up, and Down



**Figure A3** The Simulations of Rotation Object Clockwise and Counterclockwise



**Figure A4** The Simulations of Scaling Object Down and Up.

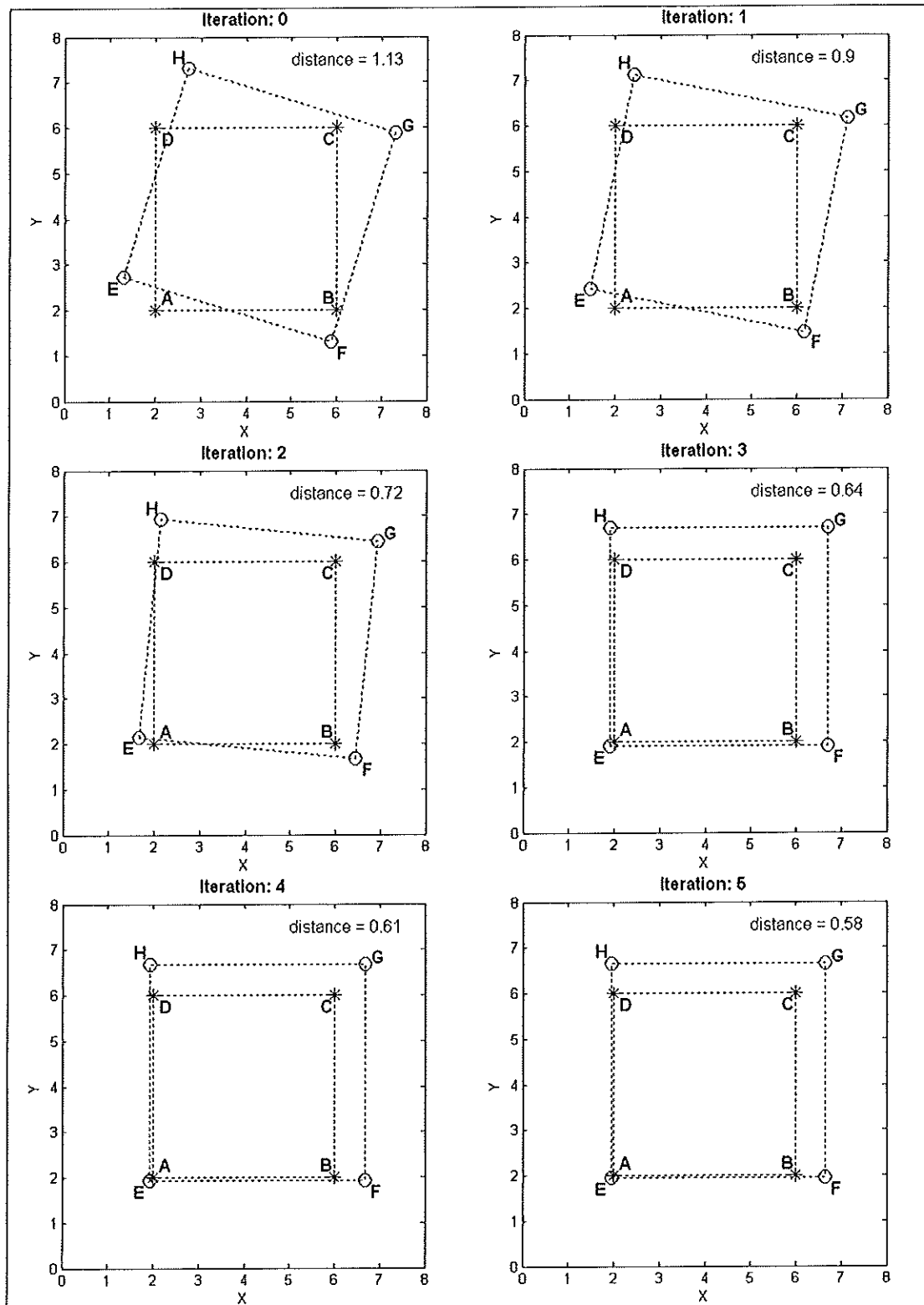


Figure A5 Progression of the ICP Algorithm Implementation from Iteration 0 to 27

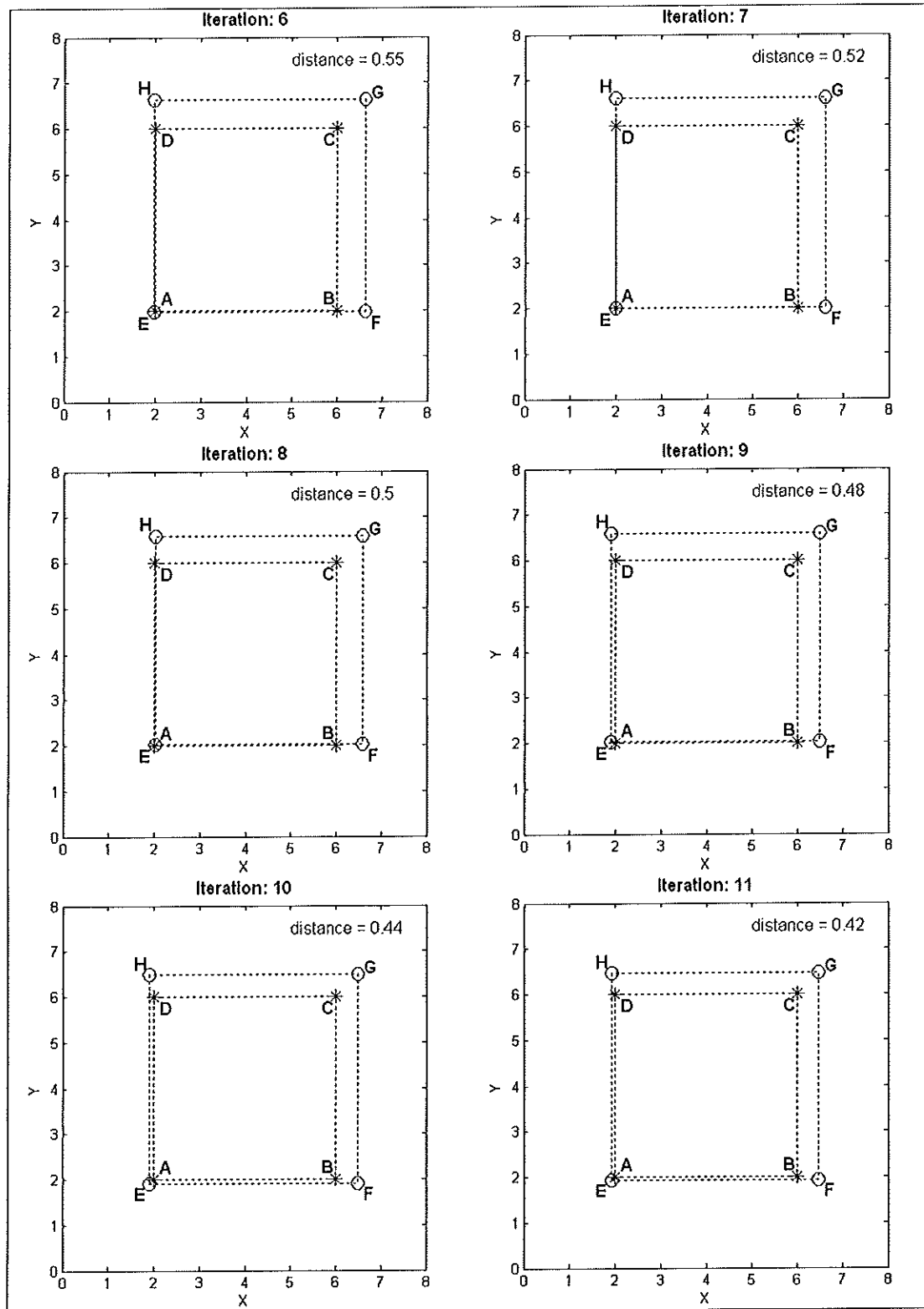


Figure A5 Progression of the ICP Algorithm Implementation from Iteration 0 to 27 (continued)

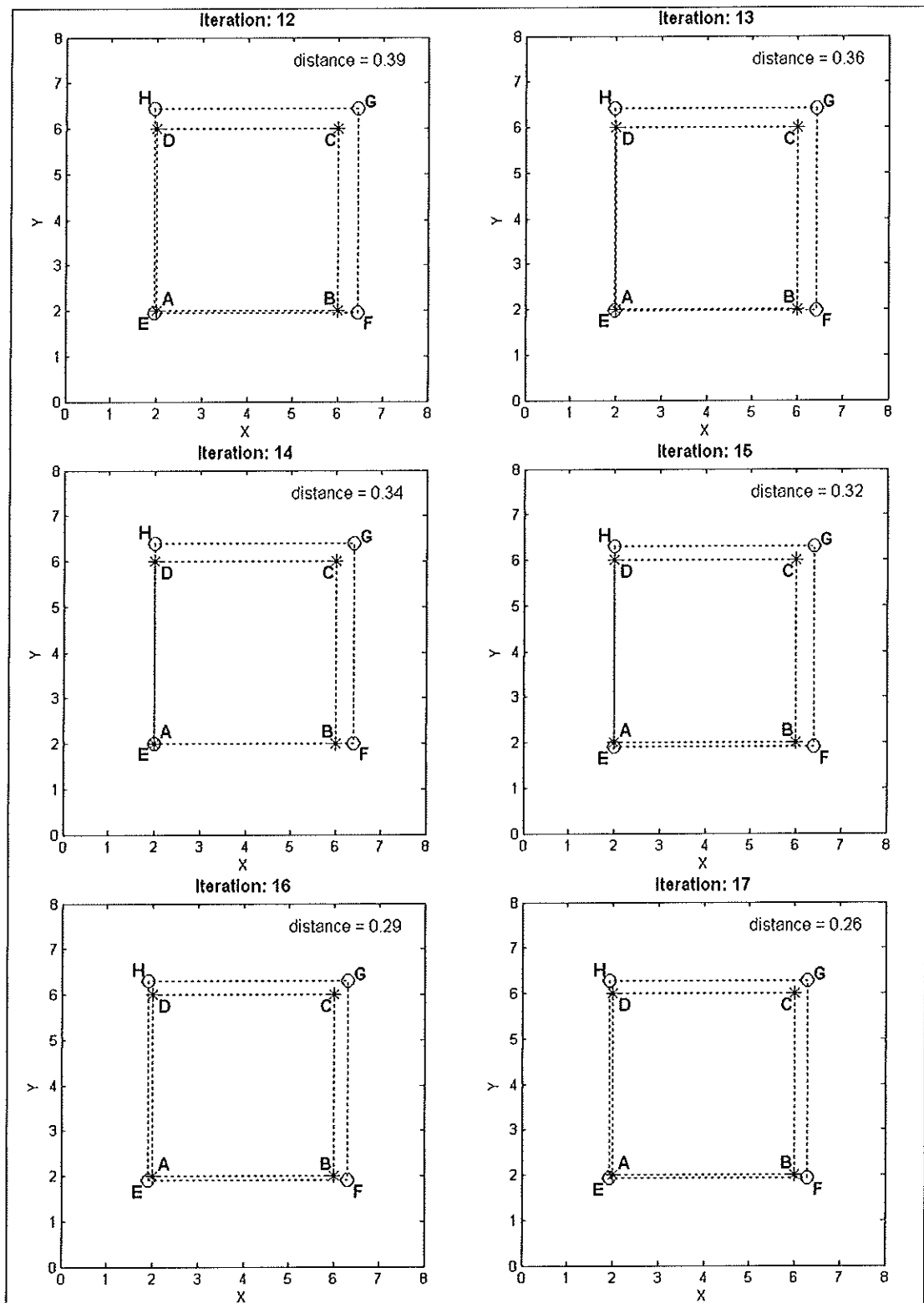


Figure A5 Progression of the ICP Algorithm Implementation from Iteration 0 to 27 (continued)

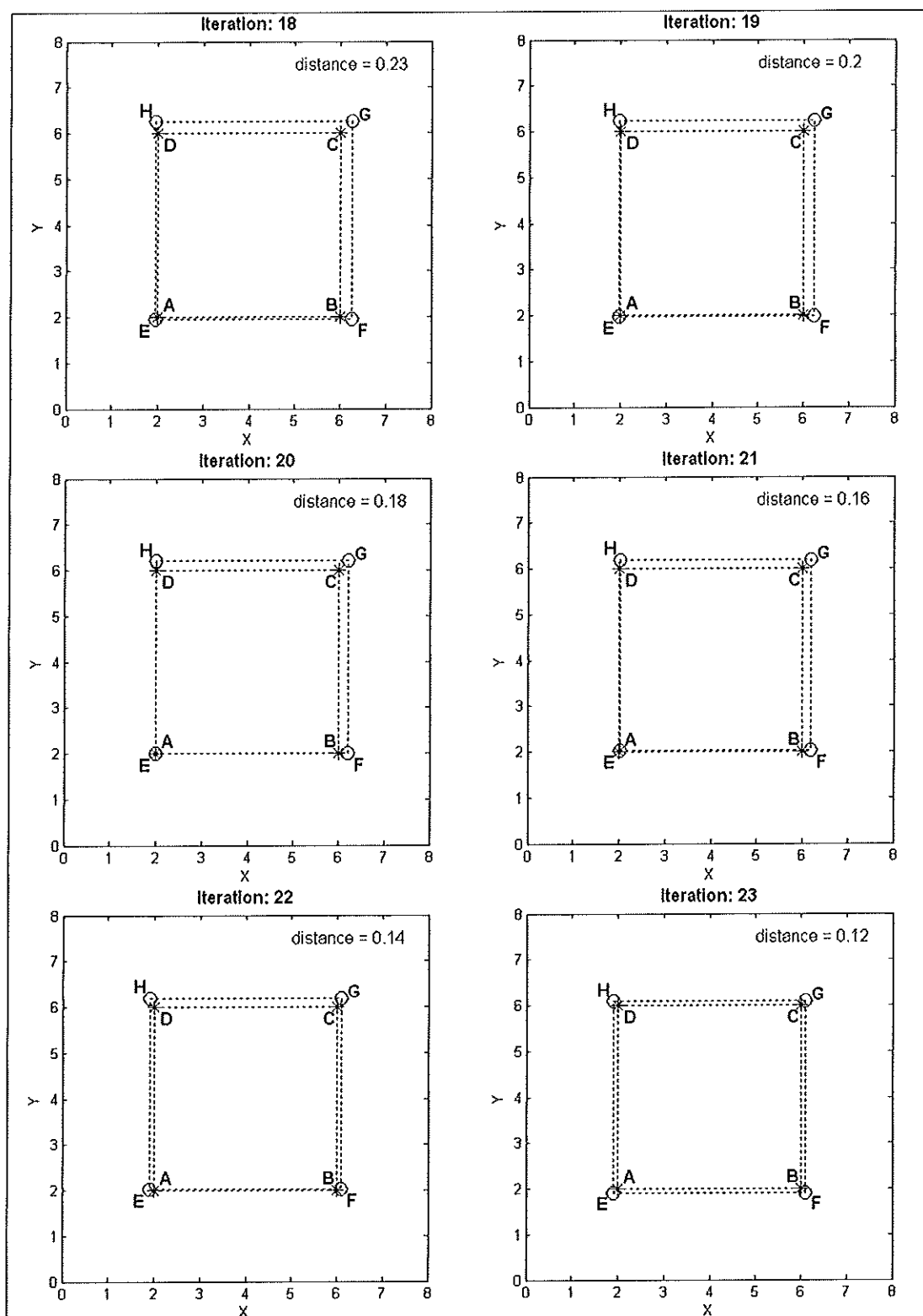


Figure A5 Progression of the ICP Algorithm Implementation from Iteration 0 to 27 (continued)

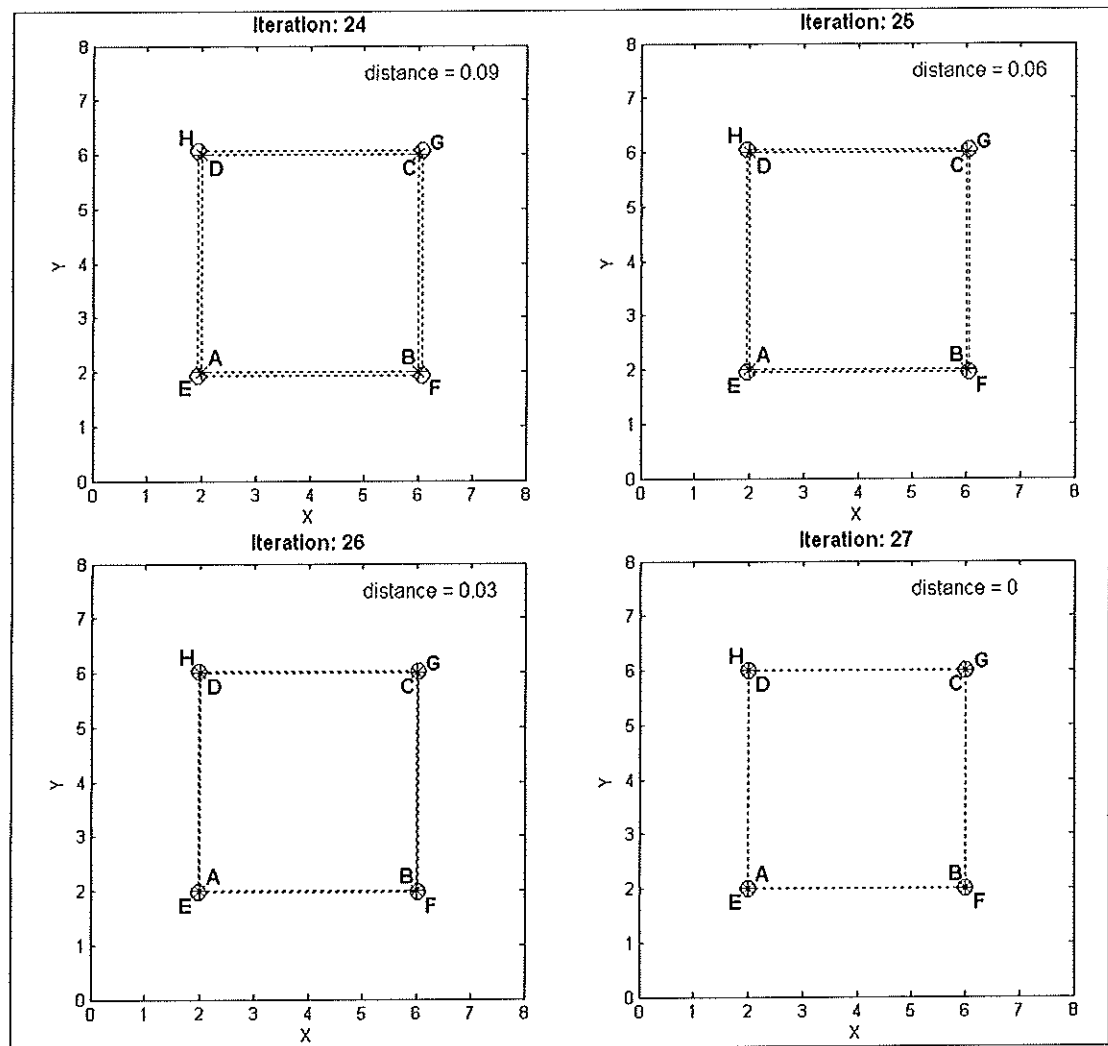
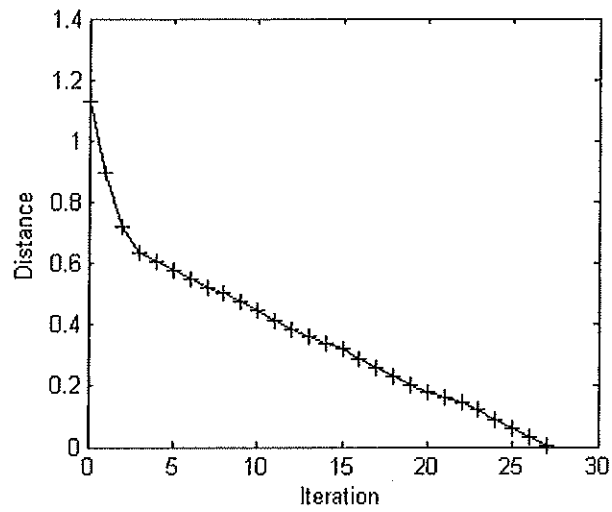


Figure A5 Progression of the ICP Algorithm Implementation from Iteration 0 to 27 (continued)





**Figure A6** Progression of the ICP Algorithm Implementation from Iteration 0 to 27

**Table A1** Progression of the ICP Algorithm Implementation from Iteration 0 to 27

Iteration	Distance	Iteration	Distance
0	1.13	14	0.34
1	0.90	15	0.32
2	0.72	16	0.29
3	0.64	17	0.26
4	0.61	18	0.23
5	0.58	19	0.20
6	0.55	20	0.18
7	0.52	21	0.16
8	0.50	22	0.14
9	0.48	23	0.12
10	0.44	24	0.09
11	0.42	25	0.06
12	0.39	26	0.03
13	0.36	27	0.00

## APPENDIX B

### FFD FORMULA DERIVATION

Free Form Deformation - FFD introduced by Sederberg and Parry (Sederberg, 2007; Sederberg & Parry, 1986; Song & Yang, 2005) is known to be a powerful shape modification method that has been applied to geometric modeling. This technique deforms an object by embedding it with in a solid defined with a control lattice. A change of the lattice deforms the solid and hence the object. FFD generally involves with 1D, 2D and also 3D data. This chapter presents the derivation of 1D, 2D and 3D FFD accordingly.

#### 1.1 1D FFD

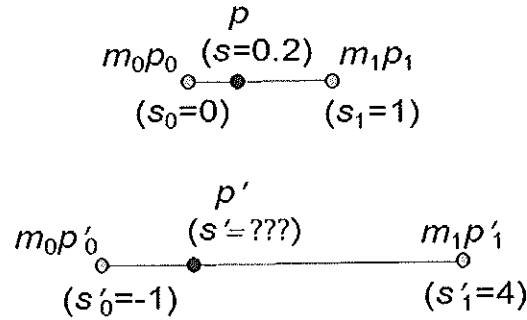


Figure B1 1D FDD, Upper: Before Deformation, Lower: After Deformation

Figure A1 shows the masses system containing two masses  $m_0$  locates at position  $p_0$  and  $m_1$  locates at position  $p_1$ . Before deformation, the position  $p_0$  has 1D position parameter  $s_0 = 0$ . The position  $p_1$  has 1D position parameter  $s_1 = 1$ . Let the position  $p$  is the center of mass system has 1D position parameter  $s$ . This system has to be satisfied with the center of mass equation (B.1).

$$p = (m_0 p_0 + m_1 p_1) / (m_0 + m_1) \quad (\text{B.1})$$

From (B.1), since there is only one position parameter we can rewrite (B.1) to (B.2) this way:

$$s = (m_0 s_0 + m_1 s_1) / (m_0 + m_1) \quad (\text{B.2})$$

Let the sum of masses in the system is equal to one as follow:

$$m_0 + m_1 = 1 \quad (\text{B.3})$$

Hence  $s_0 = 0$  and  $s_1 = 1$ , solving (B.2) from (B.3) gives the solutions

$$m_0 = 1 - s$$

$$m_1 = s$$

The deformation makes two control points move,  $p_0$  moves to  $p'_0$  and  $p_1$  moves to  $p'_1$ . We have to find the new position  $p'$  for old position  $p$  after the deformation of control point. The mass system has to be satisfied with (B.4) after the deformation.

$$p' = (m_0 p'_0 + m_1 p'_1) / (m_0 + m_1) \quad (\text{B.4})$$

From (B.4), since there is only one position parameter we can rewrite (B.4) to (B.5) this way:

$$s' = (m_0 s'_0 + m_1 s'_1) / (m_0 + m_1) \quad (\text{B.5})$$

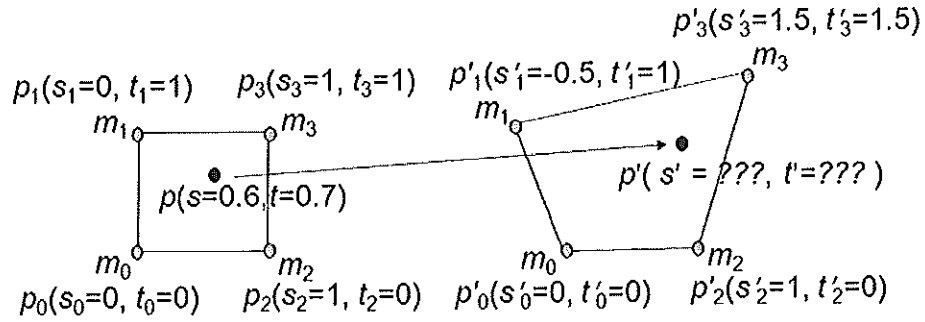
Hence  $m_0 = 1 - s$  and  $m_1 = s$ , solving (B.5) gives the solution

$$s' = (1 - s)s'_0 + ss'_1 \quad (\text{B.6})$$

Equation (B.6) is the formula of 1D FFD. The example computation of position  $p'$  locates at  $s'$  after the deformation in Figure B.1 using 1D FFD formula is as follow:

$$\begin{aligned} s' &= (1 - 0.2)(-1) + (0.2)(4) \\ &= (-0.8) + (0.8) \\ &= 0 \end{aligned}$$

## 1.2 2D FFD



**Figure B2** 2D FFD, left column: before deformation, right column: after deformation

Figure B2 shows the masses system containing four masses  $m_0$ ,  $m_1$ ,  $m_2$  and  $m_3$  locate at position  $p_0$ ,  $p_1$ ,  $p_2$  and  $p_3$  accordingly. Let the position  $p$  is the center of masses system has 2D position parameter  $s$  and  $t$ . This system has to be satisfied with the center of mass equation in two dimensions (see Equation (B.7) and Equation (B.8)).

$$s = (m_0 s_0 + m_1 s_1 + m_2 s_2 + m_3 s_3) / (m_0 + m_1 + m_2 + m_3) \quad (\text{B.7})$$

$$t = (m_0 t_0 + m_1 t_1 + m_2 t_2 + m_3 t_3) / (m_0 + m_1 + m_2 + m_3) \quad (\text{B.8})$$

Let the sum of masses in the system is equal to one as follow:

$$m_0 + m_1 + m_2 + m_3 = 1 \quad (\text{B.9})$$

Let (B.10) presents the relation between four masses. This equation also called mass balance equation.

$$m_0 m_3 = m_1 m_2 \quad (\text{B.10})$$

Hence  $s_0 = 0$ ,  $s_1 = 0$ ,  $s_2 = 1$  and  $s_3 = 1$  solving (B.7) from (B.9) gives the solution

$$s = m_2 + m_3 \quad (\text{B.11})$$

Hence  $t_0 = 0$ ,  $t_1 = 1$ ,  $t_2 = 0$  and  $t_3 = 1$  solving (B.8) from (B.9) gives the solution

$$t = m_1 + m_3 \quad (\text{B.12})$$

In this step we substitute (B.11) in (B.9), we thus obtain

$$1 - s = m_0 + m_1 \quad (\text{B.13})$$

In this step we substitute (B.12) in (B.9), we thus obtain

$$1 - t = m_0 + m_2 \quad (\text{B.14})$$

Then multiply (B.13) with (B.14) gives the solution

$$\begin{aligned} (m_0 + m_1)(m_0 + m_2) &= (1 - s)(1 - t) \\ m_0m_0 + m_0m_2 + m_0m_1 + m_1m_2 &= (1 - s)(1 - t) \end{aligned}$$

Consider (B.10) we obtain

$$\begin{aligned} m_0m_0 + m_0m_2 + m_0m_1 + m_0m_3 &= (1 - s)(1 - t) \\ m_0(m_0 + m_1 + m_2 + m_3) &= (1 - s)(1 - t) \end{aligned}$$

Consider (B.9) we obtain

$$m_0 = (1 - s)(1 - t)$$

We can find  $m_1$  in the same manner. Starting from multiplication (B.12) and (B.13)

$$\begin{aligned} (m_0 + m_1)(m_1 + m_3) &= (1 - s)t \\ m_0m_1 + m_0m_3 + m_1m_1 + m_1m_3 &= (1 - s)t \\ m_0m_1 + m_1m_2 + m_1m_1 + m_1m_3 &= (1 - s)t \\ m_1(m_0 + m_1 + m_2 + m_3) &= (1 - s)t \\ m_1 &= (1 - s)t \end{aligned}$$

We can find  $m_2$  in the same manner. Starting from multiplication (B.11) and (B.14)

$$\begin{aligned}
(m_2 + m_3)(m_0 + m_2) &= s(1 - t) \\
m_0m_2 + m_2m_2 + m_0m_3 + m_2m_3 &= s(1 - t) \\
m_0m_2 + m_2m_2 + m_1m_2 + m_2m_3 &= s(1 - t) \\
m_2(m_0 + m_1 + m_2 + m_3) &= s(1 - t) \\
m_2 &= s(1 - t)
\end{aligned}$$

We can find  $m_3$  in the same manner. Starting from multiplication (B.11) and (B.12)

$$\begin{aligned}
(m_2 + m_3)(m_1 + m_3) &= st \\
m_1m_2 + m_2m_3 + m_1m_3 + m_3m_3 &= st \\
m_0m_3 + m_2m_3 + m_1m_3 + m_3m_3 &= st \\
m_3(m_0 + m_1 + m_2 + m_3) &= st \\
m_3 &= st
\end{aligned}$$

Finally, we have all masses in form of  $s$  and  $t$  as follows:

$$\begin{aligned}
m_0 &= (1 - s)(1 - t) \\
m_1 &= (1 - s)t \\
m_2 &= s(1 - t) \\
m_3 &= st
\end{aligned}$$

After deformation, the masses system are satisfied with center of masses equation

$$\begin{aligned}
s' &= (m_0s'_0 + m_1s'_1 + m_2s'_2 + m_3s'_3) / (m_0 + m_1 + m_2 + m_3) \\
t' &= (m_0t'_0 + m_1t'_1 + m_2t'_2 + m_3t'_3) / (m_0 + m_1 + m_2 + m_3)
\end{aligned}$$

Hence the sum of all masses is equal to one, so we obtain

$$\begin{aligned}
s' &= m_0s'_0 + m_1s'_1 + m_2s'_2 + m_3s'_3 \\
t' &= m_0t'_0 + m_1t'_1 + m_2t'_2 + m_3t'_3
\end{aligned}$$

The two equations above are the formula of 2D FFD. The example computation of position  $p'$  locates at  $(s', t')$  after the deformation in Figure B2 using 2D FFD formula is as follow:

$$s' = m_0 s'_0 + m_1 s'_1 + m_2 s'_2 + m_3 s'_3$$

$$s' = (1-s)(1-t)s'_0 + (1-s)ts'_1 + s(1-t)s'_2 + sts'_3$$

$$s' = (0) + (1-0.6)(0.7)(-0.5) + (0.6)(1-0.7)(1) + (0.6)(0.7)(1.5)$$

$$s' = 0.67$$

$$t' = m_0 t'_0 + m_1 t'_1 + m_2 t'_2 + m_3 t'_3$$

$$t' = (1-s)(1-t)t'_0 + (1-s)tt'_1 + s(1-t)t'_2 + stt'_3$$

$$t' = (0) + (1-0.6)(0.7)(1) + (0.6)(1-0.7)(0) + (0.6)(0.7)(1.5)$$

$$t' = 0.91$$

### 1.3 3D FFD

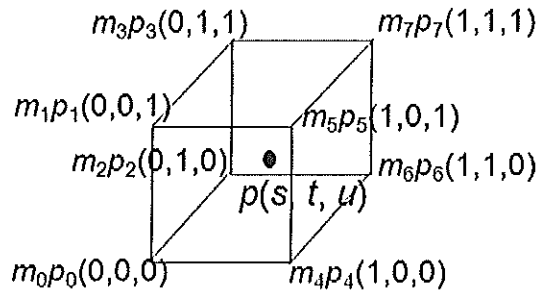


Figure B3 3D Masses System

Figure B3 shows the masses system containing eight masses  $m_0$  through  $m_7$  located at position  $p_0$  through  $p_7$  accordingly. Let the position  $p$  is the center of mass system has 3D position parameter  $s$ ,  $t$  and  $u$ . The control points  $p_i$  locate at coordinate  $(s_i, t_i, u_i)$ . This system has to be satisfied with the center of mass equation as follow:

$$p = \frac{\sum_{i=0}^7 m_i p_i}{\sum_{i=0}^7 m_i} \quad (\text{B.15})$$

Let the summation of all masses is equal to one and split (B.15) into three equations in three directions obtain

$$m_0 + m_1 + m_2 + m_3 + m_4 + m_5 + m_6 + m_7 = 1 \quad (\text{B.16})$$

$$s = \sum_{i=0}^7 m_i s_i \quad (\text{B.17})$$

$$t = \sum_{i=0}^7 m_i t_i \quad (\text{B.18})$$

$$u = \sum_{i=0}^7 m_i u_i \quad (\text{B.19})$$

Substituting  $s_i$ ,  $t_i$  and  $u_i$  from Figure A3 into (B.17), (B.18) and (B.19) accordingly gives

$$m_4 + m_5 + m_6 + m_7 = s \quad (\text{B.20})$$

$$m_2 + m_3 + m_6 + m_7 = t \quad (\text{B.21})$$

$$m_1 + m_3 + m_5 + m_7 = u \quad (\text{B.22})$$

Substituting (B.20) into (B.16) gives

$$m_0 + m_1 + m_2 + m_3 = 1 - s \quad (\text{B.23})$$

Substituting (B.21) into (B.16) gives

$$m_0 + m_1 + m_4 + m_5 = 1 - t \quad (\text{B.24})$$

Substituting (B.22) into (B.16) gives

$$m_0 + m_2 + m_4 + m_6 = 1 - u \quad (\text{B.25})$$

At this step, there are the mass balance equations as follows:

$$m_0 m_3 = m_1 m_2, m_0 m_5 = m_1 m_4, m_0 m_6 = m_2 m_4,$$

$$m_2 m_7 = m_3 m_6, m_1 m_7 = m_3 m_5, m_4 m_7 = m_5 m_6,$$

$$m_0 m_7 = m_1 m_6 = m_2 m_5 = m_3 m_4$$

Multiplying (B.23)  $\times$  (B.24)  $\times$  (B.25) gives

$$(1-s)(1-t)(1-u) = (m_0+m_1+m_2+m_3)(m_0+m_1+m_4+m_5)(m_0+m_2+m_4+m_6) \quad (\text{B.26})$$

Expanding the multiplication and consider the masses balance equation gives



$$\begin{aligned}
(1-s)(1-t)(1-u) = & m_0(m_0 + m_1 + m_2 + m_3 + m_4 + m_5 + m_6 + m_7) + \\
& m_1(m_0 + m_1 + m_2 + m_3 + m_4 + m_5 + m_6 + m_7) + \\
& m_2(m_0 + m_1 + m_2 + m_3 + m_4 + m_5 + m_6 + m_7) + \\
& m_3(m_0 + m_1 + m_2 + m_3 + m_4 + m_5 + m_6 + m_7) + \\
& m_4(m_0 + m_1 + m_2 + m_3 + m_4 + m_5 + m_6 + m_7) + \\
& m_5(m_0 + m_1 + m_2 + m_3 + m_4 + m_5 + m_6 + m_7) + \\
& m_6(m_0 + m_1 + m_2 + m_3 + m_4 + m_5 + m_6 + m_7) + \\
& m_7(m_0 + m_1 + m_2 + m_3 + m_4 + m_5 + m_6 + m_7)
\end{aligned}$$

Consider (B.16) we have

$$m_0 = (1-s)(1-t)(1-u)$$

At this step, we can find  $m_1$  through  $m_7$  in the same manner, finally we have

$$m_1 = (1-s)(1-t)u$$

$$m_2 = (1-s)t(1-u)$$

$$m_3 = (1-s)tu$$

$$m_4 = s(1-t)(1-u)$$

$$m_5 = s(1-t)u$$

$$m_6 = st(1-u)$$

$$m_7 = stu$$

After the deformation the masses system has to be satisfied with center of masses equation

$$p' = \frac{\sum_{i=0}^7 m_i p'_i}{\sum_{i=0}^7 m_i} \quad (\text{B.27})$$

Hence the summation of all masses is equal to one and all point has three dimensional coordinate, splitting (B.27) into three equations and using value of  $m_0$  through  $m_7$  gives the 3D FFD formula as follows:

$$s' = (1-s)(1-t)(1-u)s'_0 + (1-s)(1-t)us'_1 + (1-s)t(1-u)s'_2 + \\ (1-s)tus'_3 + s(1-t)(1-u)s'_4 + s(1-t)us'_5 + st(1-u)s'_6 + stus'_7$$

$$t' = (1-s)(1-t)(1-u)t'_0 + (1-s)(1-t)ut'_1 + (1-s)t(1-u)t'_2 + \\ (1-s)tut'_3 + s(1-t)(1-u)t'_4 + s(1-t)ut'_5 + st(1-u)t'_6 + stut'_7$$

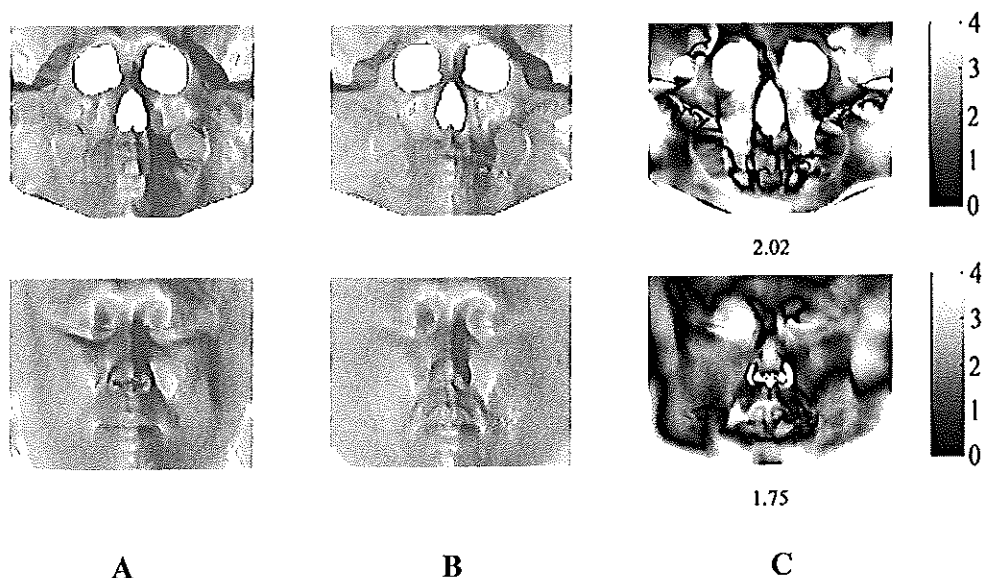
$$u' = (1-s)(1-t)(1-u)u'_0 + (1-s)(1-t)uu'_1 + (1-s)t(1-u)u'_2 + \\ (1-s)tuu'_3 + s(1-t)(1-u)u'_4 + s(1-t)uu'_5 + st(1-u)u'_6 + stuu'_7$$

These above three equations are the 3D FFD formula to find the new position  $p'$  at coordinate  $(s', t', u')$  from old position  $p$  at coordinate  $(s, t, u)$  due to the relocation of all control points from old positions  $p_0$  at coordinate  $(s_0, t_0, u_0)$  through  $p_7$  at coordinate  $(s_7, t_7, u_7)$  to new positions  $p'_0$  at coordinate  $(s'_0, t'_0, u'_0)$  through  $p'_7$  at coordinate  $(s'_7, t'_7, u'_7)$ .

## APPENDIX C

### DEMONSTRATION OF ABSOLUTE ERROR CALCULATION BETWEEN TWO CYLINDRICAL PROJECTION SURFACES

As mentioned in Chapter 3, in order to compare skull and face, the 3D head models have to be transformed onto the plane using a cylindrical projection. The advantage of cylindrical projection is the convenient to compute absolute error between two 3D surfaces which can be directly computed from the different of the intensity from each corresponded pixel. Figure C1 shows the absolute errors of cylindrical projection surfaces. In Figure C1, upper row shows the comparison between two skulls, lower row shows the comparison between two faces.



**Figure C1** Absolute Errors of Cylindrical Projection Surfaces Upper Row: The Comparison Between Two Skulls, Lower Row: The Comparison Between Two Faces (A) Target Head (B) Reference Head (C) Absolute Errors Surface when Compare Reference Head to Target Head. Errors are Measured in mm.

The calculation of absolute errors of cylindrical projection surfaces is presented in Figure C2. Figure C2A is the target skull. Figure C2B is the reference skull. Figure C2C is the absolute errors surface when compare target skull to reference skull. The pixel value in the white rectangle areas are presented in the left column. Absolute error between two surfaces can be directly computed from the different of the pixel value from each corresponded pixel as presented in Equation C1

$$C_{ij} = |A_{ij} - B_{ij}| \quad (C.1)$$

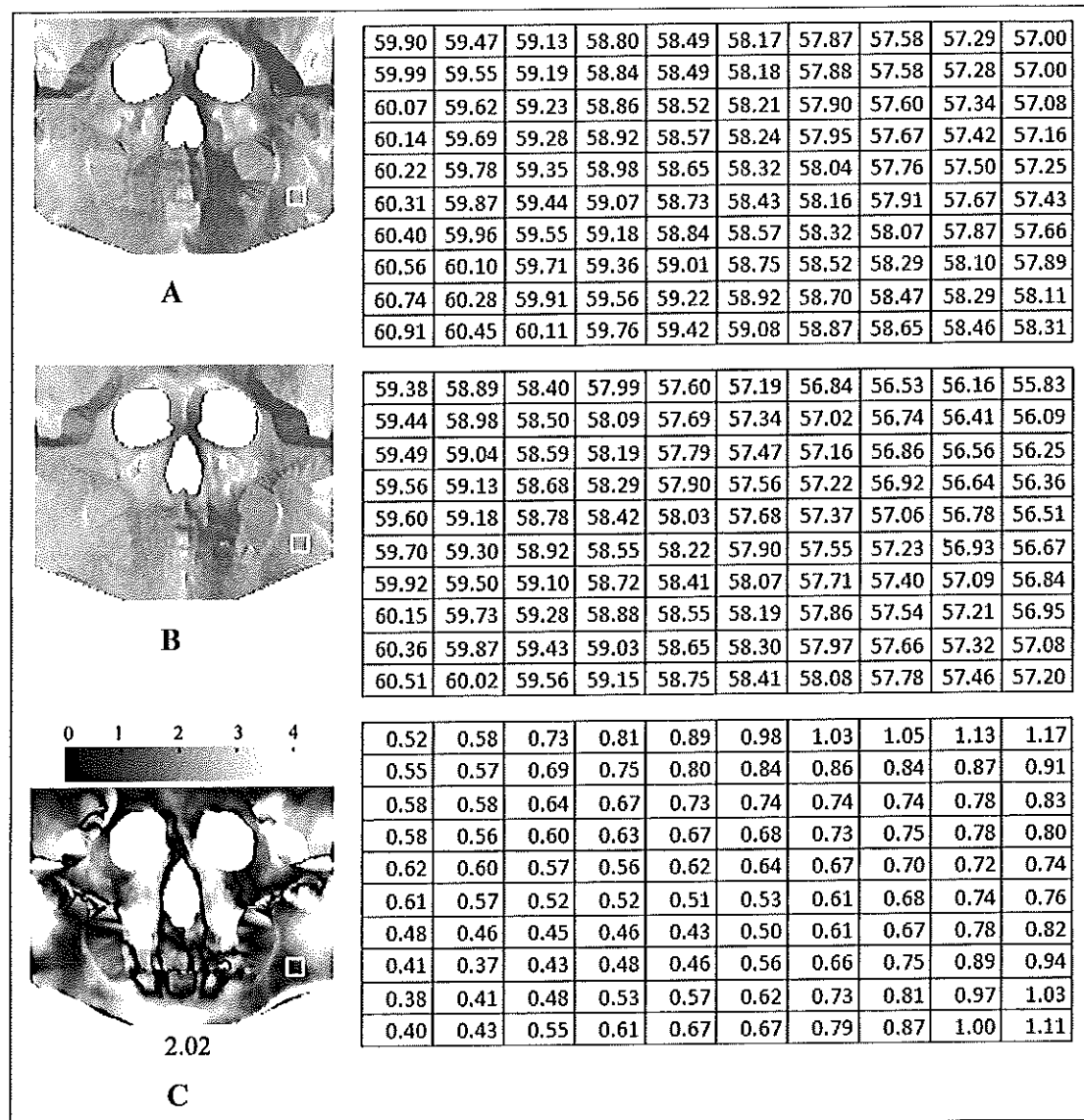
Where  $C_{ij}$  is the pixel value of image  $C$  at row  $i$  column  $j$  which is the absolute value of different between image  $A$  and image  $B$  at row  $i$  column  $j$ . In this case,  $A$  is the target head and  $B$  is the reference head.

The averaging of absolute error gives the idea of how much different between two surfaces. The calculation of this value is presented in Equation C.2.

$$C = \frac{\sum_{i=1}^M \sum_{j=1}^N C_{ij}}{M*N} \quad (C.2)$$

Where  $M$  is the number of row of image  $C$  and  $N$  is the number of column of image  $C$ .

From Figure C2C, the darker pixels indicate the lower errors and the brighter pixels indicate the higher errors. Presenting this way gives the idea of where and how different between two surfaces. The value 2.02 is the average value of all absolute errors giving the overall difference information.

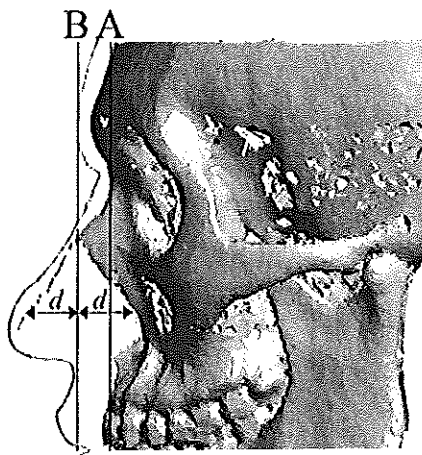


**Figure C2** Calculation of Absolute Errors of Cylindrical Projection Surfaces. (A) Target Skull (B) Reference Skull (C) Absolute Errors Surface when Compare Target Skull to Reference Skull. Errors are Measured in mm.

## APPENDIX D

### THE EVALUATION OF NOSE PROFILE ESTIMATION FROM NASAL APERTURE FOR THAI PEOPLE

In Chapter 3, we mentioned about nose profile estimation from nasal aperture in order to compare the two cylindrical projection surfaces of skull at the nasal part. Because there is less information from nasal aperture, so we have to estimate the nose profile to provide more information for comparing purpose. Figure D1 shows the nose profile estimation method used in this work which was based on the work of Prokobec and Ubelaker (2002). From Figure D1, line A dissects the nasion and prosthion. Line B is parallel to line A and intersects the foremost point on the nasal bone. For each point of nasal aperture, the distance  $d$  from line B to the nasal aperture are calculated and mirrored to form the nasal profile estimation.

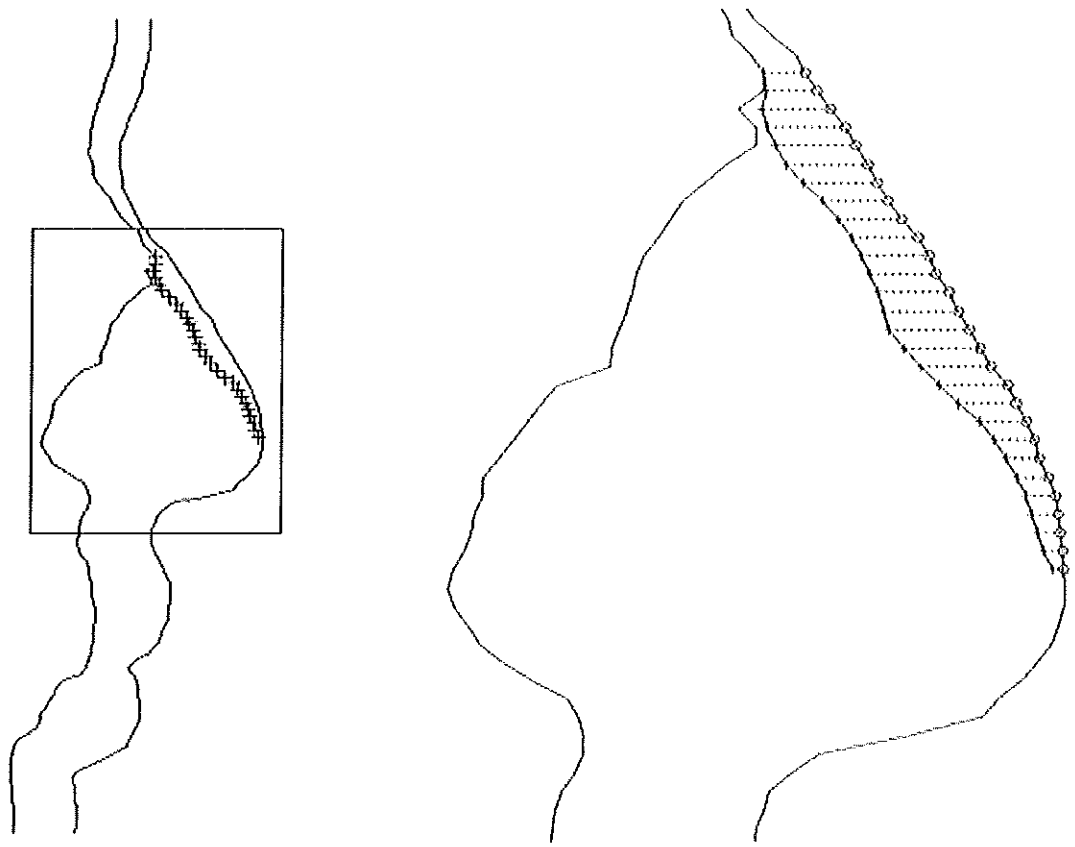


**Figure D1** Nose Profile Estimation from Nasal Aperture. Line A Dissects the Nasion and Prosthion. Line B is Parallel to Line A and Intersects the Foremost Point on the Nasal Bone. For Each Point of Nasal Aperture, the Distance From Line B to the Nasal Aperture are Calculated and Mirrored to form the Nasal Profile Estimation.

Because the purpose of this work is to reconstruct the face of Thai people but this method was originally designed for Caucasoid people, so we have to know whether this method can be used for Thai people. Therefore, the error and the result of this method should be inspected before accepted to be used in this work. Measurement of nose profile estimation error is shown in Figure D2. The rectangle region in the left column was magnified and detail added to the right column to be clearly seen. The line with cross marked indicates the estimation line. The line with circle marked indicates the expected line. The cross and the circle are marked every vertical step of 1 mm. The error of estimation is the average value of distance between all pair of cross and circle. The results and the errors of nose profile estimation for Thai people in the head database are shown in Figure D3 to D5. The summary of all estimation errors is shown in Table D1.

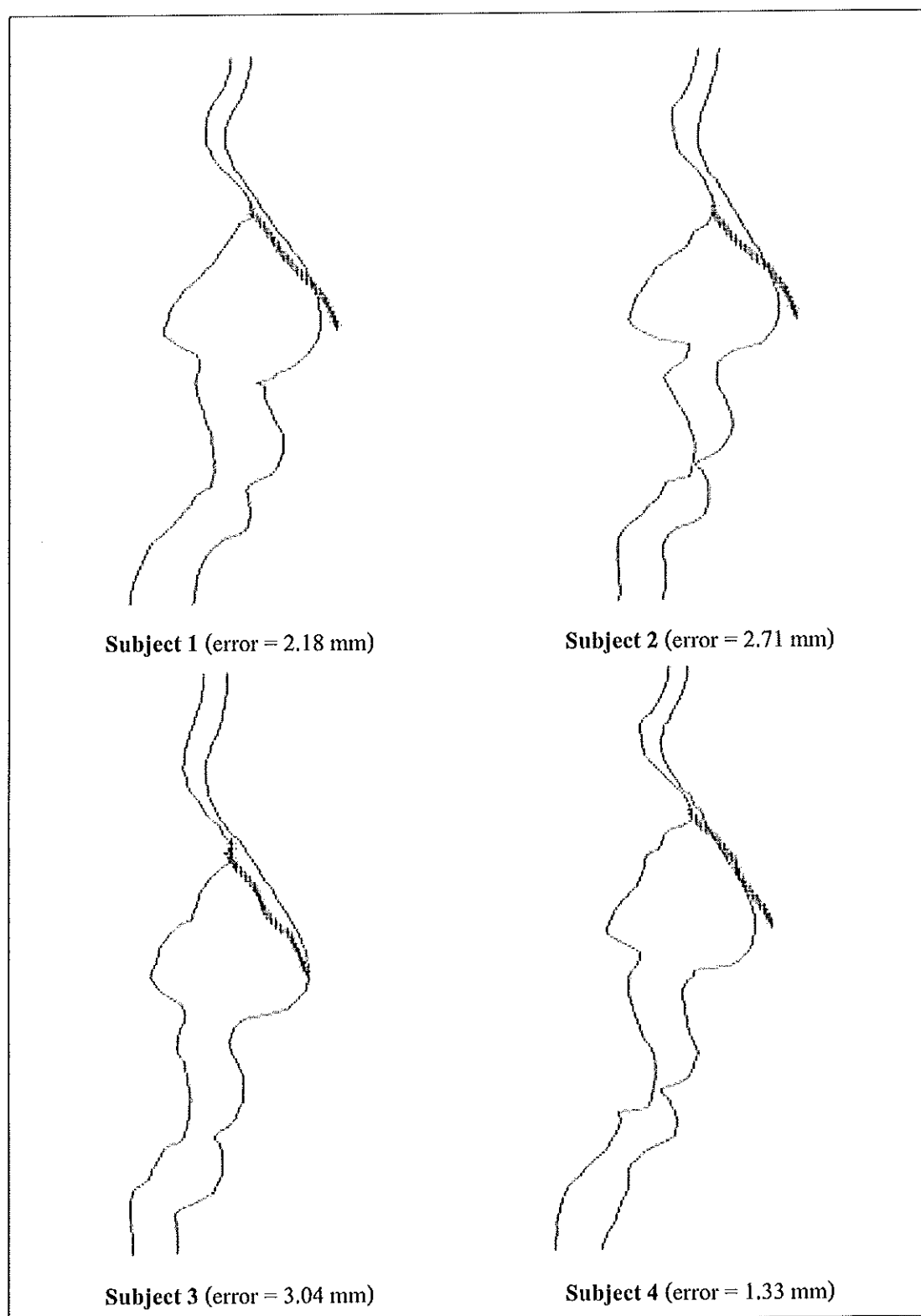
As seen in Figure D3, the estimations of subject 1 and 4 were considered as good estimation both for visual inspection and for achieving estimation errors of 1.33 mm and 2.18 mm accordingly. The estimation of subject 2 was considered as slightly too high for visual inspection corresponding to the error of 2.71 mm. The estimation of subject 3 was considered as slightly too low corresponding to the error of 3.04 mm. From Figure D4, the estimation of subject 8 was considered as best estimation both for visual inspection and achieving error of 2.41 mm. The estimations of subject 5 and subject 7 were considered as slightly too low corresponding to the errors of 3.93 mm and 4.54 mm. The estimation of subject 6 was considered as slightly too high corresponding to the error of 3.45 mm. From Figure D5, the estimations of subject 9, 10, and 11 were considered as slightly too low with the errors of 4.39 mm, 7.03, and 5.09 mm accordingly. Except for the estimation of subject 10 which was the worst estimation from this experiment, others result provided acceptable nose profile estimation. Although all the results did not much accurate estimation, it anyway can give the preliminary idea of how nose of the subject should be.

In conclusion, we are pleased with nose profile estimation results from this method because the purpose of nose profile estimation here is to provide more information about nose to be compared with other skulls, not to produce exactly the same nose profile of real subject. At this point, we considered that the results from this method was met the purpose of providing additional information apart from nasal aperture. So, we accepted to use this method in this work for the nose profile estimation phase.

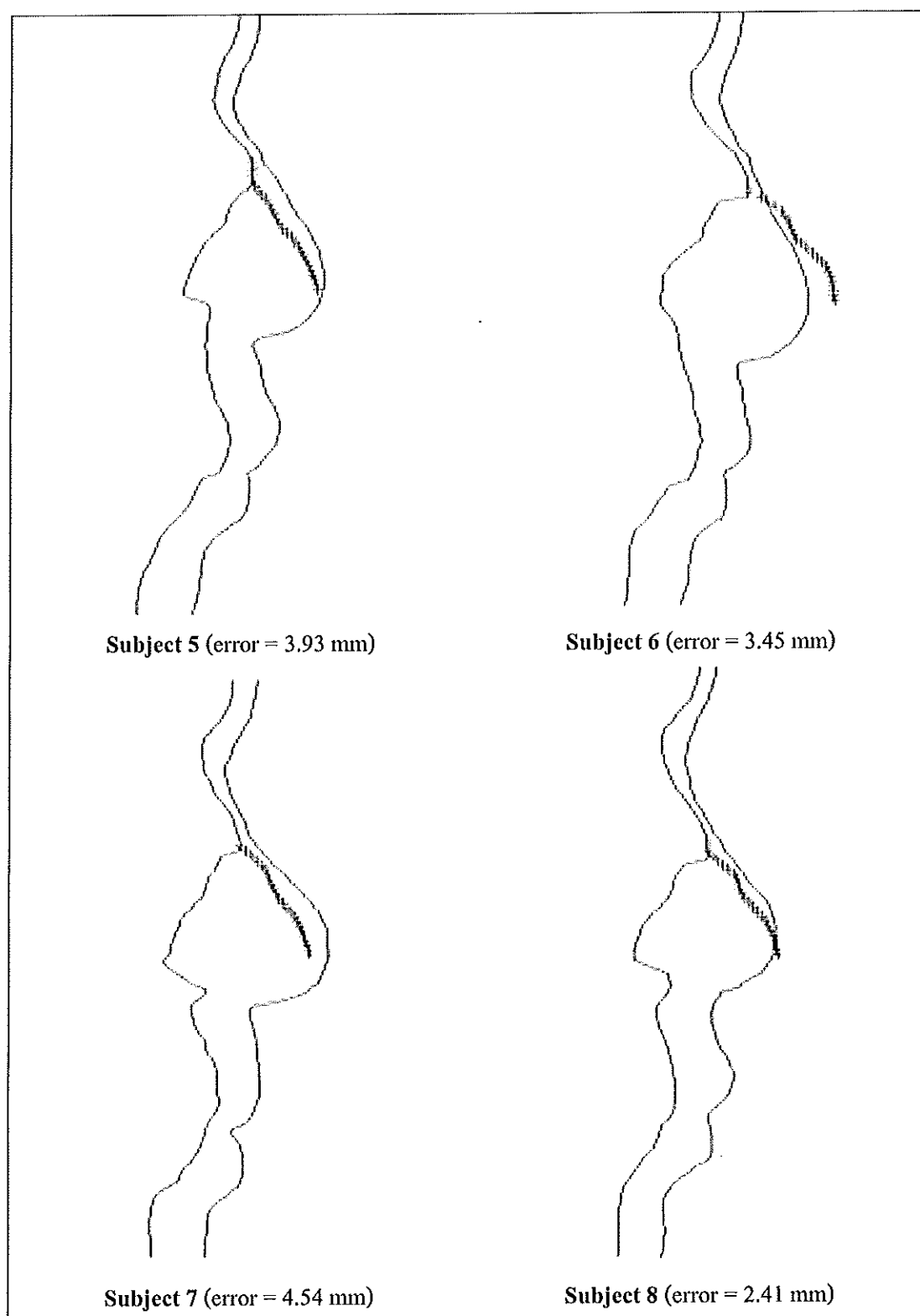


**Figure D2** Measurement of Nose profile Estimation Error. The Rectangle Region in the Left Column was Magnified and Detail Added to the Right Column to be Clearly Seen. The Line with Cross Marked Indicates the Estimation Line. The Line with Circle Marked Indicates the Expected Line. The Cross and the Circle are Marked Every Vertical Step of 1 mm. The Error of Estimation is the Average Value of Distance Between all Pair of Cross and Circle.

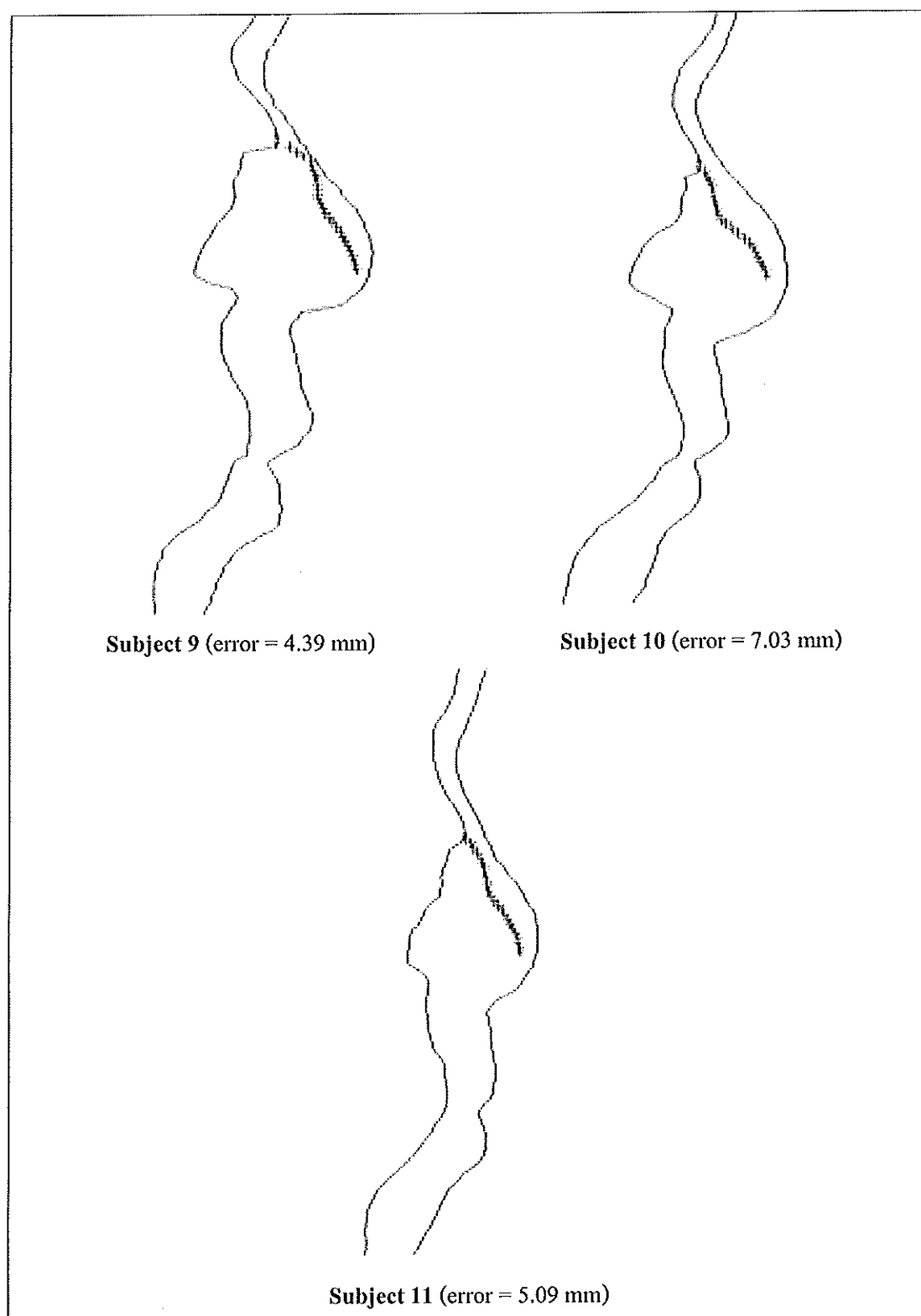




**Figure D3** Nose Profile Estimation Results and Errors of Subject 1 to 4



**Figure D4** Nose Profile Estimation Results and Errors of Subject 5 to 8



**Figure D5** Nose Profile Estimation Results and Errors of Subject 9 to 11

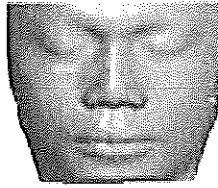
**Table B1** Errors of Nose profile Estimation for Subject 1 to Subject 11

Subject	Error of nose profile estimation (mm)
1	2.18
2	2.71
3	3.04
4	1.33
5	3.93
6	3.45
7	4.54
8	2.41
9	4.39
10	7.03
11	5.09
Mean	3.64
Maximum	7.03
Minimum	1.33
Standard deviation	1.59

## APPENDIX E

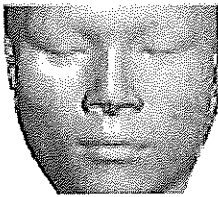
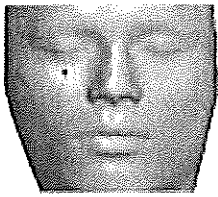
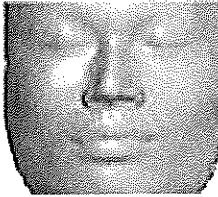
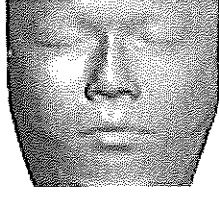
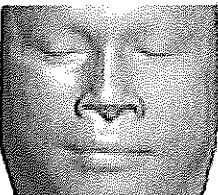
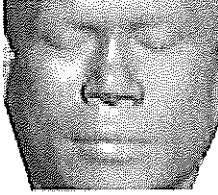
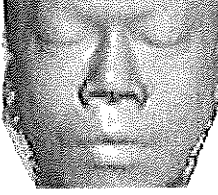
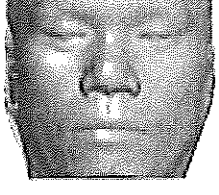
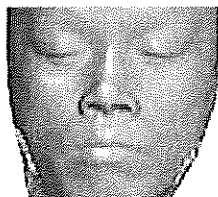
### FULL SET OF FACE POOL TEST FORM

In Chapter 4, the quantitative evaluation of facial reconstruction was performed using cylindrical projection approach. However, the goal of facial reconstruction is not reconstruction accuracy but rather recognition or identification success. As mentioned in the review of Claes and coworker (2010), a more realistic and human subjective, identification process can be simulated by generating face pool test. The full set of face pool test is presented in this section. There are 11 pages in the set according to the number of the head in the head database. Top image is the reconstructed face to be identified with the faces from the face pool. The reconstructed faces in the face pool test were from Scheme II reconstruction. Face pool are a set of faces from the face database. The reference faces in the reconstruction process of the reconstructed face were excluded from the face pool. So, the number of faces in the face pool for each test face is varied between 7 and 9 faces. For example, if the number of faces in the face pool is 7 then it means that the reconstructed face uses 4 faces as reference faces for the reconstruction process. If the number of faces in the face pool is 9 then it means that the reconstructed face uses 2 faces as reference faces for the reconstruction process. There are no face pool containing 10 faces because there are no reconstructed faces that use only one face for reference face. The check mark under the face in the face pool presents the target face. The numbers of assessors who decided the faces in the face pool to be the best three matches are presented under the face in the face pool. In this case, the best match is presented by R1, the second best match is presented by R2, and the third best match is presented by R3.



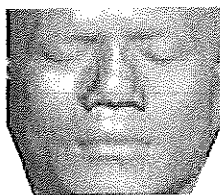
Test Face 1

## Face Pool

			
√ R1(11), R2(4), R3(2)	R1(0), R2(1), R3(3)	R1(1), R2(0), R3(0)	R1(0), R2(2), R3(2)
			
R1(1), R2(1), R3(2)	R1(4), R2(5), R3(3)	R1(1), R2(2), R3(1)	R1(1), R2(4), R3(4)
			
R1(0), R2(0), R3(2)			

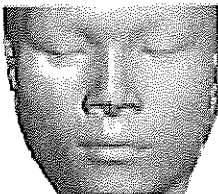
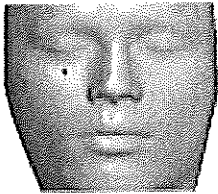
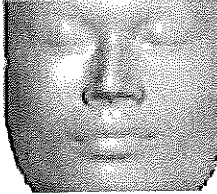
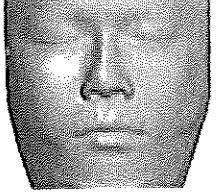
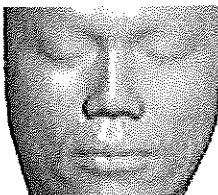

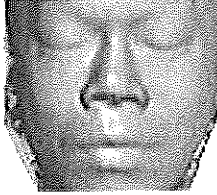
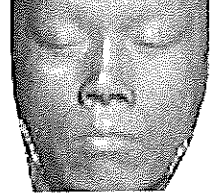
## Instruction

Please look at the Test Face and then consider the faces from Face Pool. Please select the best three match faces from the Face Pool. Please indicate the rank of the match by the number 1, 2, and 3 under the face in the Face Pool.



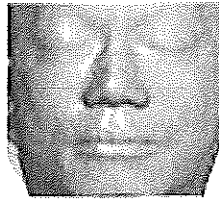
Test Face 2

## Face Pool

			
R1(4), R2(4), R3(1)	$\sqrt{R1(2), R2(2), R3(3)}$	R1(0), R2(2), R3(2)	R1(0), R2(4), R3(5)
			
R1(1), R2(0), R3(5)	R1(5), R2(0), R3(2)	R1(7), R2(3), R3(0)	R1(0), R2(4), R3(1)

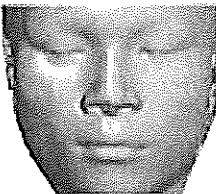
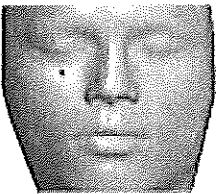
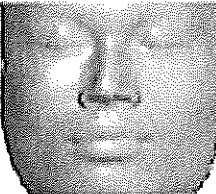
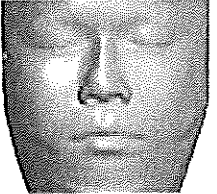

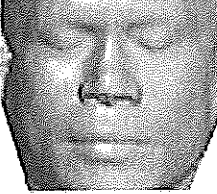
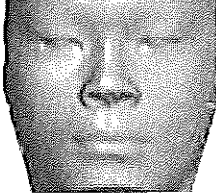
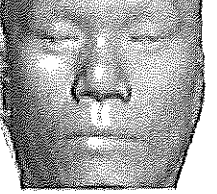
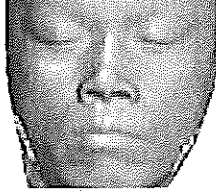
## Instruction

Please look at the Test Face and then consider the faces from Face Pool. Please select the best three match faces from the Face Pool. Please indicate the rank of the match by the number 1, 2, and 3 under the face in the Face Pool.



Test Face 3

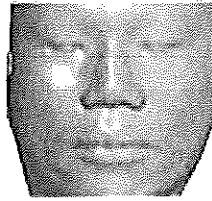
## Face Pool

			
R1(0), R2(0), R3(8)	R1(0), R2(0), R3(0)	$\sqrt{R1(3), R2(2), R3(2)}$	R1(6), R2(1), R3(1)
			
R1(5), R2(5), R3(2)	R1(2), R2(7), R3(2)	R1(0), R2(0), R3(0)	R1(3), R2(4), R3(4)
			
R1(0), R2(0), R3(0)			

## Instruction

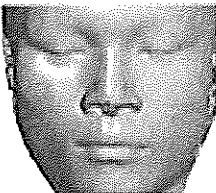
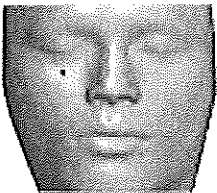

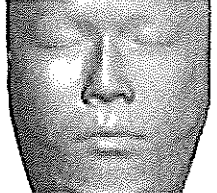
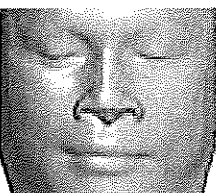
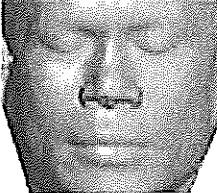

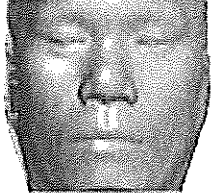
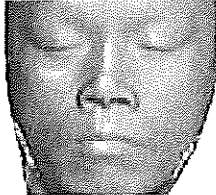
Please look at the Test Face and then consider the faces from Face Pool. Please select the best three match faces from the Face Pool. Please indicate the rank of the match by the number 1, 2, and 3 under the face in the Face Pool.





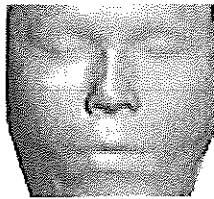
Test Face 4

## Face Pool

			
R1(1), R2(4), R3(2)	R1(0), R2(1), R3(1)	R1(0), R2(1), R3(1)	✓ R1(3), R2(7), R3(4)
			
R1(0), R2(2), R3(1)	R1(4), R2(0), R3(5)	R1(0), R2(0), R3(1)	R1(10), R2(2), R3(1)
			
R1(1), R2(2), R3(3)			

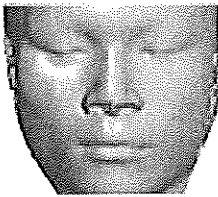
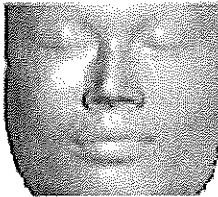
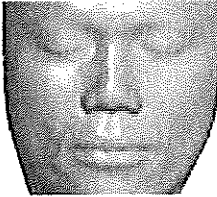
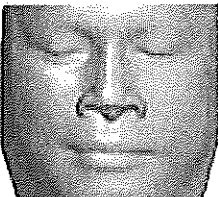
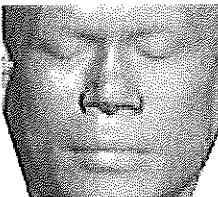
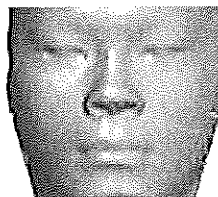
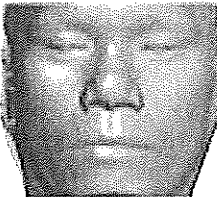
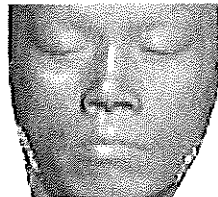
## Instruction

Please look at the Test Face and then consider the faces from Face Pool. Please select the best three match faces from the Face Pool. Please indicate the rank of the match by the number 1, 2, and 3 under the face in the Face Pool.



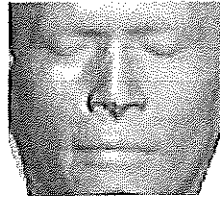
Test Face 5

## Face Pool

			
R1(5), R2(3), R3(3)	R1(0), R2(0), R3(1)	✓ R1(7), R2(3), R3(3)	R1(1), R2(1), R3(0)
			
R1(0), R2(3), R3(1)	R1(2), R2(4), R3(5)	R1(3), R2(3), R3(1)	R1(1), R2(2), R3(5)

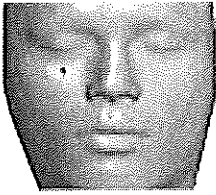
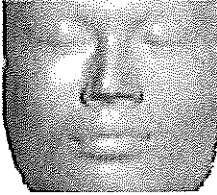
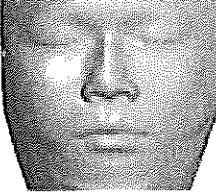
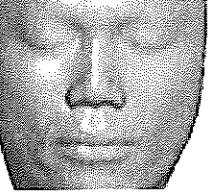
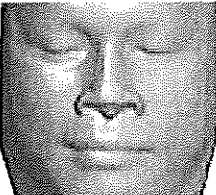
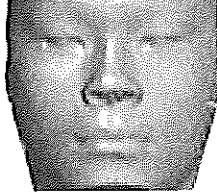
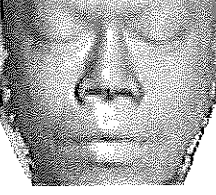
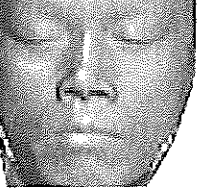
## Instruction

Please look at the Test Face and then consider the faces from Face Pool. Please select the best three match faces from the Face Pool. Please indicate the rank of the match by the number 1, 2, and 3 under the face in the Face Pool.



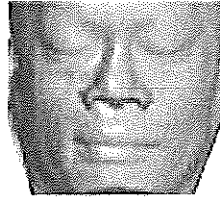
Test Face 6

## Face Pool

			
R1(0), R2(1), R3(2)	R1(0), R2(1), R3(0)	R1(3), R2(5), R3(4)	R1(4), R2(5), R3(5)
			
✓ R1(2), R2(2), R3(2)	R1(0), R2(0), R3(3)	R1(10), R2(4), R3(0)	R1(0), R2(1), R3(3)

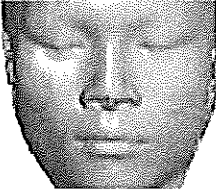
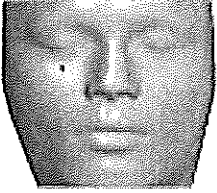

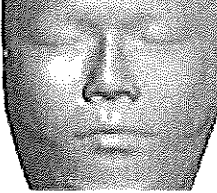
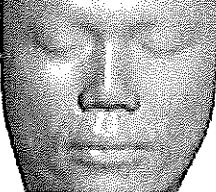
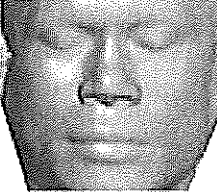

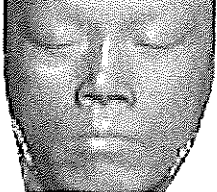
## Instruction

Please look at the Test Face and then consider the faces from Face Pool. Please select the best three match faces from the Face Pool. Please indicate the rank of the match by the number 1, 2, and 3 under the face in the Face Pool.



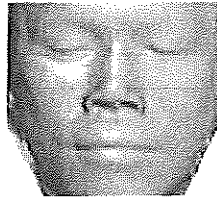
Test Face 7

## Face Pool

			
R1(5), R2(5), R3(3)	R1(1), R2(0), R3(0)	R1(0), R2(0), R3(5)	R1(2), R2(4), R3(0)
			
R1(3), R2(5), R3(4)	✓ R1(7), R2(4), R3(4)	R1(0), R2(0), R3(0)	R1(1), R2(1), R3(3)

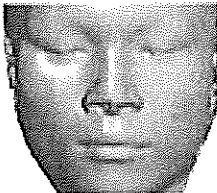
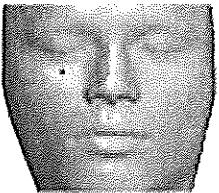
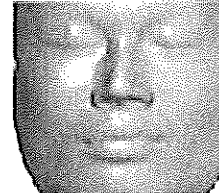
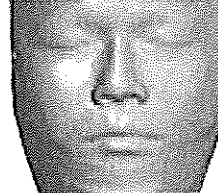
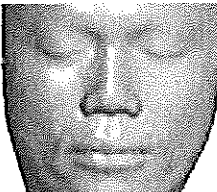
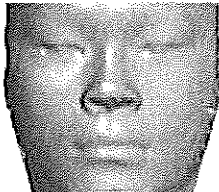

## Instruction

Please look at the Test Face and then consider the faces from Face Pool. Please select the best three match faces from the Face Pool. Please indicate the rank of the match by the number 1, 2, and 3 under the face in the Face Pool.



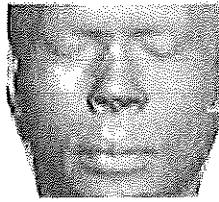
Test Face 8

## Face Pool

			
R1(9), R2(1), R3(2)	R1(1), R2(1), R3(1)	R1(0), R2(0), R3(3)	R1(0), R2(4), R3(5)
			
R1(2), R2(4), R3(5)	✓ R1(2), R2(3), R3(0)	R1(5), R2(6), R3(3)	

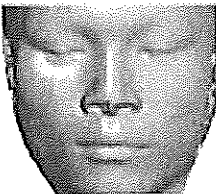
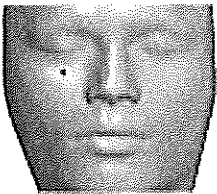

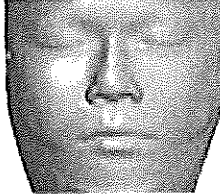

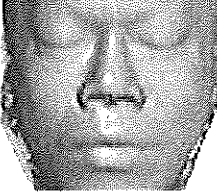
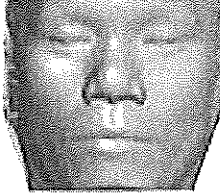
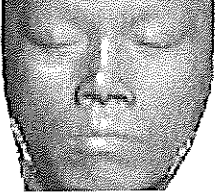
## Instruction

Please look at the Test Face and then consider the faces from Face Pool. Please select the best three match faces from the Face Pool. Please indicate the rank of the match by the number 1, 2, and 3 under the face in the Face Pool.



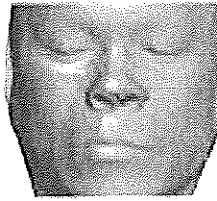
Test Face 9

## Face Pool

			
R1(2), R2(2), R3(8)	R1(0), R2(0), R3(1)	R1(0), R2(0), R3(0)	R1(0), R2(4), R3(2)
			
R1(0), R2(1), R3(2)	✓ R1(14), R2(2), R3(2)	R1(1), R2(0), R3(2)	R1(2), R2(10), R3(2)

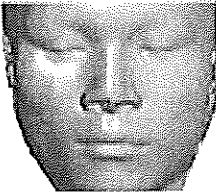
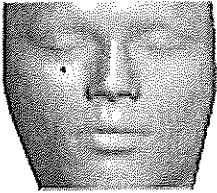
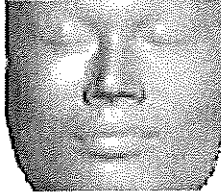
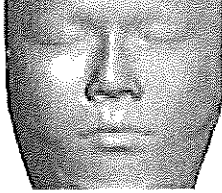
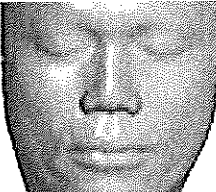

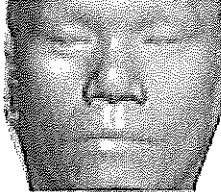
## Instruction

Please look at the Test Face and then consider the faces from Face Pool. Please select the best three match faces from the Face Pool. Please indicate the rank of the match by the number 1, 2, and 3 under the face in the Face Pool.



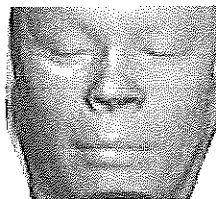
Test Face 10

## Face Pool

			
R1(2), R2(1), R3(4)	R1(0), R2(0), R3(0)	R1(0), R2(0), R3(3)	R1(2), R2(7), R3(2)
			
R1(0), R2(2), R3(2)	R1(12), R2(4), R3(2)	✓ R1(3), R2(5), R3(6)	

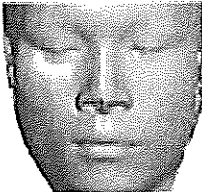
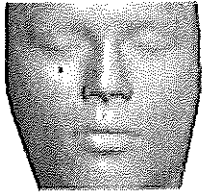
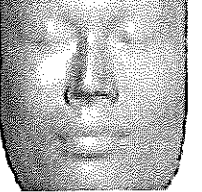
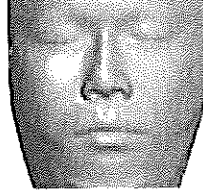
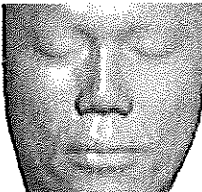
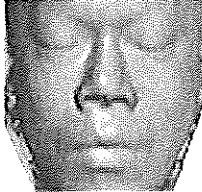
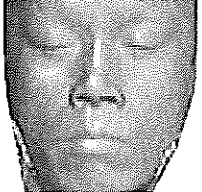
## Instruction

Please look at the Test Face and then consider the faces from Face Pool. Please select the best three match faces from the Face Pool. Please indicate the rank of the match by the number 1, 2, and 3 under the face in the Face Pool.



Test Face 11

## Face Pool

			
R1(3), R2(3), R3(4)	R1(0), R2(1), R3(2)	R1(0), R2(1), R3(0)	R1(3), R2(3), R3(5)
			
R1(3), R2(1), R3(3)	R1(7), R2(4), R3(4)	✓ R1(3), R2(6), R3(1)	

## Instruction

Please look at the Test Face and then consider the faces from Face Pool. Please select the best three match faces from the Face Pool. Please indicate the rank of the match by the number 1, 2, and 3 under the face in the Face Pool.



## **APPENDIX F**

### **PUBLICATIONS**

The following list contains three publications that have resulted from the development of the Facial Reconstruction from Skull Using Free Form Deformation presented in this dissertation.

## Facial Reconstruction from Skull

A. Namvong<sup>©</sup> and R. Nilthong

*School of Science, Mah Fah Luang University,  
333, Moo 1, Tasud, Muang, Chiang Rai, 57100, Thailand*

<sup>©</sup> E-mail: ariyanamvong@gmail.com; Fax: 053-916776; Tel. 053-916775

### ABSTRACT

The purpose of facial reconstruction is to estimate the facial outlook from skeleton remains and to aid in human identification. The reconstruction is obtained by deformation the craniometric landmarks of known skull into unknown skull. Forcing soft tissue of the known skull to the unknown skull with the same deformation gives the desired shape of the soft tissue for the unknown skull. This research uses 39 craniometric landmarks editing from five references [1,2,3,4,5]. For the deformation process, the application of Free-form deformation (FFD) is used. The 3D head model is acquired by using computed tomography (CT) with 1 mm resolution. This experiment attempts to deform the skull and skin of one 48 years old woman into another 42 years old woman. The preliminary visual result shows that it is possible to use this scheme for forensic facial reconstruction. Future development of this research will try to collect more reference head models and use the average skin deformation from various head models.

**Keywords:** Facial Reconstruction, Free-form Deformation.

### 1. INTRODUCTION

If the usual methods are impossible to identify the skeleton remains, then the possibility of facial reconstruction from the skull is considered. It is true that there are many ways in which soft tissue may cover the same skull leading to different facial outlook. So, the purpose of facial reconstruction is not to produce an accurate likeness of the person during life but the task is successful if it provides a positive effect to human identification from skeleton remains. With the assumption that the underlying skeleton affects directly the overall aspect of facial outlook, we consider that facial reconstruction is possible.

The successful of manual clay sculpting depends on combination of the ability, anatomical and anthropological knowledge of the artist, while the successful of computer-aided reconstruction depends on the number of head database and also the skill of craniometric landmarks localization of user. The facial reconstruction is obtained by deformation the craniometric landmarks of known skull into unknown skull or target skull. Forcing soft tissue of the known skull to the unknown skull with the same deformation gives the desired shape of the soft tissue for the unknown skull.

In this paper we try to develop a novel method for facial reconstruction through the use of volume deformation. Current volume deformation computer-based facial reconstruction methods differ mainly by the selection of landmarks points on the skull or craniometric landmarks, methods used for registration and deformation the model towards a given target skull.

Our procedure can be summarized as follows. For each head model we manually locate 39 craniometric landmarks taken from five references [1,2,3,4,5] then roughly register using Frankfort horizontal plane, then fine register using Iterative Closest Point (ICP). Finally we

**ANSCSE14 Mae Fah Luang University, Chiang Rai, Thailand  
March 23-26, 2010**

deform craniometric landmarks of known skull into target skull using Free-Form Deformation (FFD).

The remainder of this paper is organized as follows. In Section 2 we review theory of Free-Form Deformation. In Section 3 we describe our facial reconstruction method. Section 4 shows the results of our experiment. The paper conclusion and directions for future research are in Section 5.

## 2. FREE-FORM DEFORMATION (FFD)

Free-form deformation introduced by Sederberg and Parry [6, 7, 8] is known to be a powerful shape modification method that has been applied to geometric modeling. This technique deforms an object by embedding it with in a solid defined with a control lattice. A change of the lattice deforms the solid and hence the object as seen in Figure 1. FFD generally involves with 1D, 2D and also 3D data. We can compute a new location  $P'$  from an old location  $P$  after deforming control point from  $P_{ijk}$  to  $P'_{ijk}$  as follows:

$$\text{1D FFD:} \quad P' = \sum_{i=0}^l B_i^l(t) P'_i \quad (1)$$

$$\text{2D FFD:} \quad P' = \sum_{i=0}^l \sum_{j=0}^m B_i^l(s) B_j^m(t) P'_{ij} \quad (2)$$

$$\text{3D FFD:} \quad P' = \sum_{i=0}^l \sum_{j=0}^m \sum_{k=0}^n B_i^l(s) B_j^m(t) B_k^n(u) P'_{ijk} \quad (3)$$

$$\text{Bernstein Polynomials: } B_i^n(t) = \frac{n!}{(n-i)!i!} t^i (1-t)^{n-i} \quad (4)$$

where point  $P'$  is a new location at  $(s', t', u')$  of an old point  $P$  at  $(s, t, u)$  after deforming control point  $P_{ijk}$  to  $P'_{ijk}$ , and  $l, m, n$  are the number of control points minus 1 in x, y, z axis. ( $0 \leq s, t, u, s', t', u' \leq 1$ )

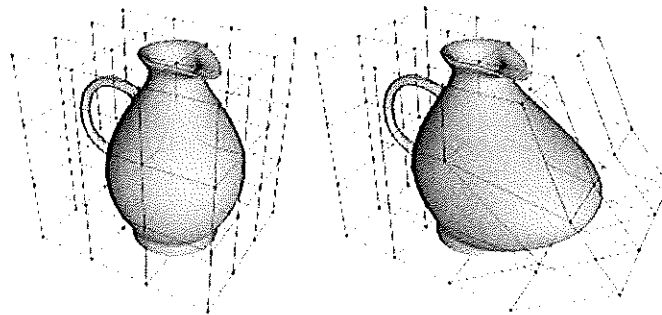


Figure 1 Example of FFD [9]

### 3. METHODOLOGY

Figure 2 shows the main step of our procedure. First step, we manually locate landmarks on both unknown skull or target and known skull or reference. Second step, we align two skulls into common position. This stage contains two processes, rough alignment and fine alignment. Rough alignment is to make two skulls into the same orientation called Frankfort horizontal plane, for supporting the performance of next process. Next process, fine alignment uses ICP algorithm. Finally, we deform craniometric landmarks of known skull into target skull using Free-Form Deformation.

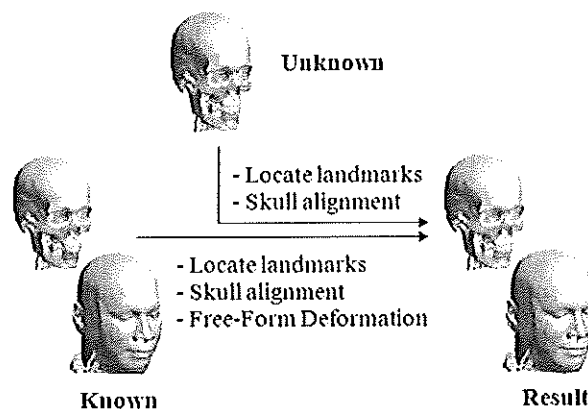


Figure 2 Methodology

#### 3.1 Craniometric Landmarks

Figure 3 and Table 1 show the 39 craniometric landmarks used in this paper. There are two types of landmarks, central landmarks and lateral landmarks. Central landmarks laid on the central of the skull and lateral landmarks laid on left and right side of the skull.

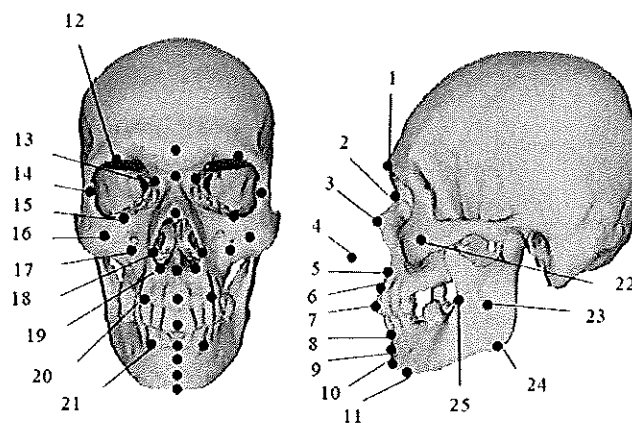


Figure 3. Craniometric landmarks

Table 1 Craniometric Landmarks

#	Central Landmarks	#	Lateral Landmarks
1	Glabella	12	Supracorbital
2	Nasal	13	Inner orbital
3	End of nasal	14	Outer orbital
4	Nose tip estimation	15	Suborbital
5	Mid-philtrum	16	Zygoma
6	Upper lip margin	17	Inferior malar
7	Incisor	18	Outer nasal
8	Lower lip margin	19	Lower nasal
9	Chin-lip fold	20	Supracanine
10	Mental eminence	21	Subcanine
11	Beneath chin	22	Outer Zygoma
		23	Mid-mandible
		24	Gonion
		25	Occlusion line

### 3.2 Skull Alignment

This stage contains two processes, rough alignment and fine alignment. First process is to make two skulls have the same orientation called Frankfort horizontal plane. The position of Frankfort horizontal Plane is like someone looking straight ahead. The technical explanation of positioning the skull this way is to have the lowest point on the lower margin of the orbit aligning horizontally with the top edge of the external auditory meatus (the ear hole) [1]. See Figure 4 for an illustration of this position.

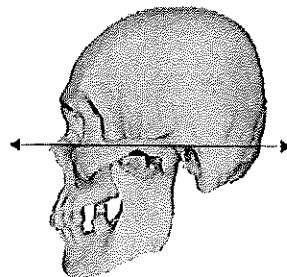


Figure 4 Frankfort horizontal plane

Second process, fine alignment uses the result from first step as an initial alignment. The method used in this process is called Iterative Closest Point or ICP. ICP is a straightforward method to align two free-form surfaces [10, 11]. The algorithms of ICP to align surface  $X$  and surface  $P$  are as follows:

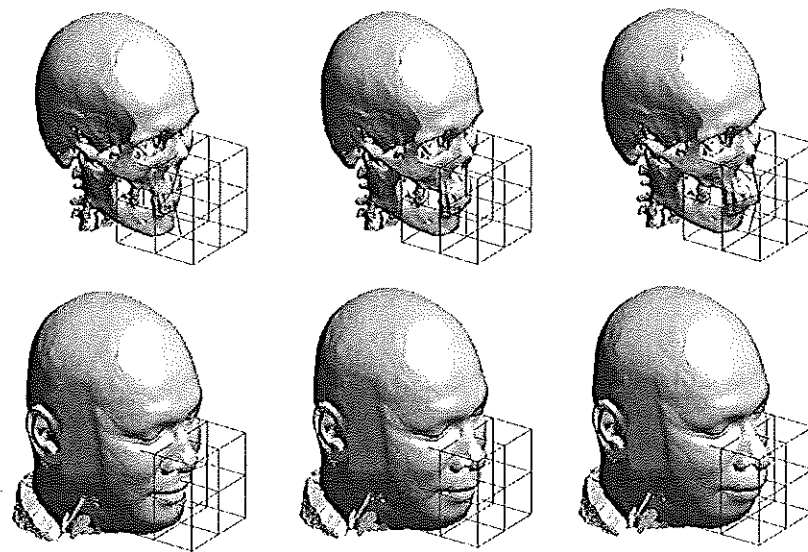
#### The Iterative Closest Point Algorithm

- Initial transformation
- Iterative procedure to converge to local minima
  1.  $\forall p \in P$  find closest point  $x \in X$
  2. Transform  $P_k \rightarrow P_{k+1}$  to minimize distances between each  $p$  and  $x$
  3. Terminate when change in the error falls below a preset threshold

### 3.3 Free-Form Deformation

From Section 2 we mention FFD in the manner called global deformation; in this research we use FFD in the manner of local deformation. As seen in Figure 5, it demonstrates the use of local FFD; the middle column shows original skull and face; the left column shows the result of pushing the skull at the upper lip margin point (point 6 from Table 1) inside resulting in deforming of the shape of face. In the right column shows the result of push this point outside.

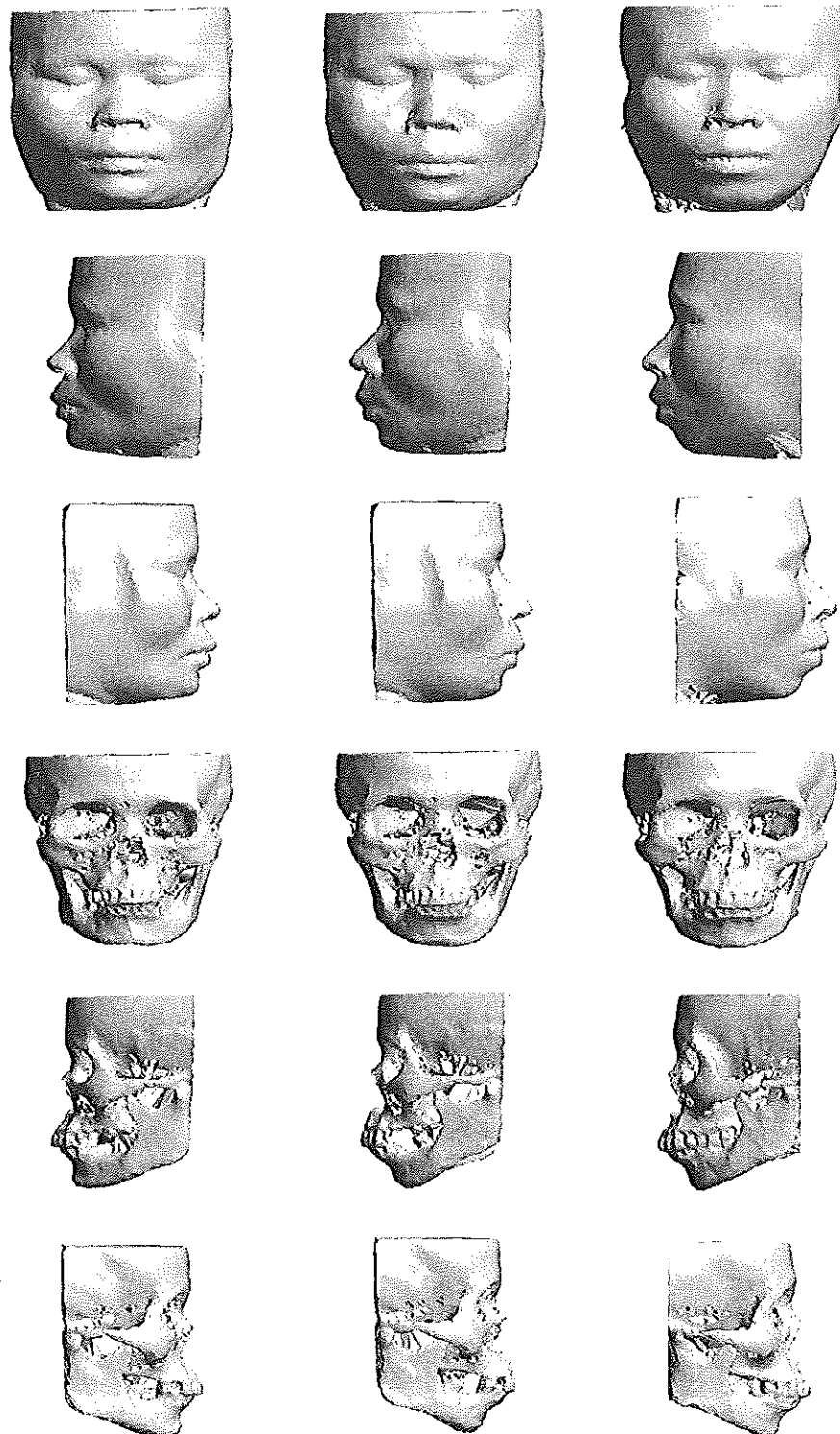
Reach to this step, two skulls have the same orientation and have the closest distance between reference skull and target skull. Now it is ready to deform all craniometric landmarks point by point from reference skull to target skull to reconstruct the face of the target skull. The reference skull, reference face, target skull, and also result from our facial reconstruction are shown in Section 4.



**Figure 5** Demonstration of local FFD, original head (middle column), pushing the upper lip margin inside (left column) and pushing outside (right column)

## 4. EXPERIMENTAL RESULTS

In this experiment, the 3D head model of reference head and target head are acquired by using computed tomography with 1 mm resolution. We attempt to deform the skull and face of one 48 years old woman into another 42 years old woman. In Figure 6 show reference skull, reference face, target skull and also target face derived from our procedure. Reference face and reference skull are in the left column. The results derived from facial reconstruction are in the middle column and real faces of target are in the right column. We can see that the result is still bias to reference face. The result face looks more like reference face than target face. However, when observing the result we can see that it is possible to use this procedure to reconstruct a face from skeleton remains.



**Figure 6** Experimental results, reference head (left column), result from the approach (middle column) and target head (right column).

**ANSCSE14 Mae Fah Luang University, Chiang Rai, Thailand  
March 23-26, 2010**

## 5. CONCLUSION

In this experiment, for each head model we manually locate 39 craniometric landmarks then do rough registration using Frankfort horizontal plane, after that do fine registration using Iterative Closest Point, and finally we deform craniometric landmarks of known skull into target skull using Free-Form Deformation. From the results, we cannot claim that this research successfully because the results cannot be quite the same as the target face. In this experiment we have the limitation of number of head database, therefore only a few head models are produced. Nevertheless, the preliminary visual result shows that it is possible to use this scheme for forensic facial reconstruction. Future development of this research we will try to collect more reference head models for facial reconstructions, and we will use the average skin deformation from various reference head models to reduce the reference bias.

## REFERENCES

1. L. Gibson, Forensic Art Essentials: A Manual for Law Enforcement Artists, 1<sup>st</sup> edition, Academic Press, London, 2008, 266-269, 303-305.
2. C. Wilkinson, Forensic Facial Reconstruction, 1<sup>st</sup> edition, Cambridge University Press, Cambridge, 2004, 71-73.
3. K.T. Taylor, Forensic Art and Illustration, 1<sup>st</sup> edition, CRC Press LLC, Washington D.C., 2001, 348-359.
4. P. Claes, D. Vandermeulen, S.D. Greef, G. Willems and P. Suetens, Statistically Deformable Faces Models for Cranio-Facial Reconstruction, Journal of Computing and Information Technology – CIT 14, 2006(1), 21-30.
5. A.F. Abate, M. Nappi, S. Ricciardi and G. Tortora, FACES: 3D Facial reconstruction from ancient Skulls using content based image retrieval, Journal of Visual Languages & Computing, 2004(15), 373-389.
6. T.W. Sederberg, Computer Aided Geometric Design Course Notes, Department of Computer Science, Brigham Young University, Utah, 2007, 133-135.
7. T.W. Sederberg and S.R. Parry, Free-form Deformation of Solid Geometric Models, Computer Graphics, 1986, 20(4), 151-160.
8. W. Song and X. Yang. Free-Form Deformation with weighted T-spline. The Journal of Visual Computer, 2005, 21(3), 139-151.
9. R. Barzel. Computer Graphics Animation Course Notes, Ecole Polytechnique, France. 2003, na.
10. P.J. Besl and N.D. McKay. A Method for Registration of 3-D Shapes, IEEE Transactions on Analysis and Machine Intelligence, 1992, 14(2), 239-255.
11. K. Bae. Automated Registration of Unorganised Point Clouds from Terrestrial Laser Scanners, Ph.D. Dissertation, Department of Spatial Sciences, Curtin University of Technology. Bentley, W.A, Australia. 2006, 1-9.

## ACKNOWLEDGMENTS

We would like to thank Mr.Sorawee Thanawong, chief of X-Ray Department, Overbrook Hospital, Chiang Rai, Thailand, for his precious help in the head computer tomography data acquisition phase and also thank to the volunteers that makes this research possible.

ANSCSE14 Mae Fah Luang University, Chiang Rai, Thailand  
March 23-26, 2010



A. Namvong<sup>c</sup> and R. Nilthong  
*School of Science, Mah Fah Luang University,  
 333, Moo 1, Tasud, Muang, Chiang Rai, 57100, Thailand*  
<sup>c</sup>E-mail: ariyanamvong@gmail.com; Fax: 053-916776; Tel. 053-916775

## ABSTRACT

The purpose of facial reconstruction is to estimate the facial outlook from skeleton remains and to aid in human identification. The reconstruction is obtained by deforming the craniometric landmarks of known skull into unknown skull. Forcing soft tissue of the known skull to the unknown skull with the corresponded deformation gives the desired shape of the soft tissue for the unknown skull. This work uses 71 craniometric landmarks edited from five references [1,2,3,4,5]. For the deformation process, the application of Free Form deformation (FFD) is used. The 3D head models are acquired by computed tomography (CT) scanner with 1 mm resolution. The questioned head is from 35 years old man. The reference heads are from 31, 38 and 24 years old men. These reference heads are chosen from the most three resembling skulls to the questioned skull. These reference skulls are deformed into questioned skull and then the reference faces are forced to deform correspondingly. Finally these deformed faces are averaged to reconstruct the desired face. The resulting face from this scheme shows promise for forensic facial reconstruction.

**Keywords:** Facial Reconstruction, Free Form Deformation.

## 1. INTRODUCTION

If the usual methods are impossible to identify the skeleton remains, then the possibility of facial reconstruction from the skull is considered. It is true that there are many ways in which soft tissue may cover the same skull leading to different facial outlook. So, the purpose of facial reconstruction is not to produce an accurate likeness of the person during life but the task is successful if it provides a positive effect to human identification from skeleton remains. With the assumption that the underlying skeleton affects directly the overall aspect of facial outlook, we consider that facial reconstruction is possible.

The successful of manual clay sculpting depends on combination of the ability, anatomical and anthropological knowledge of the artist, while the successful of computer-aided reconstruction depends on the number of head database and also the skill of craniometric landmarks localization of user. The facial reconstruction is obtained by deformation the craniometric landmarks of known skull into unknown skull or target skull. Forcing soft tissue of the known skull to the unknown skull with the same deformation gives the desired shape of the soft tissue for the unknown skull.

In this paper we try to develop a novel method for facial reconstruction through the use of volume deformation. Current volume deformation computer-based facial reconstruction methods differ mainly by the selection of landmarks points on the skull or craniometric landmarks, methods used for registration and deformation the model towards a given target skull.

ANSCSE15 Bangkok University, Thailand  
 March 30-April 2, 2011

Our procedure can be summarized as follows. For each head model we manually locate 71 craniometric landmarks taken from five references [1,2,3,4,5] then coarsely register using Frankfort plane, then fine register using Iterative Closest Point algorithm. Finally we deform craniometric landmarks of known skull into target skull using Free Form Deformation.

The remainder of this paper is organized as follows. In Section 2 we review theory of Free-Form Deformation. In Section 3 we describe our facial reconstruction method. Section 4 shows the results of our experiment. The paper conclusion and discussion are in Section 5.

## 2. FREE FORM DEFORMATION

Free Form Deformation (FFD) was introduced by Sederberg and Parry [6, 7, 8] is known to be a powerful shape modification method that has been applied to geometric modeling. This technique deforms an object by embedding it with in a solid defined with a control lattice. A change of the lattice deforms the solid and hence the object as seen in Figure 1. FFD generally involves with 1D, 2D and also 3D data. We can compute a new location  $P'$  from an old location  $P$  after deforming control point from  $P_{ijk}$  to  $P'_{ijk}$  as follows:

$$\text{1D FFD:} \quad P' = \sum_{i=0}^l B_i^l(t) P_i' \quad (1)$$

$$\text{2D FFD:} \quad P' = \sum_{i=0}^l \sum_{j=0}^m B_i^l(s) B_j^m(t) P_{ij}' \quad (2)$$

$$\text{3D FFD:} \quad P' = \sum_{i=0}^l \sum_{j=0}^m \sum_{k=0}^n B_i^l(s) B_j^m(t) B_k^n(u) P_{ijk}' \quad (3)$$

$$\text{Bernstein Polynomials: } B_i^n(t) = \frac{n!}{(n-i)! i!} t^i (1-t)^{n-i} \quad (4)$$

where point  $P'$  is a new location at  $(s',t',u')$  of an old point  $P$  at  $(s,t,u)$  after deforming control point  $P_{ijk}$  to  $P'_{ijk}$ , and  $l, m, n$  are the number of control points minus 1 in  $x, y, z$  axis. ( $0 \leq s, t, u, s', t', u' \leq 1$ )

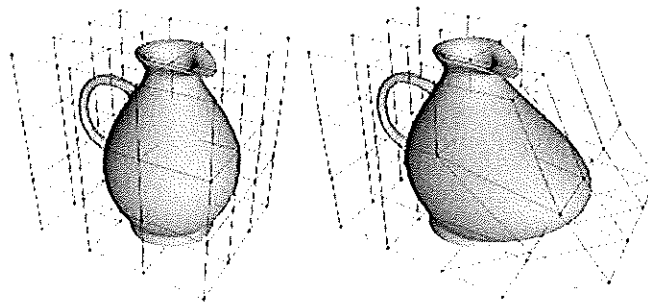


Figure 1. Demonstration of FFD [9]

### 3. METHODOLOGY

Figure 2 shows the workflow of our proposed method. The questioned skull is compared to skulls in head database. The similarity is defined by average distance between corresponded craniometric landmarks of two skulls. The craniometric landmarks used in this work are displayed in Figure 3. The  $N$  most resembling skulls are selected as references. In this work we try  $N = 1, 2$  and  $3$ . Then deform craniometric landmarks of reference skulls into questioned skull using FFD. Forcing soft tissue of the reference skulls to the questioned skull with the corresponded deformation gives the desired facial shape of the soft tissue for the questioned skull. Finally these  $N$  deformed faces are averaged to reconstruct the desired face.

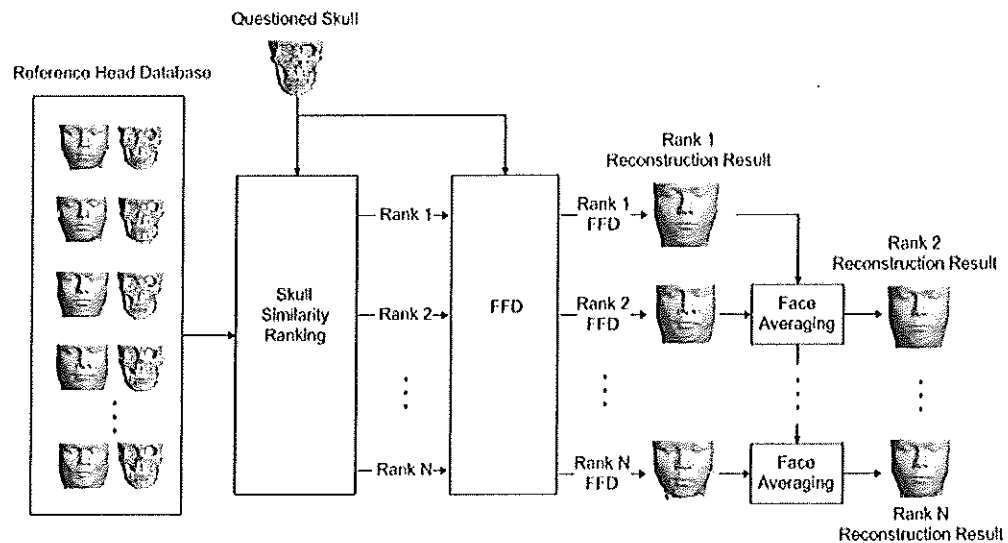


Figure 2. Facial reconstruction workflow

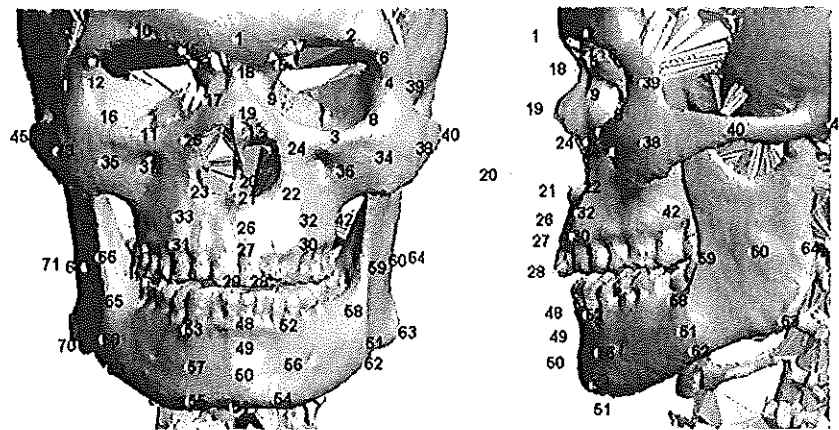
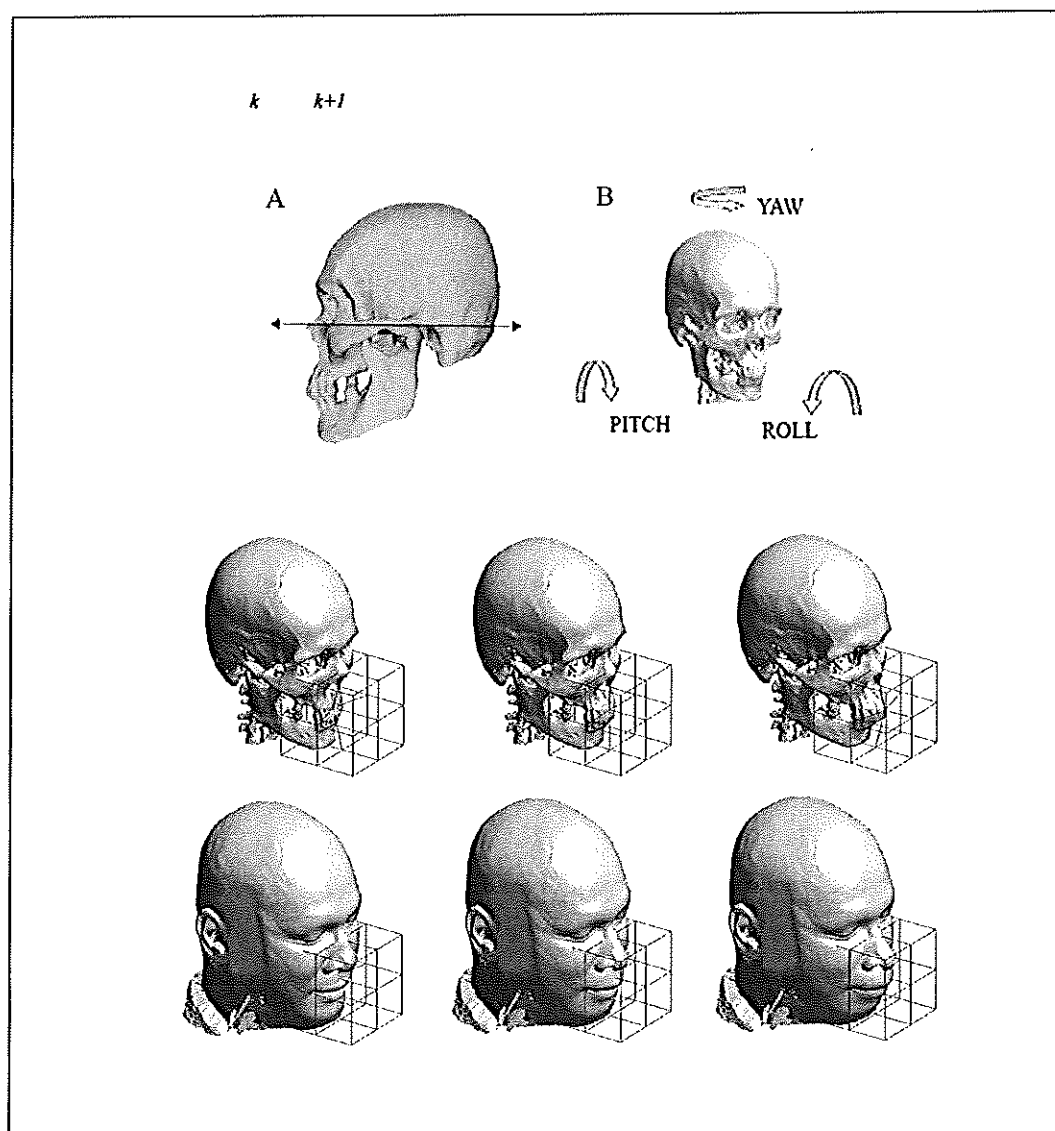


Figure 3. Craniometric landmarks



### 3.2 Free Form Deformation for Facial Reconstruction

From Section 2 we mention FFD in the global deformation manner. In this work we use FFD in the manner of local deformation by applying the local lattice to the craniometric landmarks. Figure 5 shows the local FFD demonstration of pushing the incisor inside and outside.

At this step, two skulls have the same orientation and have the closest distance between reference skull and target skull. Now it is ready to deform all craniometric landmarks point by point from reference skull to target skull to reconstruct the face of the target skull.

## 4. EXPERIMENTAL RESULTS

In this experiment, the 3D head database containing six heads are acquired by using CT scanner. The heads with craniometric landmarks are displayed in Figure 6. The label M indicated male gender and number indicated age at scanned date. All skulls in head database are paired up and then the distance between paired skulls are calculated as seen in Table 1. The similarity rank for each skull is displayed in Table 2. For the experiment, M35 is picked out from the reference database to be assumed as questioned skull or so called target skull. From Table 2, we can see that the most three resembling to target skull are M31, M38 and M24 accordingly. From Figure 7, the R1 result is reconstructed from M31 only, the R2 result is reconstructed from M31 and M38, the R3 result is constructed from M31, M38 and M24. From visual evaluation, R3 result shows promise for forensic facial reconstruction.

Table 1. Distance between skulls (mm.)

Head	M24	M29	M31	M35	M38	M55
M24	X	5.49	4.52	4.70	5.80	5.69
M29	5.49	X	4.94	5.62	4.91	3.77
M31	4.52	4.94	X	4.05	5.01	4.79
M35	4.70	5.62	4.05	X	4.18	5.36
M38	5.80	4.91	5.01	4.18	X	5.05
M55	5.69	3.77	4.79	5.36	5.05	X

Table 2. Similarity rank

Head	Rank				
	1	2	3	4	5
M24	M31	M35	M29	M55	M38
M29	M55	M38	M31	M24	M35
M31	M35	M24	M55	M29	M38
M35	M31	M38	M24	M55	M29
M38	M35	M29	M31	M55	M24
M55	M29	M31	M38	M35	M24

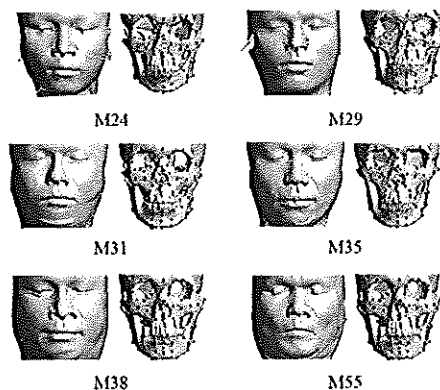


Figure 6. Head database with landmarks

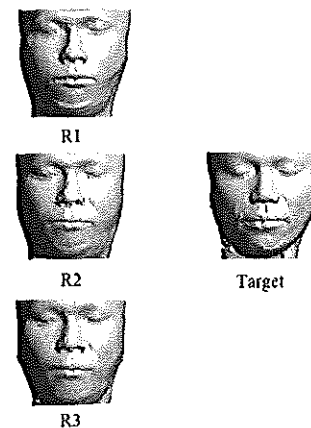


Figure 7. Reconstruction results

## 5. CONCLUSION AND DISCUSSION

Manual facial reconstruction has a long tradition both in forensic and archaeological fields, but, as long as progressive studies and medical imaging technology leads to the development of alternative computer-based facial reconstruction methods. We have to remark that there is no way to exactly reproduce the face of discovered skull. In stead of using small set of facial soft tissue thickness data and then interpolate the large remaining area, we can use whole facial soft tissue thickness data from 3D head models derived from CT scanner and then approximate questioned face from reference face in face database. The approach presents possibility to use this scheme as a support tool for forensic facial reconstruction.

In this paper, the skull similarity is considered in a whole. In the future, we will try to consider the dissections of skull instead and do the reconstruction from most resembling section. In addition, we will try to consider other factors apart from only skull shape such as age and nutrition condition.

## REFERENCES

1. L. Gibson, *Forensic Art Essentials: A Manual for Law Enforcement Artists*, 1<sup>st</sup> edition, Academic Press, London, 2008, 266-269, 303-305.
2. C. Wilkinson, *Forensic Facial Reconstruction*, 1<sup>st</sup> edition, Cambridge University Press, Cambridge, 2004, 71-73.
3. K.T. Taylor, *Forensic Art and Illustration*, 1<sup>st</sup> edition, CRC Press LLC, Washington D.C., 2001, 348-359.
4. P. Claes, D. Vandermeulen, S.D. Greef, G. Willems and P. Suetens, Statistically Deformable Faces Models for Cranio-Facial Reconstruction, *Journal of Computing and Information Technology – CIT* 14, 2006(1), 21-30.
5. A.F. Abate, M. Nappi, S. Ricciardi and G. Tortora, FACES: 3D Facial reconstruction from ancient Skulls using content based image retrieval, *Journal of Visual Languages & Computing*, 2004(15), 373-389.
6. T.W. Sederberg, *Computer Aided Geometric Design Course Notes*, Department of Computer Science, Brigham Young University, Utah, 2007, 133-135.
7. T.W. Sederberg and S.R. Parry, Free-form Deformation of Solid Geometric Models, *Computer Graphics*, 1986, 20(4), 151-160.
8. W. Song and X. Yang. Free-Form Deformation with weighted T-spline. *The Journal of Visual Computer*, 2005, 21(3), 139-151.
9. R. Barzel. *Computer Graphics Animation Course Notes*, Ecole Polytechnique, France. 2003, na.
10. P.J. Besl and N.D. Mckay. A Method for Registration of 3-D Shapes, *IEEE Transactions on Analysis and Machine Intelligence*, 1992, 14(2), 239-255.
11. K. Bae. *Automated Registration of Unorganised Point Clouds from Terrestrial Laser Scanners*, Ph.D. Dissertation, Department of Spatial Sciences, Curtin University of Technology. Bentley, W.A, Australia. 2006, 1-9.

## ACKNOWLEDGMENTS

We would like to thank Overbrook Hospital, Kasemrad Sriburin Hospital and Kratumban Hospital for precious help in the head computer tomography data acquisition phase and also thank to the volunteers that make this work possible.

ANSCSE15 Bangkok University, Thailand  
March 30-April 2, 2011



## FACIAL RECONSTRUCTION FROM SKULL USING FREE FORM DEFORMATION

Arlyu NAMVONG, Rungrote NILTHONG

School of Science, Mae Fah Luang University, Chiang Rai, Thailand

### Abstract

*The purpose of facial reconstruction is to estimate the facial outlook from a discovered skull with the intention to provide a positive effect for deceased identification. In this paper, we tried to develop a novel method for facial reconstruction through the use of Free Form Deformation. The target face was obtained by deforming the craniometric landmarks of known skull into unknown skull. Forcing soft tissue on the known skull to the unknown skull with correspondent deformation gives the desired shape of the soft tissue for the unknown skull. Modified from Rhine's landmarks, the 33 craniometric landmarks were used in this work. For the deformation process, the application of Free Form Deformation was employed. The resulting face from this scheme shows promising forensic facial reconstruction.*

**Keywords:** Facial Reconstruction; Free Form Deformation

### Introduction

One of the most complicated tasks for criminal investigation is dealing with unidentified skeleton remains. There are several reasons why identification is essential. For every unidentified deceased person, there might be someone who cared about. Family members should have known what happened to their lover. Most of the time, an unidentified body is found, crime remains unsolved and the murderer may be still walking around. If usual protocols are impossible to identify the skeleton remains, then possibility of facial reconstruction from skull shall be considered. It is true that there are many ways in which soft tissue may cover such the same skull leading to different facial outlook. So, the purpose of facial reconstruction is not to produce an accurate likeness of the person during life but the task is considered successful if it is able to provide a positive effect on deceased identification. With an assumption that the underlying skeleton directly affects the overall aspects of facial

outlook, we considered that facial reconstruction from skull is possible.

Being still in use and constantly evolving, an old technique is a manual clay facial reconstruction also known as sculptural technique (Wilkinson, 2004). This method utilizes average skin thickness data derived from the craniometric landmarks. From tissue thickness of the landmarks, the remaining open spaces are interpolated to form the features of the face. This process is done according to the discretion of the artist resulting in a very subjective and not reproducible face (Taylor, 2001). There are no exact rules for the manual clay facial reconstruction which makes computerization of the process more challenging.

This paper introduces a novel approach to computerize facial reconstruction through the use of Free Form Deformation method. This approach differs from other researches that try to interpolate all face features from small set of tissue thickness data. Stephen et al (2008) stated that the relationships between connective tissue and skull are not completely known at this moment. The assumption behind this novel

approach is the changing in the facial soft tissue responding to the changing in the skull. The reconstruction is obtained by deforming the craniometric landmarks of known skull into unknown skull. Forcing soft tissue on the known skull to the unknown skull with the associated deformation offers a desired shape of the soft tissue for the unknown skull.

The remainders of this paper are organized as follow. Materials and related theories to the method are mentioned in the next section. After that, the methodology workflow is presented. Then, the result and

discussion of this approach are mentioned. The paper conclusion is summarized in the last section.

## Materials and Method

### Image Acquisition

The 3D data of skull and face used in this paper are acquired from CT scanner (Fig. 1). The Cartesian coordinate is used to represent 3D data in the form of (x, y, z) also known as point cloud. Meshing, shading and shadowing are used for the visualization purpose.

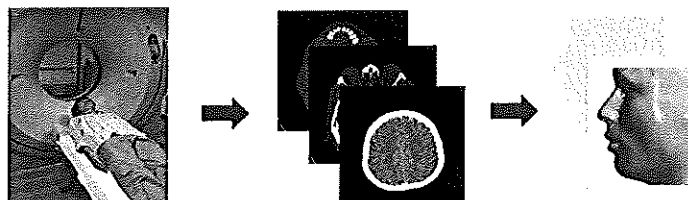


Fig. 1. 3D head data acquisition from CT scanner.

### Craniometric Landmarks

Craniometric landmarks are anatomical landmarks on the skull. For manual clay sculpturing method, average skin thickness data table is applied. From tissue thickness at the landmarks, the remaining open spaces are interpolated to form the features

of the face. In this work, the reconstruction is obtained by deforming the craniometric landmarks of known skull into unknown skull giving a desired shape of the soft tissue for the unknown skull. The craniometric landmarks used in this work are modified from Rhine's landmarks (Fig. 2).

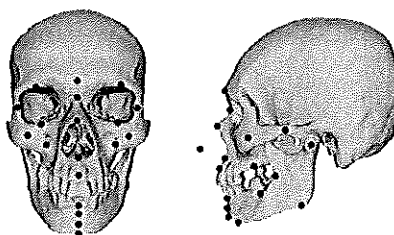


Fig. 2. Craniometric landmarks used in this work.

### Frankfort Plane

All heads in the database have to be aligned to the same orientation and position. The favorite standard orientation

of skull used in forensic facial reconstruction is called Frankfort plane. The position of Frankfort plane is like someone looking straight ahead. The





technical explanation of positioning the skull this way is to have the lowest point on the lower margin of the orbit aligning horizontally with the top edge of the ear hole (Gibson, 2008).

#### Iterative Closest Point

Iterative Closest Point (ICP) is a straight forward method to align two free form surfaces (Besl & McKay, 1992). In this paper, this method is used to align reference skull to questioned skull before doing the facial reconstruction. The algorithms of ICP to align surface  $X$  and surface  $P$  are as follows:

#### The Iterative Closest Point Algorithm

- Initial transformation
  - Iterative procedure to minimize the distance
1.  $\forall p \in P$  find closest point  $x \in X$

$$\text{1D FFD:} \quad P' = \sum_{i=0}^l B_i^l(t) P_i' \quad (1)$$

$$\text{2D FFD:} \quad P' = \sum_{i=0}^l \sum_{j=0}^m B_i^l(s) B_j^m(t) P_{ij}' \quad (2)$$

$$\text{3D FFD:} \quad P' = \sum_{i=0}^l \sum_{j=0}^m \sum_{k=0}^n B_i^l(s) B_j^m(t) B_k^n(u) P_{ijk}' \quad (3)$$

$$\text{Bernstein Polynomials:} \quad B_i^n(t) = \frac{n!}{(n-i)! i!} t^i (1-t)^{n-i} \quad (4)$$

where point  $P'$  is a new location at  $(s', t', u')$  of an old point  $P$  at  $(s, t, u)$  after deforming control point  $P_{ijk}$  to  $P'_{ijk}$ , and  $l, m, n$  are the

2. Transform  $P_k \rightarrow P_{k+1}$  to reduce the average distances
3. Terminate when next transformation step does not reduce the average distance

#### Free Form Deformation

Free Form Deformation (FFD) was introduced by Sederberg and Parry (Sederberg & Parry, 1986) is known as a powerful shape modification method that has been applied to geometric modeling. This technique deforms an object by embedding it with in a solid defined with a control lattice. A change of the lattice deforms the solid and hence the object (Fig. 3). FFD generally involves with 1D, 2D and also 3D data. We can compute a new location  $P'$  from an old location  $P$  after deforming control point from  $P_{ijk}$  to  $P'_{ijk}$  as follows:

number of control points minus 1 in x, y, z axis.  
( $0 \leq s, t, u, s', t', u' \leq 1$ )

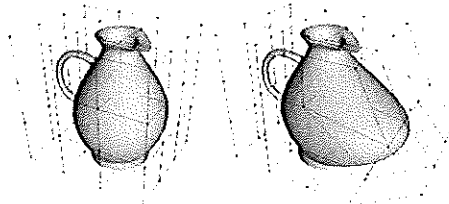


Fig. 3. Demonstration of global FFD (Barzel, 2003).

In this work, we use FFD in the manner of local deformation by applying the local lattice to the craniometric landmarks. Fig.

4 shows the deformation of face according to the deformation of incisor.

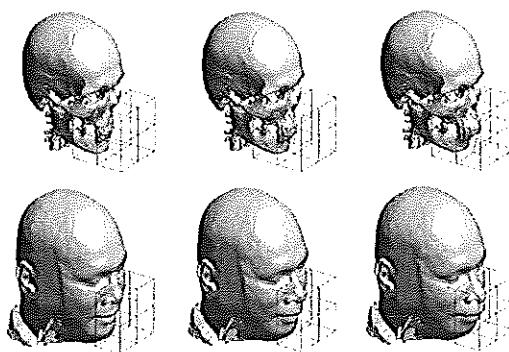


Fig. 4. Demonstration of local FFD. Middle column: original head. Left Column: moving incisor inside. Right column: moving incisor outside.

#### *Cylindrical Projection*

In this paper, to compare skull and face, we transform head 3D models onto plane using a cylindrical projection and resample

them with a specified rate. Fig. 5 shows the cylindrical projection of skull and face. Fig. 6 shows the absolute errors of cylindrical projection surfaces of skull and face.



Fig. 5. Cylindrical projection of face and skull

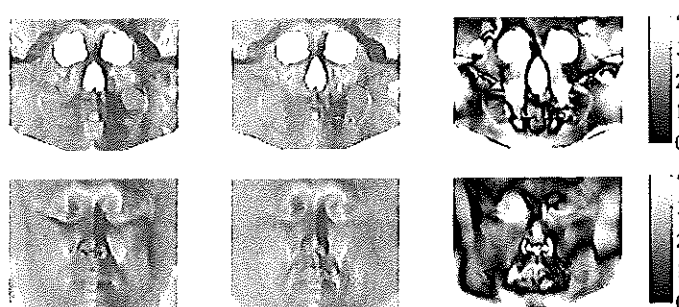


Fig. 6. Absolute errors of cylindrical projection surfaces. Errors are measured in mm.



### Nose Profile Estimation

In order to compare the two cylindrical projection surfaces of skull at the nasal part, we have to estimate the nasal profiles due to there are less information from nasal aperture. Fig. 7 shows the nose profile estimation method modified from Prokobe and Ubelaker (2002). Line A dissects the nasion and prosthion. Line B is parallel to line A and intersects the foremost point on the nasal bone. For each point of nasal aperture, the distance from

line B to the nasal aperture are calculated and mirrored to form the nasal profile estimation.

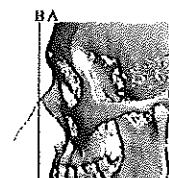


Fig. 7. The nose profile estimation method.

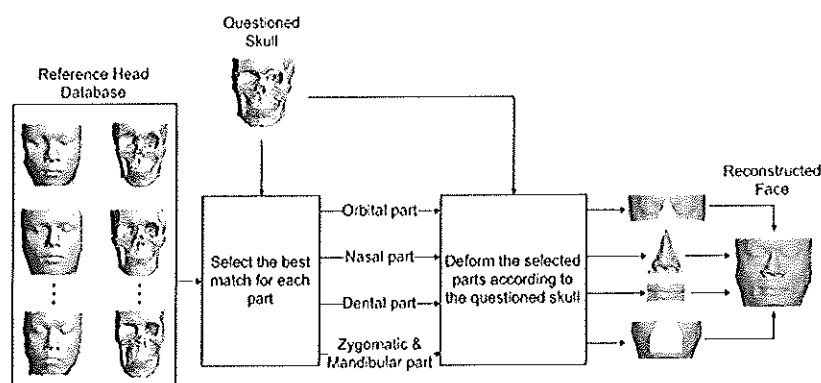


Fig. 8. Facial reconstruction workflow

### Methodology

There are 11 three dimensional head models in the head database. Each of them is picked out as questioned skull and the remaining heads are used as reference heads. Fig.8 shows the workflow of the proposed method. First of all, the questioned skull is compared to all skulls in head database each part separately. In this work, the skull is sectioned into 4 parts consisting of orbital part, nasal part, dental part and zygomatic & mandibular part. This work is developed from our previous research which considering zygomatic part and mandibular part separately. In this work, we consider zygomatic part and mandibular part together because these two

bones are linked by masseter muscle. It is one of the major muscles responsible for facial appearance. It is a very large and thick muscle originates at zygomatic bone and terminates at mandibular bone (Fig. 9). The best match for each part is selected as reference part. Then all of the reference parts are deformed according to the questioned skull. Finally, the deformed parts are combined to reconstruct the new face.

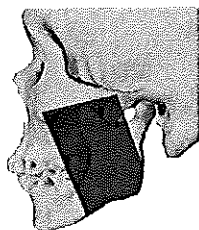


Fig. 9. Masseter muscle

column and second column demonstrate the target faces and reconstructed faces accordingly. These two columns are displayed for visual evaluation. Third column and fourth column present the cylindrical projection of target faces and reconstructed faces accordingly. Then the absolute errors are computed and displayed in fifth column. Although the result shows that we cannot produce exactly the same face as the target face, it still shows a promising forensic facial reconstruction.

#### Result and discussion

Fig. 10 and 11 present the facial reconstruction of subjects 1 – 11. First

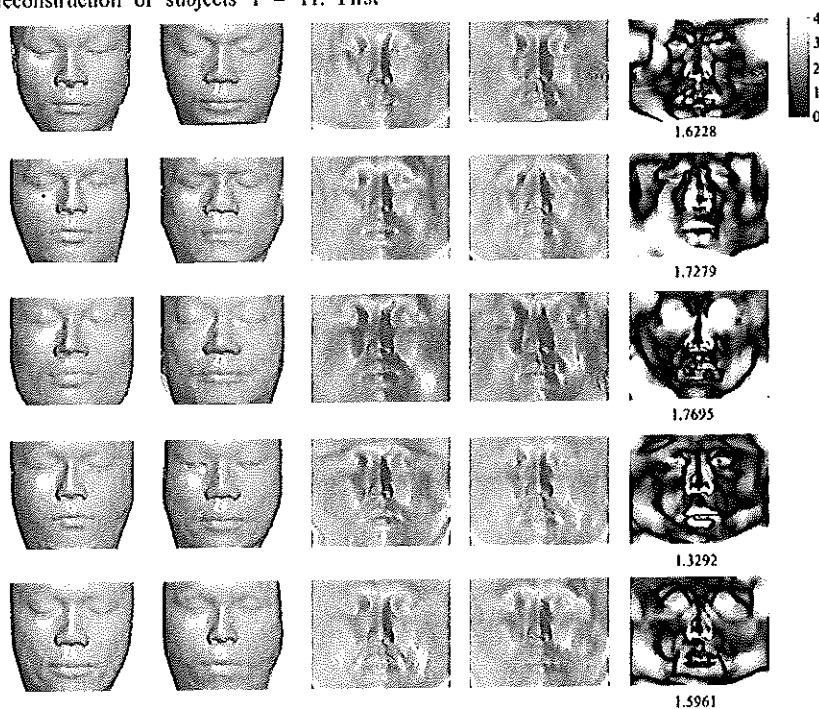


Fig. 10. Facial reconstruction of subjects 1 - 5. First column: target faces. Second column: reconstructed faces. Third column: cylindrical projection of target faces. Fourth column: cylindrical projection of reconstructed faces. Fifth column: absolute reconstruction errors. Errors are measured in mm.

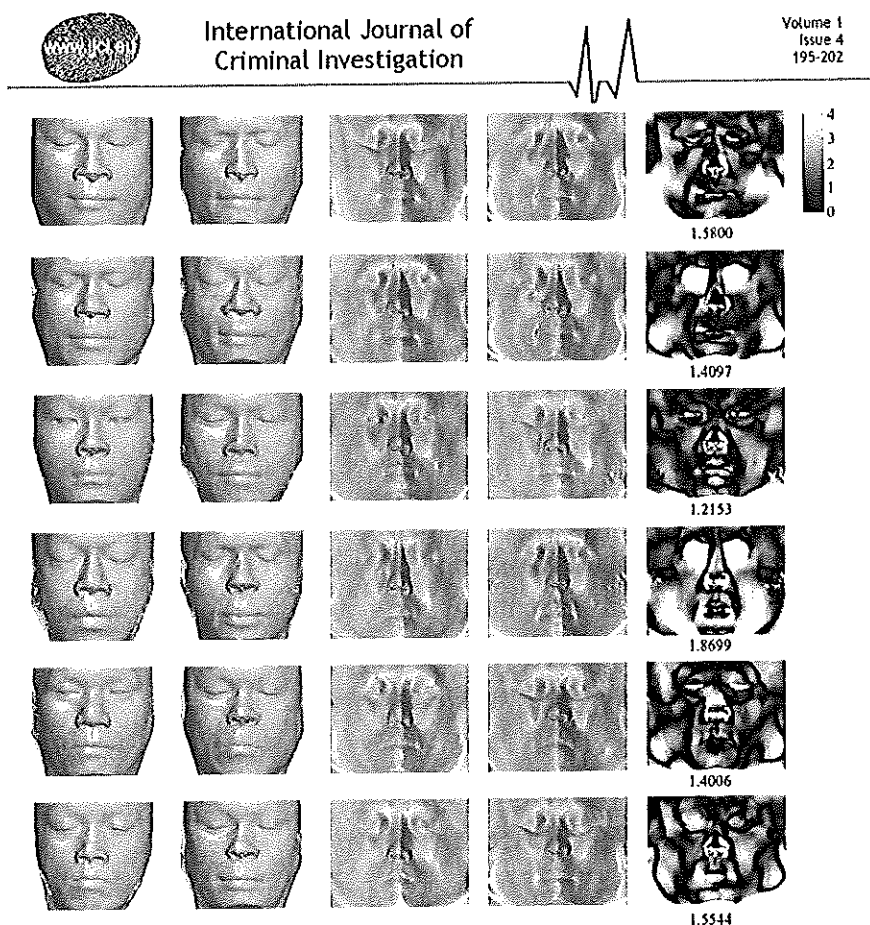


Fig. 11. Facial reconstruction of subjects 6 - 11. First column: target faces. Second column: reconstructed faces. Third column: cylindrical projection of target faces. Fourth column: cylindrical projection of reconstructed faces. Fifth column: absolute reconstruction errors. Errors are measured in mm.

### Conclusions

A traditional manual facial reconstruction has been used for a long time in both forensic and archaeological fields. However, the progressive studies and medical imaging technology leads to the development of alternative computer-based facial reconstruction methods. We have to remark that there is no way to reproduce exactly the same face for discovered skull. Instead of using small set of facial soft

tissue thickness data and then interpolate the large remaining area, we can use whole facial soft tissue thickness data from 3D head models derived from CT scanner and then the approximate questioned face from reference faces in face database. The approach presents possibility to use this scheme as a support tool for forensic facial reconstruction.

### Acknowledgement

We would like to thank Overbrook Hospital, Kasemrad Sriburin Hospital and

### References

- Barzel, R. Computer Graphics Animation Course Notes, Ecole Polytechnique, France. 2003.
- Besl, P.J.; McKay, N.D. A Method for Registration of 3D Shapes, IEEE Transactions on Analysis and Machine Intelligence, 1992, 14(2), 239-255.
- Gibson, L. Forensic Art Essentials: A Manual for Law Enforcement Artist, 1<sup>st</sup> edition, Academic Press, London, 2008.
- Prokopec, M.; Ubelaker, D.H. Reconstructing the shape of the nose according to the skull, Forensic Science Communications, 2002, 4(1).
- Sederberg, T.W.; Parry, S.R. Free Form Deformation of Solid Geometric Models, Computer Graphics, 1986, 20(4), 151-160.
- Kratumban Hospital for precious help in the head CT data acquisition phase and also thank to the volunteers that make this work possible.
- Stephan, C.N.; Taylor, R.G.; Taylor, J.A. Methods of Facial Approximation and Skull-Face Superimposition, With Special Consideration of Method Development in Australia. In M. Oxenham (Ed.), Forensic Approaches to Death, Disaster and Abuse, Australian Academic Press, Queensland, 2008, 133-147.
- Taylor, K.T. Forensic Art and Illustration, 1<sup>st</sup> edition, CRC PRESS LLC, Washington D.C., 2001.
- Wilkinson, C. Forensic Facial Reconstruction, 1<sup>st</sup> edition, Cambridge University Press, Cambridge, 2004.



## **CURRICULUM VITAE**

## CURRICULUM VITAE

**NAME** Ms. Siriluk Pongpunyayuen

**DATE OF BIRTH** 20 October 1986

**ADDRESS** 29 M.9 Sunshine, Maechan, Chiang Rai, Thailand 57110

**EDUCATION BACKGROUD**

2008 Bachelor Degree of Science (Cosmetic science)  
Mae Fah Luang University, Thailand

**WORK EXPERIENCE**

2008 – 2009 Research and Development Product (Hair care) at  
ModerncassInternational cosmetic Co.,Ltd.

**PRESENTATION**

Siriluk Pongpunyayuen & Nattaya Lourith. (2011). Radical scavenging activity and phenolic compounds in Rambutan peels extract. In: **Pure and Applied Chemistry International Conference 2011** (pp. 168). 5-7 Janurary 2011, Bangkok, Thailand.

Siriluk Pongpunyayuen & Nattaya Lourith. (2011). Appraisal of antityrosinase activity and phenolic compounds from Rambutan peels for cosmetics In: **The 3<sup>rd</sup> International Conference on Natural Product for Health and Beautiful 2011** (pp. 172-187). 16-18 March 2011, Bangkok, Thailand.